Addis Ababa University
Addis Ababa Institute of Technology
School of Chemical and Bio Engineering

Photocatalysis of titanium dioxide nanoparticles for drinking water disinfection under vis-LEDs and sunlight illumination

Shimelis Kebede Kassahun

PhD Dissertation

In partial fulfillment of the requirements for the attainment of \the degree of Doctor of Philosophy in Chemical Engineering (Environmental Engineering)

Addis Ababa University
Addis Ababa, Ethiopia
October, 2017

Photocatalysis of titanium dioxide nanoparticles for drinking water disinfection under vis-LEDs and sunlight illumination

Shimelis Kebede Kassahun

A Ph.D. Dissertation Submitted to the School of Chemical and Bio Engineering, Addis Ababa Institute of Technology, Addis Ababa University in Partial Fulfillment of the Requirements for the Degree of Doctor of Philosophy (Ph.D.) in Chemical Engineering (Environmental Engineering).

Submitted to: School of Chemical and Bio Engineering

Advisor:

Dr.- Ing. Zebene Kiflie

Addis Ababa University
Addis Ababa, Ethiopia
October, 2017

Addis Ababa University
School of Graduate Studies
School of Chemical and Bio Engineering

Titanium dioxide (TiO_2) based photocatalysis for drinking water disinfection under vis-LED and sunlight

By

Shimelis Kebede Kassahun

Approved by:

Dr.- Ing. Zebene Kiflie Zebene Kiflie (Main Advisor)

Prof. Dong-Woo Shin _____ (Co Advisor)

Prof. Young-Ryun Chung _____ (Co Advisor)

Declaration

I, Shimelis Kebede declare that this thesis and the work presented in it are my own and has been generated by me as the result of my own original research.

Photocatalysis of titanium dioxide nanoparticles for drinking water disinfection under vis-LEDs and sunlight illumination

I confirm that:

- ✓ *This work was done wholly while in candidature for the Degree of Doctor of Philosophy at Addis Ababa University.*
- ✓ *Where any part of this thesis has not previously been submitted for a degree or any other qualification at this university and other institution.*
- ✓ *Where I have consulted the published work of others, this is always clearly attributed.*
- ✓ *Where I have quoted from the work of others, the source is always given. With the extension of such quotations, this thesis is entirely my own work.*
- ✓ *I have acknowledged all main sources of help.*

Signed:..... Shimelis Kebede .....

Date:.....6/ October /2017.....

ABSTRACT

Response surface methodology, Box-Behnken experimental design, was applied to investigate and find optimum synthesis parameters for preparing visible-light active nitrogen doped titanium dioxide (N-TiO_2) by sol-gel method. Nitrogen to titanium molar ratios, calcination temperature and calcination time have been selected as the study parameters. X-ray diffraction (XRD) crystal phase compositions, Brunauer-Emmett-Teller (BET) specific surface area and visible-light decolorization of methylene blue have been examined as experimental responses.

A total of 15 tests were conducted, and all the samples have demonstrated different photoactivity under visible light. Furthermore, the important synthesis parameters which affect the three selected responses were investigated using the analysis of variance (ANOVA). Calcination temperature was found to be the most significant parameter which has direct influence on the crystal phase compositions, the specific surface area and photoactivity of the synthesized catalysts. The model adequacy test and regression analysis have shown that the results were well fitted with quadratic model equations. Model predictions were in good agreement with experimental data with 96.68 %, 96.88 %, and 96.96 % variability. N/Ti molar ratio of 6, calcination temperature of 400^{O}C and calcination time of 3 h was found to be the optimum condition.

The doped and undoped TiO_2 prepared at the optimum condition were characterized using X-ray diffraction (XRD), nitrogen absorption-desorption analysis, Fourier Transformed Infrared spectrometer (FTIR), Raman spectrometer, X-ray photoelectron spectroscopy (XPS), UV/Vis/NIR Spectrophotometer, High-resolution transmission electron microscopy (HR TEM), field emission scanning electron microscope (FE SEM), thermo gravimetric analysis (TGA), differential scanning calorimeter (DSC) and fluorescence spectrophotometer. From all characterization techniques, the results show the successful preparation of the N-doped TiO_2.

N-doped TiO_2 catalyst prepared under the optimum condition was immobilized on the surface glass beads using tetraethylorthosilicate (TEOS) as a binder. Simplified and low temperature sol-gel preparation method was investigated at different concentration of TEOS for better adhesive strength to glass support and photocatalytic decolorization activities on methylene blue. The physical and chemical characteristics of pure N-doped TiO_2 and property changes due to addition of TEOS were studied using X-ray diffractometer (XRD), Brunauer Emmett Teller (BET) analyzer, UV-Vis spectrometer, Fourier transform infrared spectroscopy (FT-IR), Field emission scanning electron microscope (FE-SEM) and High-resolution transmission electron microscopy (HR-TEM). The results showed that the addition of TEOS significantly improved the BET surface area, surface hydroxyl group and adhesive strength of the catalyst. However, the photoactivity of the catalyst was suppressed at the higher concentrations of TEOS (20 and 30%). Based on these results 5% TEOS was found to be an optimum value for successful immobilization of N-doped TiO_2 on the glass beads. The catalytic activity did not deteriorate, even after repeated application only 6 % loss in its photoactivity at the 5^{th} cycle test.

In the selection and design of appropriate types of photoreactor system configuration in terms of total irradiated surface area of catalyst per unit volume, reaction kinetics and light distribution within the reactor are the most important factors in photocatalysis reaction. Though several photoreactor system configurations has been reported in the literature, most of them have been applied in degradation of hazardous organic compounds. In this thesis work, photocatalytic bacterial inactivation is studied with immobilized N-doped TiO_2 using a novel multi stage fixed bed photoreactor. The photoreactor has been developed from N-doped TiO_2 nanoparticles immobilized on glass beads using tetraethoxysilicate (TEOS) as a binder with low temperature synthesis route. The reactor was irradiated under visible light emitting diodes (vis-LED) and sun light. The photocatalytic bacterial inactivation efficiency was investigated by varying selected reactor operating

parameters such as initial bacterial load (10^3 to 10^9 CFU mL^{-1}), TiO_2 concentration (0.3 to 0.6 gm), flow rate (40 to 60 mL min^{-1}), and light incident photon flux (2.24 x 10^{16}, 3.36 x 10^{16}, and 5.23 x 10^{16} photons/s) using *E. coli* as test organism. The results demonstrated that, the lower percentage of surviving *E. coli* were found at initial bacterial concentration of 10^6 CFU mL^{-1}, TiO_2 concentration of 0.6 g, flow rate of 40 mL min^{-1} and light intensity of 5.23 x 10^{16} photons/s was selected as optimum operating parameters.

The photocatalytic inactivation efficiency was further investigated on different types of Gram-negative (*E. coli, S. flexneri and S. typhimurium*) and Gram-positive bacteria (*B. subtilis and S. aureus*) in water. The inactivation log unit reduction for *E. coli, S. typhimurium, S. flexneri, S. aureus and B. subtilis* were found to be 5.22, 4.69, 4.65, 4.03, and 3.08 in 120 min under vis-LED irradiation and 5.70, 5.05, 4.97, 4.25 and 3.90 in 40 min under sunlight irradiation, respectively. In both cases, the Gram-positive bacteria demonstrated the least log unit reduction. The rate of photocatalytic inactivation, calculated based on Chick-Watson disinfection kinetic model, indicated faster disinfection kinetics in the case of Gram-negative bacteria. The bacterial cell membrane damage, examined on *S. aureus, and S. flexneri* using field emission scanning electron microscope clearly showed the effects of TiO_2 nanoparticle on bacterial cell structure.

Immobilized TiO_2 recycling studies were performed using the proposed photoreactor with *E. coli* as test organism. The photocatalytic bacterial inactivation efficiency was evaluated and compared between the reuse cycles and results show that the log unit reduction of *E. coli* only decreased by about 0.89 after five-time reuse.

ACKNOWLEDGEMENTS

I would like to express my deep gratitude to my advisor, Dr.-Ing Zebene Kiflie for his insightful guidance, encouragement and supervision starting from proposal development and throughout my Ph. D studies.

I also would like to thank Prof. Dong-won Shin for his kind academic guidance and financial support during my stay in South Korea as research scholar. He is the one who gave me the opportunity to conduct this research in Nano Co., Ltd., advanced research laboratory and facilitated my stay at Gyeongsang National University, Plant Molecular Biology and Biotechnology Research Center to carry out part of the experimental work.

I also want to extend my gratitude Prof. Young-Ryne Chung for allowing me to use his research laboratory and for the continuous follow up during my research activity. I have enjoyed a very good working environment, laboratory facility and encouragement from his M.Sc. and Ph. D students: Mr. Kbd Rajon, Mr. Harun Rashid, Mr. Ajmal Khan, and Mr. Yeong Jeon.

I also would like to express my appreciation and thanks to Professor Whasik Min for facilitating my stay in South Korea and his continuous follow-up.

I was very lucky to have the opportunity to work in Nano Co., Ltd. Advanced Research Laboratory. My gratitude goes to Dr. Sam-Sik Park and his research groups for offering invaluable supports.

I thank all members of Department of International and External Cooperation, Gyeongsang National University for their support. My special thank goes to Mr. Kim Hoe-Dong for his unlimited assistance in every matter during my stay in S. Korea.

Besides, I would like to acknowledge Mr. Sintayehu Nibret and Mr. Kebede Taye for finding time in their busy schedule to read my publication manuscript, comments and valuable suggestions.

In South Korea, I received the support and have special memories of my friends Mr. Tewodros Nigatu, Mr. Sintayehu Nibret, Mr. Adane Tilahun, Mr. Anteneh Wedajo, Mr. Lemesa Etana, Mr. Nebiyou Getachew and Mr. Dereje Azmeraw.

It is indeed, a great pleasure for me to express my heartfelt gratitude to my wife and my families for their encouragement, support and help during my Ph. D studies.

I really appreciate the members of school of Chemical and Bio Engineering staffs at Addis Ababa institute of Technology, Addis Ababa University, for their direct or indirect contribution. My special thanks go to Mr. Zerihun Abate for handling any matter which was concerned me during my absence.

I am very thankful to all staff members of Gyeongsang national University Centralized Scientific Instrumentation Facility (CSIF) for their support during material characterization. I am also grateful to Prof. Jeoung Ju Lee for his kind support during XPS sample scanning.

Finally, I would like to thank and acknowledge Addis Ababa University for giving me the opportunity to study my Ph. D and covering all of the required course fees and research expenses. I am grateful for providing financial support granted by Germany Academic Exchange service (DAAD). In addition, I also like to thank the National Institute for International Education (NIIED), Korean Ministry of Education scholarship program and Gyeongsang National University. I would like also to extend my appreciation for Nano Co., Ltd for allowing me to use their advanced research facilities and for their unlimited cooperation.

TABLE OF CONTENTS

LIST OF FIGURES

LIST OF TABLES

LIST OF PUBLICATIONS

1. Kassahun SK, Kiflie Z, Shin DW, Park SS, Jung WY, Chung YR. Optimization of sol-gel synthesis parameters in the preparation of N-doped TiO2 using surface response methodology. J Sol-Gel Sci Technol. 2017;82(2):322–334.
2. Kassahun SK, Kiflie Z, Shin DW, Park SS, Jung WY, Chung YR. Photocatalytic decolorization of methylene blue by N-doped TiO2 nanoparticles prepared under different synthesis parameters. J Water Environ, Nanotechnol. 2017;2(3):136–144.
3. Kassahun SK, Kiflie Z , Shin DW, Park SS, Jung WY, Chung YR. Facile low temperature immobilization of N-doped TiO2 prepared by sol–gel method. J Sol-Gel Sci Technol. 2017;83(3):698–707.
4. Study the effect of operational parameters on the new type of Vis-LED illuminated photoreactor for bacterial inactivation: Ready to Submit.
5. Novel multi-stage fixed bed photoreactor for bacterial inactivation using N-doped TiO2 under Vis-LED and sunlight : Under review (international Journal of Environmental Research)

Chapter 1

INTRODUCTION

1.1. Background of the study

Access to safe and reliable potable water in sufficient amount is fundamental for good health and wellbeing. The availability and distribution of this valuable resource is uneven in most continents.

An estimated 748 million people worldwide still do not have access to safe potable water [1]. Most of these people are from the developing countries, especially in the rural areas and low- income communities [2]. Furthermore, reports show that 50 % of the population from these regions is exposed to polluted water sources [3]. Lack of access to safe drinking water is responsible for several infectious diseases and thus, constitutes one of the major causes of mortality in these countries. It is estimated that each year 200 million cases of water-related diarrheal illness are reported worldwide leading to 2.1 million deaths [4]. In Africa, despite an increase in drinking water coverage from 56 per cent in 1990, to 66 per cent in 2010, the population relying on unimproved drinking water source increased from 279 million in 1990, to 344 million in 2010 [5]. There is almost five times as many people in rural areas without an improved drinking water source than in urban areas, 1990-2010 [6].

Cholera, malaria, guinea worm and river blindness are the major water-related and waterborne diseases which are associated with limited access to water and sanitation in Africa [7]. Approximately fifty present of all patients occupying African hospital beds suffer from water- borne illnesses [8].

In particular in Sub-Saharan Africa, access to water remains a major concern for states and populations [9]. There are 25 countries in Sub-Saharan Africa in which

the percentage point gap between use of improved drinking water in urban and rural areas is more than 25% [5]. In seven countries - Congo, Democratic Republic of Congo, Ethiopia, Gabon, Niger, Sierra Leone and Somalia - it is more than 50%. Difficulties in accessing water are significant health issues, particularly in terms of diarrheal morbidity and malnutrition in children under 5 years of age in this region [10].

Surface, ground and lake water are considered as the main sources of drinking water. Today, roughly a third of the world's population depends on ground water for drinking, which is generally seen as a safe alternative to drinking untreated, microbial contaminated surface water [11]. However, several human activities can affect the ground water quality. Furthermore, it is estimated that roughly 10 % of wells are contaminated with the most widespread geogenic contaminants, arsenic and fluoride [11].

Deficiencies in piped water distribution systems, also common in many developing countries, have been linked to contamination of water at consumer taps and outbreaks of water-borne illnesses [12]. In Sub-Saharan Africa only 50 % of the population has access to piped water, which is the lowest coverage rates compared to other part of the world [13].

Contaminated drinking water is one of the most significant environmental contributors to the human disease burden and in terms of waterborne contaminants, which include inorganic and organic chemicals as well as pathogens/microbes, the World Health Organization (WHO) considers that microbial hazards remain the primary concern in both developing and developed countries [14]. For this reason, more effective, lower-cost, robust methods to disinfect waters from source to point-of-use are needed, without further stressing the environment or endangering human health by the treatment itself.

Conventional methods of water disinfection can address many of these problems. However, these treatment methods are often chemical, energy and operationally intensive. They are focused on large systems and thus require considerable amount of capital, trained man power and infrastructure. Furthermore, generations of undesirable disinfection by-products (DBPs) are of primary concern in the case of chemical treatment methods since many of them have been found to be carcinogenic and/or mutagenic.

On the other hand, advanced oxidation processes (AOPs) are alternative treatment methods for decontamination of water containing organic pollutants, classified as bio-recalcitrant, and/or for disinfection removing current and emerging pathogens [15]. These methods depend on the generation of highly reactive chemical species which are capable to disinfect and inactivate wide range of drinking water related diseases and mineralizing organic pollutants [15], [16]. All of them are characterized by the same chemical feature: production of hydroxyl radicals ($^{\cdot}OH$), which are able to degrade these pollutants into readily biodegradable compounds, and eventually mineralize them to innocuous CO_2, H_2O, and inorganic ions [17]. Most importantly, these methods are less energy intensive [18].

In addition, several researches have been also done in the area of heterogeneous catalysts. But, water treatment processes using heterogeneous photocatalysts has gained much attention due to its effectiveness in degrading and mineralizing the recalcitrant organic compounds, disinfecting wide variety of micro-organisms as well as the possibility of utilizing the solar UV and visible spectrum [19]. Some semiconductor catalysts such as TiO_2, ZnO, Fe_2O_3, CdS, GaP and ZnS are considered as heterogeneous photocatalysts. However, titanium dioxide (TiO_2) has played a much larger role in this application compared to other semiconductor photocatalysts due to its unique characteristics such as inexpensive, inert nature, chemically stability, non-hazardous, highly reactive and ecofriendly. Considering the above

advantages related with TiO_2 photocatalyst, this research work aims to develop an alternative drinking water disinfection system using titanium dioxide photocatalyst.

1.1. Justification of the study

A shortage of clean drinking water is high and water related infectious diseases are chronic in rural parts of the world especially in developing countries. Infectious diseases caused by pathogenic bacteria, viruses and protozoan parasites are among the most common and widespread health risk associated with drinking water. Mainly elderly people and young children who leave in these countries are vulnerable to these infections diseases.

Though several well-developed water disinfection technologies already exist, they are usually characterized by large investment and infrastructure requirement, high operation and distribution cost, difficulty in maintenance, ineffectiveness, non-residual effect, potentially toxic by-products, and technical complexity. More importantly these technologies are not easily applicable in rural parts of the world.

In view of tackling these disadvantages the development of an alternative drinking water disinfection system is desirable.

1.2. Scope of the study

The main aim of this study was to develop a novel and simple type of photoreactor for photocatalytic bacterial inactivation. The reactor was developed from immobilized visible light active nitrogen doped titanium dioxide (N-doped TiO_2) on glass beads and irradiated under Vis-LED and sun light.

1.3. Statements of the problem

Three-quarters of the earth's surface is water. However, only one percent of that water is available for human consumption; and that one percent often contains micro-organisms that can cause life threatening waterborne diseases. Water-related

diseases are a growing human tragedy. Billions of people suffer from diseases linked to dirty water. Some 60 % of all infant mortality worldwide is linked to infectious and parasitic diseases and most of them are water-related. At any given time, about half the population in the developing world is suffering from one or more of the six main diseases associated with water supply and sanitation.

Water quality is the composition of water as affected by natural processes and human activities. Many different diseases are spread by contaminated drinking water, caused by *Campylobacter*, *Vibrio cholerae*, *Amoebic dysentery*, *Giardia* (beaver fever), *Cryptosporidium* etc. In the future, more pathogenic micro-organisms will emerge and spread through water because of agricultural magnification, increased population growth, increased migration and climate change. Pathogenic micro-organisms can also emerge because they build up resistance to disinfectants. The existing drinking water disinfection technologies are not properly addressing these water quality concerns. Besides, these technologies have a number of drawbacks as discussed detail in section 6.3.1 and 6.3.2. Some of the main drawbacks are summarize as follow:

I. Difficulties in controlling certain process parameters like temperature and pH related with chemical disinfection methods. Some of the disinfection process like Ozonation require quite high exposure time to disinfect the pathogenic micro-organisms
II. Chlorination and Ozonation disinfection process create substantial amount of undesired disinfection by-products, which are considered to be potential human carcinogen.
III. High initial and operational investment requirement

IV. Larger treatment area requirement.

V. Environmental incompatibility, for example, mercury lump disposal problem with UV disinfection technologies.

VI. Some pathogens such as viruses, and certain bacteria like *Campylobacter, Yersina, Mycobacteria,* or *Legionella*, and protozoans *Cryptosporidium* or *Giardia lamblia* cysts have been known to be resistant to chlorine disinfection

VII. Safety concern, in particular Ozone being highly unstable gas can create an explosion at low concentration.

VIII. Low residual effect characteristics related with ozonation and UV disinfection treatment.

IX. Unsuitability of these technologies for rural areas.

These have led to the rapid research and development in the field of "Advanced Oxidation Processes (AOPs)" as the innovative water treatment technologies and avoiding the drawbacks related with already existing technologies.

Therefore, this study emphasizes on development of alternative drinking water disinfection technologies using heterogeneous photocatalyst in particular with titanium dioxide (TiO_2). This was achieved by synthesized the photocatalyst to activate in visible light spectrum and improving its recoverability through immobilizing on other support material.

So far, considerable efforts that have been done to reduce its band-gap energy of TiO_2 and utilize the visible-light which is the larger portion of the solar spectrum. One of the major approaches in this regard is doping, a modification of TiO_2 by influencing the electron structure with metal and non-metal ions via different physical and chemical synthesis routes that include implantation, sputtering, ball mill, solvothermal and sol-gel methods for synthesis of nitrogen doped titanium dioxide (N-doped TiO_2). Due to several advantages on sol-gel synthesis method, different

researchers have been tried to investigate the effects of sol-gel synthesis parameters on the preparation of N-doped TiO_2 using the conventional "one-parameter-at-a-time approach" [20]–[27]. Although this approach is widely acceptable, it has a limitation in estimating the interaction effects between the factors and lacks a predictive capability [17]. Furthermore, it has been ignored to obtain the optimum synthesized parameters which simultaneously satisfy specific surface area, pore size, crystal size, crystallinity, and crystal phase which is the photocatalytic activity of a TiO_2 powder depends on.

On the other hands, immobilization TiO_2 have been reported by the series of process such as sol-gel synthesis, coating on the glass support followed by heat treatment at high temperature. The coating and the heat treatment processes were repeated several times to achieve the required coating strength. Though this method is easy to control the microstructure of the film, solution composition, and film thickness, it however affects photoactivity due to significant surface area reduction during repeated higher heat treatments [28]. Furthermore, the method is time consuming and an energy intensive process that typically takes place above 400 ^oC. Some researchers have also pointed out the influences on catalyst activity that result from diffusion of sodium ion from the glass into coated TiO_2 catalyst at high calcination temperature [28]. On the other hand, it has been reported that water or other solvent (such as Ethanol based TiO_2 sol-gel immobilization lacks adhesive strength which decreases the performance of repeated usability of the catalyst [29].

Furthermore, Several immobilized type photoreactor designs such as rotating corrugated drum reactor [30], fixed-bed reactor [31], tubular photoreactor [32], multi tubular photoreactor [33], UV/TiO_2 immobilized optical-fiber photoreactor [34], annular photocatalytic reactor [35], corrugated plate photocatalytic reactor [36], stirred annular photoreactor [37], Taylor- vortex reactor [38] have been proposed in different applications. However, most of them were complex, focused on degradation

of hazardous organic compounds and their application has been very limited for pathogenic microorganism inactivation applications.

1.5. Research objectives

1.5.1. General objective

The general objective of this study is to synthesize and characterize a visible light active nitrogen-doped TiO_2 and investigate the photocatalytic microbial inactivation performance in the form of immobilized photoreactor.

1.5.2. Specific objectives

The specific objectives of this study are:

- ✓ To synthesize nitrogen-doped titanium dioxide (N-doped TiO_2) using sol-gel methods and optimize the synthesis parameters using surface response methodology.
- ✓ To investigate the chemical and physical properties of the doped and undoped TiO_2 nanoparticles.
- ✓ To prepare immobilized N-doped TiO_2 nanoparticle on the surface of glass beads via dip-coating technique.
- ✓ To study the physical and chemical properties of immobilized N-doped TiO_2.
- ✓ To design and construct a multi-stage fixed bed photoreactor system for the continuous bacterial photocatalytic inactivation using N-doped TiO_2 and investigate its performance under Vis-LED/sunlight irradiation.
- ✓ To investigate the photocatalytic bacterial inactivation efficiency under different operating parameters such as initial bacterial load, TiO_2 concentration, flow rate, and light intensity using *E. coli* as test organism.
- ✓ To investigate the photocatalytic bacterial inactivation efficiency and rate of disinfection on selected Gram-negative (*E. coli, S. typhimurium and S. flexneri*) and Gram-positive bacteria (*B. subtilis and S. aureus*).

- ✓ To examine bacterial cell membrane damage due to N-doped TiO_2 nanoparticles under scanning electron microscope.

Chapter 2

LITERATURE REVIEW

2.1. Drinking water related waterborne pathogens

Drinking water related waterborne diseases are caused by pathogenic micro-organisms that most commonly are transmitted in contaminated fresh water. These pathogens have the potential to cause widespread waterborne disease within communities [39]. Three different groups of pathogenic micro-organisms can be transmitted via drinking water to humans these are protozoans (unicellular eukaryotes), bacteria, and viruses. All are transmitted by the fecal–oral route, so largely arise either directly or indirectly by contamination of water resources and supplies by sewage or animal feces [40].

It is theoretically possible, although unlikely, that helminthes (eukaryotic parasites) (>100 mm) such as nematodes (roundworm or hookworm) and cestodes (tapeworm) may also be transmitted via drinking water.

The main characteristics that distinguish prokaryotes from eukaryotes are the following:

1. Eukaryotic cells are generally more complex than prokaryotic cells.
2. DNA is enclosed in a nuclear membrane and is associated with histones and other proteins only in eukaryotes.
3. Organelles are membrane-bound in eukaryotes.
4. Prokaryotes divide by binary fission whereas eukaryotes divide by mitosis.
5. Some structures are absent in prokaryotes: for example, Golgi complex, endoplasmic reticulum, mitochondria, and chloroplasts.

❖ Bacteria

Bacteria are single-celled, constitute a large domain of prokaryotic micro-organisms. The cells occur in three basic shapes: cocci (spherical shape; e.g., *Streptococcus*), bacilli (rods; e.g., *Bacillus subtilis*), and spiral forms (e.g., *Vibrio cholera*; *Spirillum volutans*). They are much smaller than eukaryotic cells, there cell size generally ranges between 0.3 mm (e.g., *Bdellovibrio bacteriovorus*; *Mycoplasma*) and 1-2 μm (e.g., *E. coli*; *Pseudomonas*). A typical cytoplasmic membrane of the bacteria comprises about one third lipid and two thirds protein. It contains synthetic enzymes for components of all layers of the cell wall together with proteins involved in transport, energy generation and so on. Cell wall is the most important part of the bacteria structure, which confer the characteristic cell shape and provide the cell with mechanical protection. Many functions, such as semi-permeability, respiration, and oxidative phosphorylation reactions, rely on an intact membrane structure [16]. There are broadly speaking two different types of cell wall in bacteria, a thick one in the gram-positives and a thinner one in the gram-negatives. The names originate from the reaction of cells to the gram stain. However, this difference in staining is due to fundamental differences in cell wall structure and chemical composition.

Gram-positive bacteria possess a thick cell wall containing many layers of peptidoglycan and teichoic acids. In contrast, Gram-negative bacteria have a relatively thin cell wall consisting of a few layers of peptidoglycan surrounded by a second lipid membrane containing lipopolysaccharides and lipoproteins. Figure 2.1 illustrate the comparison of the cell wall of Gram-positive and Gram-negative bacteria. Between the cell wall and cell membrane is periplasmic space, where contains various degradative enzymes, binding proteins, membrane-derived oligosaccharides, and electron mediators. Within the cytoplasm of bacteria is a nucleoid, a region where the genetic material (DNA) resides. Also within the cytoplasm are numerous ribosomes, whose function is protein synthesis. Cytoplasm also contains plasmid in some bacteria. Plasmids are extra-chromosomal DNA, which

often code for pathogenesis factors and antibiotic resistance factors. Some bacteria also have surface structures, such as flagella, pili (fimbriae), capsules, and so on.

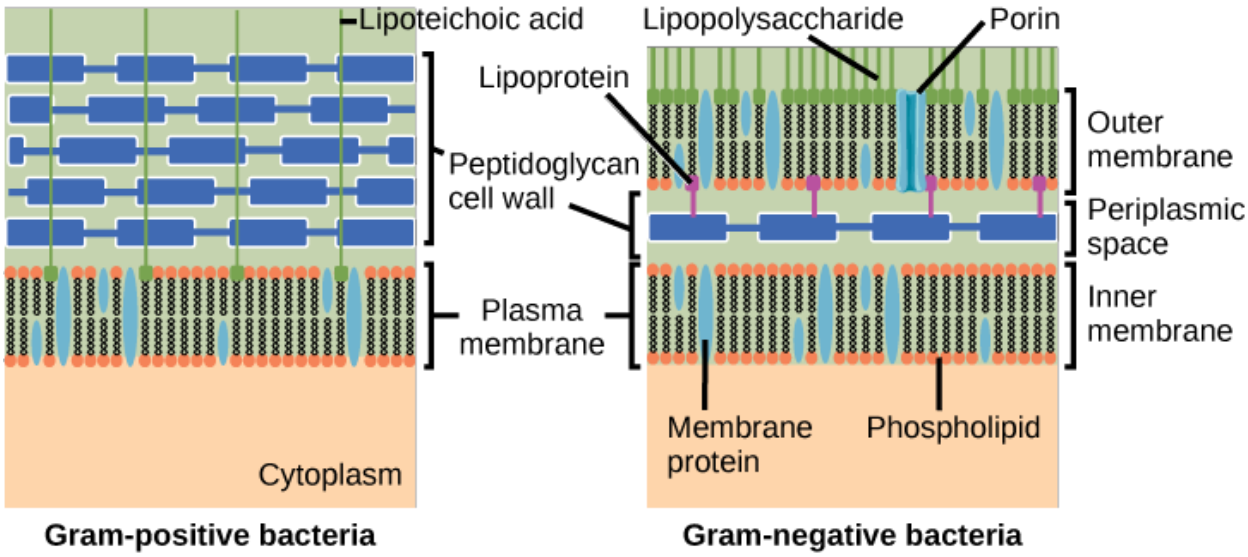

Figure 2. 1 Comparison of the cell wall of Gram-positive bacteria with Gram-negative bacteria [41].

The vast majority of the bacteria in the body are rendered harmLess by the protective effects of the immune system, and some are beneficial. However, several species of bacteria are pathogenic and cause infectious diseases. They can contaminate the water system through various ways. Drinking water pathogens originate primarily from the contamination of water resources, although pathogens can also contaminate water during treatment, within the distribution system or even within the home [39]. A great majority of evident water-related health problems are the result of bacteriological contamination [42].

2.2. Drinking water-related waterborne diseases in Ethiopia

Coverage levels for water and sanitation in Ethiopia are among the lowest in the world. According to WHO/UNICEF joint monitoring program for water supply and sanitation 2014 report, the portion of population that gained access to improved drinking water (piped onto premises and other improved sources) in Ethiopia is estimated around 97 % (51% piped onto premises and 46% other improved sources)

in urban area and 42% (1% piped onto premises and 41% other improved sources) in rural area. This clearly indicates that there is high disparity between urban and rural part of the country in terms of improved drinking water.

In addition to access to safe drinking water, water quality is another major problem, as evidenced by frequent outbreaks of water related epidemics in both rural and urban areas. Over 60% of the communicable diseases occurring in Ethiopia are due to poor environmental health conditions as a result of unsafe and inadequate water supply and poor hygienic and sanitary practices [43].

Since a large majority of the rural population get their water supplies from unprotected sources such as streams, ponds wells, etc., waterborne diseases are one of the most significant public health problems [44]. These diseases are the number one causes of infant mortality in Ethiopia. Children under the age of five die every year associated to diseases transmitted through unsafe water. The most common drinking water-related waterborne diseases in Ethiopia includes Shigellosis, Typhoid fever, Cholera, Acute Gastroenteritis, Infectious hepatitis (Hepatitis A), Amebiasis and Giardiasis [45].

2.3. Water disinfection technologies

Disinfection or inactivation is the most crucial process in the treatment of drinking water supply and is the final barrier against pathogenically impurities in drinking water [46]. Disinfection of potable water commonly has two goals: the immediate destruction or inactivation of pathogens, and persistent inactivation of pathogens through residual action (known as residual effect) [47].

In general water disinfection technologies categorized as conventional and advanced oxidation processes (AOPs).

2.3.1. Conventional drinking Water disinfection technologies

There are different disinfection technologies have been developed for inactivation or killing of drinking water pathogenic micro-organisms. The most common conventional methods for water disinfection are chemicals, ultraviolet irradiation, and filtration processes etc. [48]. Chlorine, chlorine dioxide, and chloramines are the most common chemical disinfectants [49]. Among these chemical disinfectant, chlorine has been successfully used to disinfect drinking water for more than a century [46]. The basic principles of these technologies are discussed as follow:

i) Chlorination

The chlorination disinfection has been in use as far back as early twentieth century for inactivation of photogenic microorganisms [50]. It is the most widely used disinfectant, both in centralized water distribution systems and for point-of use treatment. It is also the most effective methods against a broad spectrum of pathogens, and it provides residual effect to continue to disinfect water as it passed through the distribution system [46]. Chlorination is still the most widely used and relatively cost effective means of disinfectant in water and wastewater [46], [51], [52].

The most commonly used chlorination disinfectants are chlorine (chlorine gas chlorine dioxide, and hypochlorite solution) which is the first and the most widely used disinfectant for municipal wastewater, and other chlorine compounds such as chloramines, chloride, bromine, fluorine and iodine [53]–[56].

Chlorine inactivates a microorganism by damaging its cell membrane. Once the cell membrane is weakened, the chlorine can enter the cell and disrupt cell respiration and DNA activity (two processes that are necessary for cell survival) [57].

In addition to controlling disease-causing organisms, chlorination offers a number of benefits including:

- ✓ Reduces many disagreeable tastes and odours;
- ✓ Eliminates slime bacteria, molds and algae that commonly grow in water supply reservoirs, on the walls of water mains and in storage tanks;
- ✓ Removes chemical compounds that have unpleasant tastes and hinder disinfection;
- ✓ Helps remove any iron, manganese and/or hydrogen sulphide that are present in raw water.

A disadvantage of using chlorination to disinfect drinking water is the potential formation of harmful byproducts if too much chlorine is used in the presence organic compounds in the water [58]. These harmful byproducts (DBPs) of the chlorination including trihalomethanes, halogenated acetic acid, and halogenated acetonitriles are known to be toxic and associated with reproduction and carcinogenic risk in humans [59]. Another disadvantage of chlorination is ineffectiveness against Cryptosporidium and Mycobacterium and it is inefficiency is that in eliminating some epidemic micro-organism at low chlorine dose [52].

Moreover, chlorination process is highly dependent on certain process parameters. For example mixing characteristics of chlorine contactors ,the presence of suspended solids, contact time and chlorine dose are strongly affect the efficiency of the process [60], [61].The strong chlorine taste and smell that result from the free chlorine residuals due to overdosing are also an issue of chlorination [62].

ii) Ultraviolet (UV) irradiation

Light is a form of electromagnetic energy where the shorter the wavelength of the light, the greater the amount of energy emitted. Ultraviolet light is classed as the range that occurs below the visible range (400-700 nm) and is found at wavelengths of between 100 and 400 nm. It is broken down into four ranges, UV-A, UV-B, UV-C and vacuum UV as shown in Table 2.1.

It is UV-C range (200–280 nm) that is used for water disinfection. While it is absorbed by RNA, DNA and proteins, which leads to cellular damage, mutation, cancer and cell death.

Ultraviolet light in the UV-C band is also known as ultraviolet germicidal radiation (UVGI) and is widely used for sterilizing equipment and creating sterile environments, as well as in the food and the water industry to inactivate micro-organisms.

Table 2. 1 Wavelength (Nanometers) and Energy Emitted (eV) by Different Bands of Ultraviolet Light.

Ultraviolet Range (abbreviation)	Wavelength (nm)	Energy per Photon (eV)
A (UVA)	400 - 315	3.10 – 3.94
B (UVB)	315 - 280	3.94 – 4.43
C (UVC)	280 - 100	4.43 – 12.4
Vacuum (VUV)	200 - 100	6.20– 12.4

The cell nucleus in bacterial and protozoan waterborne pathogens contains DNA, which comprises strands of nucleotides that join to form pairs held together by hydrogen bonds. These form the characteristic double stranded helix. There are four nucleotides that form pairs, cytosine with guanine and adenine with thymine. Viruses do not have a nucleus but can contain either DNA or RNA within a protein shell. RNA also has four types of nucleotides like DNA, but thymine is replaced by uracil. UV light generally inactivates microbes by damaging material in their DNA and RNA. Nucleotides absorb UV light in the wavelength range 220-300 nm. After UV exposure, energy opens up the double bond in thymine and cytosine bases in DNA then dimers (covalent bonds) form between these complementary nucleotides, this causes blocking protein synthesis and disabling the proper replication of the DNA helix during cell division cycle.

UV disinfection does not kill pathogens rather it inactivates them so that they are unable to reproduce and cause infection, but remain alive.

This disinfection technology uses open channel equipped with low or medium pressure mercury arc lamps: The low pressure (LP), which emits nearly monochromatic light at 254 nm and medium pressure (MP), which emits polychromatic light over a wide range of wavelengths, including those associated with germicidal [63].

Advantages of UV Disinfection

- ✓ Highly effective at inactivating on broad range of pathogens including those which are resistant to chlorine/ chloramines.
- ✓ Forms no harmful disinfection by-products (eg. Trihalomethanes)
- ✓ Inactivation independent of pH and temperature
- ✓ No unpleasant taste or odor
- ✓ No transportation, storage or handling of chemicals. Disadvantages of UV Disinfection
- ✓ It can be used in combination with a secondary chemical disinfectant to provide a residual for distribution of drinking water.
- ✓ It is not environmental compatible because of mercury lump disposal problem.
- ✓ The efficiency can be influenced by factors including suspended particles, particle sizes, or concentrations of dispersed micro-organisms.
- ✓ The micro-organisms can recover from the damage after the disinfection processes.

iii) Filtration

Filtration process, specifically membrane filtration such as Microfiltration (MF) and Ultra filtration (UF) are increasingly applied in advanced drinking water treatment processes for disinfection and removal of colloids and larger molecular weight organics [45]. These technologies are based on a physical barrier concept which is used for the separation of solids from fluids by interposing a medium through

which only the fluid can pass. Therefore, the relative sizes of the filter pores and the micro-organisms present in the fluid should be considered during the filtration process. In addition, multiple separation approaches should be taken into consideration.

This technology is advantageously used for complete wastewater treatment in compact units before recycling or reclamation either for municipal or industrial wastewater including zero toxic residue [60]. However, the following disadvantages are the main issues. These are:

- ✓ The technology recommended for low or very low contaminated waters. Particularly recommended for groundwater recharge and potable wastewater reuse.
- ✓ Some micro-organisms that are capable of passing the filtration process
- ✓ Much more expensive (capital and operating cost)
- ✓ No residual effect in distribution system

2.3.2. Advanced Oxidation Processes (AOPs) drinking water disinfection technologies

Advanced oxidation processes (AOPs) refers to a set of chemical treatment procedures designed for mineralization of refractory organic compounds, water pathogens and disinfection by- products by oxidation through situ generation of highly reactive transitory species (i.e. H_2O_2, $OH^{\cdot}$, $O_2^{\cdot-}$, O_3) [17]. Among these reactive transitory species the hydroxyl radical ($^{\bullet}OH$) is one of the most powerful known oxidants which are responsible to destroy/convert organic contaminants to harmLess substances [64]. The versatility of AOPs is also enhanced by the fact that they offer various alternative methods of hydroxyl radical production, thus allowing a better compliance with specific treatment requirements [16]. Furthermore, the eco-friendly end products like CO_2, H_2O and, inorganic ions are the special feature of these processes. The hydroxyl radical can be formed by a number of methods in aqueous systems, these includes:

i) Ozonation

The method of disinfecting drinking water and wastewater is ozone disinfection (also known as Ozonation). Ozone is a molecule made of three oxygen atoms that occurs naturally in the earth and that can also be manmade. It is a strong oxidizing agent with a standard redox potential of 2.07 V, which is used extensively for water disinfection [65]. This method is effective in destroying bacteria, viruses but also cyst-forming protozoan parasites like Giardia and *Cryptosporidium* which are particularly resistant to most other disinfectants [66]. Apart from pathogen control, today ozone is being used for a wide range of purposes in water treatment including: 1) oxidation of inorganic compounds, especially reduced metals; 2) oxidation of synthetic organic compounds (including pesticides); 3) removal of natural organic compounds, which includes chlorination DBP precursors, reduction in total organic carbon (TOC) concentrations, and the removal of taste and odor, algal toxins, and color; and finally, 4) particle (turbidity) reduction.

During ozonation, the pollutants can be degraded by two different pathways: direct reactions with O_3 and indirect reactions with hydroxyl radicals [67]. The direct oxidation with aqueous ozone is relatively slow (compared to hydroxyl free radical oxidation) but the concentration of aqueous ozone is relatively high. On the other hand, the hydroxyl radical reaction is fast, it can react 10^6–10^{12} times faster than ozone, but the concentration of hydroxyl radicals under normal ozonation conditions is relatively small [68]. The overall reaction is:

$$3O_3 + OH^- + H^+ \rightarrow 2OH^O + 4O_2$$

Ozone and hydroxyl radials are two of the strongest chemical oxidants known, with both compounds involved in the destruction of micro-organisms [69]. But ozone can easily diffuse through a microbial membrane into the cytoplasm of cells due to the

high oxidation power. Inactivation of microorganism by ozonation is mainly caused by the direct oxidation of dissolved ozone molecules [59].

Ozone disinfection produces less disinfection by-products which will enable these facilities to meet more stringent drinking water standards and regulations [70].

However, some of the major drawbacks associated with ozonation disinfection methods discussed as follows:

- ✓ No residual effect to control contamination of the water after the disinfection process has been completed.
- ✓ The ozone exposure required to inactivate these micro-organisms is quite high.
- ✓ The quality of the wastewater to be treated highly influences the efficiency of ozonation.
- ✓ Ozonation equipment is expensive.
- ✓ The process is highly dependent on pH.
- ✓ Ozone is highly unstable gas it cannot be stored in pressurized vessels and transported such as chlorine and it can lead to an explosion if the concentration above 23%.

ii) **Hydrogen peroxide (H_2O_2)**

Hydrogen peroxide (H_2O_2) is rarely used in drinking water treatment as a stand-alone treatment process. However, there are a number of technologies where H_2O_2 is used as part of the treatment methods. The advanced oxidation process (AOP) uses H_2O_2 in conjunction of O_3 and/or UV light to produce hydroxyl radicals ($\cdot OH$), which are very effective in removing taste and odor compounds, and inorganic and organic micro pollutants. H_2O_2 can also be catalyzed with iron, to produce hydroxyl radicals by Fenton's reaction.

The mechanism of H_2O_2 to kill vegetative bacteria involves in destroying molecules essential for normal metabolism (DNA, RNA, enzymes, and phospholipids) [55].

H_2O_2 is a weak mirobiocide compared to chlorine, ozone, and other commonly used disinfectants. Consequently, it is not approved by regulatory agencies as a stand-alone disinfection treatment process.

iii) **Ultrasonic**

Ultrasonic technology has been used as a non-chemical approach. Its disinfection power is related to the occurrence of cavitation phenomena. It consists of the production of micro-bubbles, which are generated when a great negative pressure is applied to a liquid. Compression and rarefaction waves rapidly move through the liquid media. If the waves are sufficiently intense they will break the attractive forces in the existing molecules and create gas bubbles. As ultrasound energy enters the liquid, the gas bubbles grow until they reach a critical size beyond which they either implode or collapse, thus releasing a great energy amount and promoting sonochemical reactions cause the formation of hydrogen atoms and hydroxyl radicals and the generation of shear and tensile stresses [71].

Micro-organisms may be inactivated by several mechanisms. First, cell membranes can be disrupted as a result of the stresses produced by implode or collapse of gas bubbles. Second, the combined effects of fluid shear, tensile stresses, and hydroxyl radicals may lead to the inactivation of micro-organisms [72].

Advantages and disadvantages of ultrasound-induced disinfection systems presented as follow: Advantages

- ✓ Simple, flexible design with low capital costs
- ✓ Easy upgrading of conventional treatment unit
- ✓ High efficiency of several bacteria inactivation

- ✓ Oxidation of natural organic matter and degradation of chemicals pollutants
- ✓ No production of conventional disinfection by-products (THMs,etc.)
- ✓ High synergy/improved efficiency in combination with conventional disinfection treatments (O_3; Cl_2; UV).

Disadvantages

- ✓ Design criteria still developing
- ✓ Increase of water turbidity
- ✓ Energy consumption
- ✓ Maintenance/replacement of ultrasound probe
- ✓ Lack of remaining disinfection capacity

iv) **Fenton Processes**

Fenton process is a strong oxidation system amongst advanced oxidation processes and has been successfully put into use for removal of recalcitrant organic contaminants as well as inactivation of pathogenic micro-organisms [73]. The mechanism of the Fenton reaction is the reaction between H_2O_2 and Fe^{2+} in an acidic aqueous medium (pH≤3) produces $HO^{\cdot}$ radicals and involves the following steps: pH adjustment to low acidic values, oxidation reaction, neutralization, and coagulation.

$$Fe^{3+} + H_2O_2 \rightarrow Fe^{2+} + OH + OH^{o}$$

A combination of hydrogen peroxide and UV radiation with Fe^{2+} or Fe^{3+} oxalate ion (photoFenton (PF) process) produces more hydroxyl radicals compared to conventional Fenton method or photolysis and in turn increases the rate of degradation of organic pollutants and disinfection capacity [18].

The microbial inactivation of Fenton process is due to hydroxyl radical attack of the cell membrane.

The primary advantage of Fenton and photo Fenton are the prevention of regrowth potential of the microbes [74].

The disadvantages of these processes are: (i) iron ions have to be separated from the system at the end of the process by precipitation, which is expensive in labor, reagents and time; (ii) it is limited by a narrow pH range (pH 2–3); and (iii) iron ions may be deactivated due to complexion with some iron complexing reagents such as phosphate anions and intermediate oxidation products [75].

v) **Heterogeneous photocatalysis**

Both conventional and some of AOPs technologies for microbial disinfection have limitations, such as, production of toxic by-products, generation of secondary pollution, or energy and labor intensiveness and so on. Among AOPs, heterogeneous photocatalysis has shown a great potential to solve these drawbacks as a low-cost, environmental friendly and sustainable treatment technology [76].

Photocatalysis is one of the very successful and active areas of research that have provided important ways to harvest readily available solar energy to destroy harmful organic contaminant as well as inactive photogenic micro-organisms [77], [78]. It is by far one of the most superior technology in the environmental purification because unlike many other technologies, photocatalysis does not serve as a mere phase transfer but completely degrades the organic pollutants by converting to innocuous substances such as CO_2 and H_2O [79].

Heterogeneous photocatalysis through illumination by UV or visible light on a semiconductor surface generates hydroxyl radicals [16]. The common photocatalysts are primarily metal oxides or sulphides, i.e., TiO_2, ZnO, ZrO_2, SnO_2, WO_3, CeO_2, Fe_2O_3, Al_2O_3, ZnS and CdS [80]. Among these metal oxides the most popular choices of photocatalysts are TiO_2 and ZnO. Both TiO_2 and ZnO has a wide difference in energy between the highest permitted energy level for the electron in the valence

band and the lowest permitted energy level in the conduction band (known as band gap). Because of these characteristics they can be used as photocatalysts under UV radiation [81].

TiO_2 has been exhaustively used in many applications, this is due to the fact that TiO_2 photocatalysis has a number of important features, and these are:

i. The catalyst is relatively inexpensive.
ii. It operates at ambient temperature.
iii. The by-products are usually harmLess to the environment.
iv. No other chemical reagent is needed.
v. Biological and chemical inertness and resistant to photo and chemical corrosion.
vi. Capable of repeated use without substantial loss of catalytic ability.
vii. Can inactivate bacteria, virus and protozoa

2.4. Titanium Dioxide (TiO_2)

Titanium dioxide belongs to the family of transition metal oxides. It is well known as a kind of n-type semiconductor material. It is the most active photocatalyst under the photon energy of $300nm < \lambda < 390nm$ and remains stable after the repeated catalytic cycles [17].

TiO_2 exists as three different polymorphs/ crystal phases; anatase, rutile and brookite (Figure 2.2). Among these three polymorphs, rutile is the most thermodynamically stable phase, whereas anatase and brookite are meta stable phases and easily transformed into rutile by thermal treatment [82]. In general anatase has superior photocatalytic properties and widely applied in different practical applications [83], [84]. Whereas, rutile is claimed as a catalytically inactive or much less active form [85]. Brookite generally does not show appreciable photocatalytic activity [86].

The minimum band gap energy required by these three polymorphs is 3.2 eV, 3.0 eV and 3.2 eV, for anatase, rutile and brookite, respectively.

Moreover, the most active commercially available anatase based photocatalyst is Degussa P-25 which is based on a mixture of 75 % anatase and 25 % rutile phases produced by Degussa Chemical Company (Germany) [87]. It is 99.5 % nonporous photocatalyst with Brunauer Emmett Teller (BET) surface area of 55 ± 15 m^2/g and crystallite sizes of 30 nm [88]. Degussa P-25 is standard photocatalyst in photocatalysis process having superior properties with higher photoactivity than pure TiO_2.

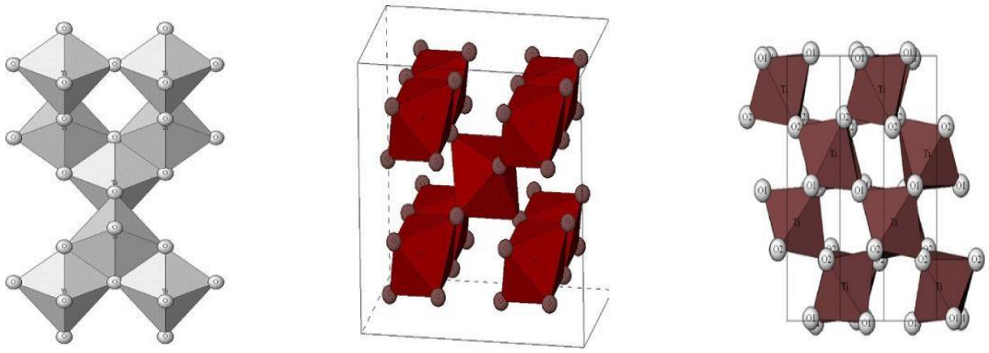

(a) Anatase *(b) Rutile* *(c)Brookite*

Figure 2. 2 The three polymorphs of titanium dioxide.

2.4.1. Application of TiO_2

TiO_2 an important material in many practical applications, and, in commercial products ranging from drugs to foods, cosmetics to catalysts, paints to pharmaceuticals, and sunscreens to solar cells in which TiO_2 is used as a desiccant, brightener, or reactive mediator [89].

Furthermore, various applications of TiO_2 photocatalyst had been investigated that include selective synthesis of organic compounds, phototreatment of pathogenic organisms, cancer treatment, self-cleaning and anti-fogging, air cleaning,

detoxification and remediation of water, mineralization of hazardous inorganic compounds, decontamination of soil and treatment of heavy metals [90].

2.4.2. Mechanism of TiO_2 photocatalysis

The basic mechanism of TiO_2 [v] photocatalysis involves three major steps: (i) light absorption and generation of electron-hole pairs; (ii) separation of charge carriers; and (iii) oxidation and reduction reactions at the surface of semiconductor [91](Figure 2.3). When titanium dioxide is irradiated with UV light with an energy (hv) equal or greater than the band gap electrons (e^-) are promoted from valence band (VB) to conduction band (CB) leaving holes (h^+) behind in aqueous solution. Simultaneously, a large percentage of excited-state electrons and holes can recombine due to electrostatic force of interaction and dissipate the input energy as heat [92]. This recombination of photogenerated electrons and holes is the reason behind the low photoactivity of TiO_2 [93].The conduction band electrons (e^-_{vb}) reduce dissolved oxygen present in the water to generate superoxide radical anion ($O_2^{\cdot -}$), and valence band holes (h^+_{vb}) oxidize water or hydroxide ions to produce the hydroxyl radicals [94]. The required energy that has to be supplied by the photons for the promotion of the electrons depends on the band gap for the specific material [95].

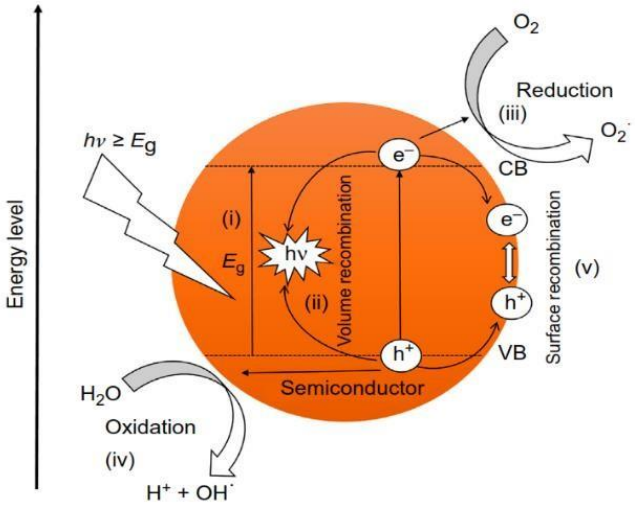

Figure 2. 3 Schematic of semiconductor nanoparticle and photocatalysis mechanism [91] .

The general TiO_2 photocatalysis mechanisms are summarized as follow.

$$TiO_2 + h_v \rightarrow h^+ + e^-$$

$$H_2O + h^+ \rightarrow \cdot OH + H^+$$

$$h^+ + OH^- \rightarrow \cdot OH$$

$$O_2 + e^- \rightarrow \cdot O_2^-$$

$$\cdot O_2^- + H^+ \rightarrow \cdot OOH$$

$$\cdot OOH \rightarrow O_2 + H_2O_2$$

$$H_2O_2 + \cdot O_{2-} \rightarrow \cdot OH + OH^- + O_2$$

$$H_2O_2 + h_v \rightarrow 2 \cdot OH$$

Oxidation of the organic pollutants via successive attack by ·OH radicals

$$\text{Pollutant} + \cdot OH \rightarrow \text{pollutant}^+$$

Or by direct reaction with holes

$$\text{Pollutant} + h^+ \rightarrow \text{degradation products}$$

For oxidation reactions to occur, the valance band must have a higher oxidation potential than the material under consideration.

It has been suggested that the hydroxyl radical (·OH) and superoxide radical anions ($\cdot O_2^-$) are the primary oxidizing species in the photocatalytic oxidation processes [96]. In comparison with other oxidant .OH (hydroxyl radical) has superior oxidation potential (Table 2.2).

Table 2. 2 Oxidation potentials of various oxidants [97].

Oxidants	Oxidation potential (V)
·OH (hydroxyl radical)	2.8
O_3 (ozone)	2.07
H_2O_2 (hydrogen peroxide)	1.77
ClO_2 (hypochlorous acid)	1.49
Cl (chlorine)	1.36

There are two main drawbacks in practical applications TiO_2 photocatalysis. The first drawback is that it is only be excited by ultraviolet (UV) light wavelength ($\lambda < 388$ nm) which only accounts for about 4% of the incoming solar energy on the Earth's surface and consequently its efficiency remains too low under natural sunlight [98]. The second drawback is associated with TiO_2 powder is the difficulty in recycling and reusing [99]. The first drawback can be improved by modification of the crystal structure of TiO_2 through doping with metals and nonmetals. And immobilization of the catalyst on certain supporting materials can also increase the recoverability of the catalyst for repeated usability.

2.4.3. Photocatalytic disinfection of TiO_2

There are many micro-organisms which could potentially contaminate a water source, including bacteria (*Legionella, Coliform Enter- obacteriaceae, Vibrio, Shigella, Helicobacter, Clostridium,* and *Salmonella*), protozoans (*Cryptosporidium* and *Giardia*), viruses and fecal matter, particularly human fecal matter [96].

Titanium dioxide in the anatase form appears to be the most photoactive and the most practical of the semiconductors for widespread environmental application such as water purification, waste water treatment, hazardous waste control, air purification, and water disinfection [100].

The photocatalytic reaction has been shown to be capable of killing a wide range of organisms, including gram-negative and gram-positive bacteria, fungi, algae, protozoa, viruses and bacteriophages [101]. The biocidal action of the TiO_2 photocatalyst has been frequently ascribed to two major photochemical oxidants: OH radical and reactive oxygen species (ROS) [102]. Generation of hydroxyl radicals through the partial oxidation of water is sufficient to kill micro- organisms such as bacteria, destroy viruses, and remove alternative organic contaminants from water and associated cathodic reaction leads to the formation of superoxide species, which also exhibit a strong oxidation power [96].

For photocatalytic disinfection to occur, microbes must be in close proximity or make contact with the surface of the semiconductor to allow for the exchange of electrons and subsequent chemical reactions [103].

The mechanism of bactericidal action of TiO_2 photocatalysis, is attributed to the combination of cell membrane damage due to ROS attack of extra-cellular components (e.g. peptidoglycan, polysaccharides and phospholipid) and further oxidative attack of internal cellular components (e.g. enzymes, coenzymes and nucleic acid), ultimately resulting in cell death [104], [105]. It also further elucidated as cumulative damage leads to the cell membrane disorder, increasing its permeability, demonstrated by the leakage of potassium ions , and finally the cell lysis and death [106].

To date, the most convincing research suggests that the critical targets of ROS attack are polyunsaturated fatty acids and that the resulting lipid peroxidation is the key factor in the bactericidal effect [101]. The process of lipid peroxidation is shown in Figure 2.4. Lipid peroxidation is a complex process known to occur in both plants and animals. It involves the formation and propagation of lipid radicals, the uptake of oxygen, a rearrangement of the double bonds in unsaturated lipids and the eventual destruction of membrane lipids, with the production of a variety of breakdown products, including alcohols, ketones, alkanes, aldehydes and ethers [17]. This radical chain reaction leads to the oxidation of biomolecules significantly distant from the initial site of the ROS attack [107].

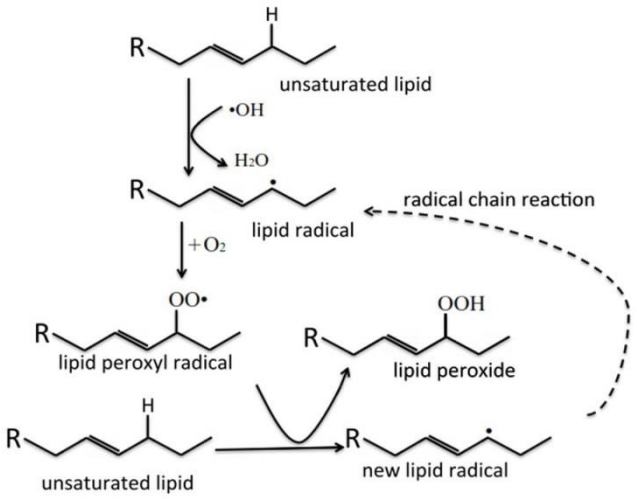

Figure 2. 4 Schematic of lipid peroxidation [107].

.

2.4.4. Immobilization of Titanium Dioxide

Photocatalytic reactors can utilize TiO_2 in the form of aqueous suspension or immobilized on a solid substrate [108]. In conventional process of wastewater treatment, TiO_2 nanoparticles are generally used as a slurry system due to the large surface area of catalysts available for better mass transfer and high photocatalytic efficiency [109].

Nevertheless, the filtration to eliminate and recycle the powdered TiO_2 suspended in the treated water increases running cost, and induces the secondary pollution, which has become a main limiting factor for practical application [110]. Besides, the TiO_2 nanoparticles tend to aggregates and suspensions are difficult to apply to continuous flow systems. In order to overcome this disadvantage and allow a continuous operation, immobilization of the catalyst through coating on other supporting materials has been adopted [17], [111]. Consequently, it could help to eliminate the costly phase separation processes and to promote the practicality of such catalysts as an industrial process [112]. The advantages of immobilization system are also

including superior adsorption properties and increased surface hydroxyl groups or reduced charge recombination [113].

As disadvantage, the immobilized photocatalysts usually show lower activities when compared with powder TiO_2, mainly due to the decrease in the interphase surface available and the increase in the restrictions to the mass transfer. Moreover, the immobilization procedure must guarantee the long-term stability of the TiO_2, avoiding the possible leaching of TiO_2 particles to the solution, and must permit the regeneration of the catalyst in case of deactivation [31].

Apart from immobilization techniques pelletized form of TiO_2 can also be used to eliminate post- treatment catalyst recovering problem. But Pelletized TiO_2 has been known to 'crumble' due to mechanical abrasion, which again raises filtration problems [33].

Immobilization and the support material influences the photocatalyst activity [114]. In order to have high photocatalytic efficiency the support should have the following characteristics [115] (a) transparent to irradiation; (b) strong surface bonding with the TiO_2 catalyst without negatively affecting the reactivity; (c) high specific surface area; (d) good absorption capability for organic compounds; (e) separability; (f) facilitating mass transfer processes and (g) chemical inert.The strong interactions between substrates and TiO_2 nanoparticles are always required to avoid the loss of TiO_2 nanoparticles during the long-term process of recycling, this strong interaction is achieved through physical adsorption, electrostatic interaction, hydrogen bonding interaction and chemical bonding interaction [110].

Many techniques have been developed for immobilization of TiO_2 catalysts onto a solid substrate, this includes, dip-coating from suspension, spray coating, sputtering, sol-gel related methods, thermal treatment, chemical vapor deposition (CVD) and electrophoretic deposition. Among these techniques, dip-coating method has several

advantages. Some of the advantages include the methods can be applied for a range of coating thickness with reasonable coating quality, the coating equipment is inexpensive and relatively simple to operate, and high-speed capability of the process should lead to low costs and high productivity.

i) Dip-coating Method

Dip coating is the precision controlled immersion and withdrawal of any substrate into a reservoir of liquid for the purpose of depositing a layer of material. Coating thickness generally increases with faster withdrawal speed. The method is used to make thin films with the sol-gel technique.

The thickness is determined by the balance of forces at the stagnation point on the liquid surface. A faster withdrawal speed pulls more fluid up onto the surface of the substrate before it has time to flow back down into the solution. The thickness is primarily affected by fluid viscosity, fluid density, and surface tension.

The applied coating may remain wet for several minutes until the solvent evaporates. This process can be accelerated by heated drying. In addition, the coating may be cured by a variety of means including conventional thermal, ultra violet (UV), or infra-red (IR) techniques depending on the coating solution formulation. Once a layer is cured, another layer may be applied on top of it with another dip-coating / curing process. In this way, a multi-layer stack is constructed.

In general, TiO_2 immobilization with sol-gel and dip-coating methods consists of 3 steps:

1. Preparation of the suspension (sol-gel)
2. Coating of the substrate via dip-coating method
3. Sintering: thermal treatment of the coated substrate at high temperature.

Different types of substrates have been tested for immobilizing TiO_2, some of the materials are glass beads [116], glass tubes [32], fiberglass [34], woven mesh [117], steel mesh [118], quartz [119], stainless steel [109], and many types of plastics [120] and ceramics [121] ,alumina [112] and silica [122].

For glass-supported TiO_2 catalysts, it has been reported that oxygen bridges are formed between OH groups bound to the TiO_2 catalyst surface and the supporting glass plate during thermal treatment, and these strengthen the adherence of the catalysts to the glass plate. Therefore, a mechanically stable coating should be expected from a properly coated TiO_2 layer on glass plates [123]. Furthermore, affordability, recyclable and contain silicon dioxide is a good adsorbent are additional benefits.

2.4.5. Doping of Titanium Dioxide (TiO_2)

Doping is the process the addition of a small percentage of foreign atoms as an impurity in the regular crystal lattice of the semiconductor materials in a controllable manner in order to define the electrical properties. These impurity atoms are known as dopants. The impurities are dependent upon the type of semiconductor. Lightly and moderately doped semiconductors are referred to as *extrinsic*. A semiconductor doped to such high levels that it acts more like a conductor than a semiconductor is referred to as *degenerate*.

Basic conditions that are required for the doping process are:

- ✓ The atom which is to be doped in the crystal must be placed at the position same as that of the position of the semiconductor atom.
- ✓ There should be no distortion in the crystal after the insertion of the dopants.
- ✓ The size of the dopants should be exactly same as that of the size of the atom of the crystal.

- ✓ In a crystal, the percentage of doping should not be more than one percent

Developing an efficient sunlight-sensitive TiO_2 by narrowing its band gap is an important challenge [124]. There are many techniques to improve photoactivity of TiO_2 such as control of phase morphology, crystallite size, and reducing band gap energy [125].

In order to improve its adsorption capacity, and interfacial charge transfer rate as well as the response into the visible spectrum of solar light, TiO_2 has been doped with certain transition metals, non-metals and ionic components [88], [126].

i) TiO_2 Doping Mechanisms

In doping process, modifications can be effected either in bulk by doping metals/non-metals or on the surface of TiO_2 by anchoring colored inorganic semiconductors or organic dyes, where they act as sensitizers [127]. Surface modification using appropriate element dopant could reduce the recombination rate of electron-hole pairs and increase the photocatalytic efficiency [128]. There are three different main opinions regarding modification mechanism of TiO_2 doped with nonmetals. (1) Band gap narrowing; (2) Impurity energy levels; and (3) Oxygen vacancies [92].

Nonmetals such as C, S, F and N are effectively applied in the synthesis of visible light active TiO_2 catalyst via band gap narrowing [129], [130]. It is believed that when non-metallic elements are doped into the TiO_2 anatase lattice they forms a donor state just above the top of the valence band and this process leads to the narrowing of the band gap of TiO_2 and the creation of oxygen vacancy, both of which enhance visible light absorbance (hv_3) Figure 2.5 [98]. On the other hand, theoretical calculations showed that the p-orbitals of these dopants significantly overlapped with the valence band O 2p orbitals, which facilitated the transport of photo-generated charge carriers to the surface of the catalyst [131].

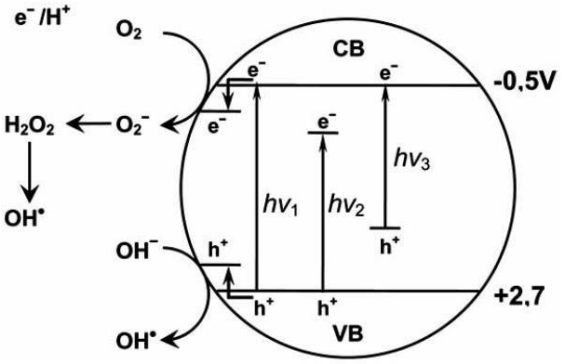

Figure 2. 5 . Mechanism of TiO_2 photocatalysis: hv1: pure TiO_2; hv2 metal-doped TiO_2 and hv3: nonmetal-doped TiO_2 [70].

In band gap narrowing process, the anodic shift of the quasi-Fermi potential, the visible-light absorption, and the transfer of photoexcited carriers to the reactive sites at the catalyst surface have been noticed as a result of non-metal anion doping affecting its visible-light activity [132].

The visible light photoactivity of metal-doped TiO_2 can be explained by a new energy level produced in the band gap of TiO_2 by the dispersion of metal nanoparticles in the TiO_2 matrix. Electron can be excited from the defect state to the TiO_2 conduction band by photon with energy equals hv_2 (Figure 2.5).

In the case of noble metals (such as, Ru^{3+} and $V4^{+}$), when a small amount of a noble metal is doped into the TiO_2, the electrons and holes produced by the light irradiation are retained on the noble metal and TiO_2 semiconductor, respectively because the noble metal trap the electrons, which limit the recombination of the electrons and photo holes, and thus improve the reactivity of the photo catalyst [17]. In general photocatalytic activity of TiO_2 is related to many factors such as the method of preparation, amount and type of dopant, crystalline structure, surface properties, surface area, density of surface OH^- group, and parameters of post process treatment (e.g., temperature of annealing) [133]. Many producing methods were proposed to dope

(or incorporate) trace impurity in TiO_2 including: ion-assisted sputtering, plasma, ion-implantation, chemical vapor deposition (CVD) and sol-gel [92].

2.4.6. Nitrogen-doped TiO_2 and its techniques

Titanium dioxide (TiO_2) is one of the most promising semiconductor materials which have attracted a lot of attention because of its successful application in different areas as a heterogeneous photocatalyst. Some of the main application areas include degradation of organic pollutants [22], inactivation of pathogenic microorganisms from water and air [134], and degradation of dyes [135], [136]. Relative inexpensiveness, high efficiency, environmentally friendliness, chemical and biological stabilities are its unique advantages [137], [138]. Most importantly, it can be used repeatedly with its catalytic capability for a long period of time [105]. However, its main drawback is that it is only activated by ultraviolet (UV) light, which accounts for 4-5 % of the solar energy that reaches the earth's surface due to its wide band-gap energy (3.2 eV) [139].

So far, considerable efforts that have been done to reduce its band-gap energy and utilize the visible-light which is the larger portion of the solar spectrum. One of the major approaches in this regard is doping, a modification of TiO_2 by influencing the electron structure with metal and non-metal ions [134], [140]. In comparison with the metal dopants, nonmetals such as C, S, F and N are effectively applied in the synthesis of visible light active TiO_2 catalyst via band gap narrowing [129], [130]. After Asahi et al. [141],who first, introduced successful doping of nitrogen and prepared a visible light active TiO_2 in the wavelength range of less than 500 nm, nitrogen atom has been widely investigated [130], [140]. This is because nitrogen can be easily introduced into the titanium structure as it has comparable atomic size and ionization energy [142].

Inorganic and organic nitrogen dopants (such as aqueous ammonia, urea, ammonium chloride, triethylamine, and diethylamine) are widely used in the synthesis of

nitrogen-doped TiO_2 [143]. The ammonia nitrogen dopant was more efficient than other dopant [144].

Various methods have been reported for the nitrogen doping of TiO_2. The methods are generally classified into three ways: (1) sputtering and implantation techniques, which were mainly used to prepare single crystalline or polycrystalline nitrogen-doped TiO_2 thin films; (2) sintering TiO_2 at high temperatures under a nitrogen containing atmosphere; and (3) wet methods, which involved sol-gel and solvothermal methods [144]. The wet method has been one the most successful method in the preparation of nitrogen doped TiO_2 nanomaterial, because of its convenient control of titanium sources, the nitrogen doping amount, the hydrolysis condition, pH solvent solution, and solvent systems [145]. In addition, simple variation in experimental conditions can lead to the required particle size and crystal structure.

Solvothermal synthesis generally refers to a reaction occurring in the presence of any kind of solvent in a sealed system (e.g. in an autoclave) with the temperature raised above the boiling point of the solvent.

Compared to other techniques, the sol-gel method has several additional advantages. These include the possibility of making deposits on complex-shaped substrates, inexpensive start-up materials, and simple equipment [146]. Therefore, wet method using sol-gel technique is the first choice to determine suitable nitrogen dopant, and it is simple nitrogen doping method for better photocatalytic efficiency.

i) Sol-gel method

The sol-gel process is a wet-chemical method widely employed recently in the fields of materials science and ceramic engineering [147]. It involves the evolution of inorganic networks through the formation of a colloidal suspension (sol) and gelation of the sol to form a network in a continuous liquid phase (gel). The precursors for synthesizing these colloids consist usually of a metal or metalloid element

surrounded by various reactive ligands. The starting material is processed to form a dispersible oxide and forms a sol in contact with water or dilute acid. Removal of the liquid from the sol yields the gel, and the sol/gel transition controls the particle size and shape. Calcination of the gel produces the oxide.

A sol is a stable dispersion of colloidal particles or polymers in a solvent. The particles may be amorphous or crystalline. An aerosol consists of particles in a gas phase, while a sol consists of particles in a liquid.

A gel consists of a three-dimensional continuous network, which encloses a liquid phase in a colloidal gel, the network is built from agglomeration of colloidal particles. In a polymer gel the particles have a polymeric sub-structure made up of aggregates of sub-colloidal particles. Generally, the sol particles may interact by van der Waals forces or hydrogen bonds. A gel may also be formed from linking polymer chains. In most gel systems used for materials synthesis, the interactions are of a covalent nature and the gel process is irreversible. The gelation process may be reversible if other interactions are involved. The idea behind sol-gel synthesis is to "dissolve" the compound in a liquid in order to bring it back as a solid in a controlled manner. Multi component compounds may be prepared with a controlled stoichiometry by mixing sols of different compounds. The sol-gel method prevents problems of co-precipitation, which may cause inhomogeneity and enables mixing at an atomic level and results in small particles, which are easy to sinter.

Removal of the remaining liquid (solvent) phase requires a drying process, which is typically accompanied by a significant amount of shrinkage and densification. The rate at which the solvent can be removed is ultimately determined by the distribution of porosity in the gel. The ultimate microstructure of the final component will be strongly influenced by changes imposed upon the structural template during this phase of processing. Afterwards, a thermal treatment, or a firing process, is also necessary in order to favor further poly-condensation and to enhance the mechanical

properties and structural stability via final sintering, densification, and grain growth. One of the distinct advantages of this methodology, as opposed to the more traditional processing techniques, is that densification is often achieved at much lower temperatures.

2.4.7. Nitrogen-doped titanium dioxide as drinking water disinfectant

There are a number of applications of nitrogen-doped titanium dioxide photocatalyst in water and waste water treatment is presented by different authors in most previous research works. However, the application this photocatalyst is limited to degradation of organic pollutants from wastewater. Nitrogen-doped photocatalyst based antimicrobial disinfectant technologies are still in the developmental stage.

This section discusses some of the previous works on application of nitrogen-doped photocatalyst in microbial inactivation process.

Wong *et al*. [148] have investigated the antibacterial activity of photocatalytic titanium dioxide as a pure, nitrogen- and carbon-doped TiO_2 substrates. According to their study, nitrogen-doped TiO_2 substrates have shown superior visible-light-induced bactericidal activity against *Escherichia coli* compared to pure TiO_2 and carbon-doped TiO_2 substrates. In this pathogen- killing experiment, a significantly higher proportion of all tested pathogens, including *Shigella flexneri*, *Listeria monocytogenes*, *Vibrio parahaemolyticus*, *Staphylococcus aureus*, *Streptococcus pyogenes*, and *Acinetobacter baumannii*, were killed by visible-light-illuminated nitrogen-doped TiO_2 substrates than by pure TiO_2 substrates. They achieved 90% reduction in the *E. coli* population using an incandescent light and nitrogen-doped TiO_2.

Wu *et al*. [149] have also studied the modified metal-ion and non-metal co-doped TiO_2 (palladium- modified nitrogen-doped titanium dioxide (PdO/TiON)) effect on selected gram-negative bacteria (*E. coli*). The authors shown that, PdO/TiON treatment

resulted in *E. coli* survival ratio of ~80% after 5-min treatment, and ~10% survival ratio upon 30 min irradiation from initial ~10^7 cfu/mL cell population. 10^{-4} surviving at 1-h irradiation, and <10^{-8} survival ratio upon 90 min treatment which indicates a complete killing. They have also stated photocatalysis oxidative damages on the cell membrane.

Le *et al.* [150] have tested the nitrogen-doped titanium dioxide for air cleaning and disinfecting. The preparation parameters and their impact on the material's structure were carried out by multiple techniques: thermogravimetric and differential scanning calorimetric analysis, x-ray diffraction, scanning electron microscope, transmission electron microscopy, energy dispersive x-ray spectroscopy and UV–Vis diffuse reflectance spectrophotometry showed that the nitrogen- doped TiO_2 calcined at 500 ◦C for 3 h exhibited a spherical form with a particle size about 15–20nm and crystal phase presented a mixture of 89.12% anatase. They have prepared air photocatalytic cleaner by depositing nitrogen-doped TiO_2 on a porous quartz tube (D =74mm; l=418mm). The created air cleaner was able to remove 98.5% of bacteria (total aerobic bacteria and fungi, 300 cfu/m^3) within 120 min.

Ledezma *et al.* [151] have also investigated the inactivation kinetics of *Escherichia coli* using a solar photocatalytic process that employs nitrogen-doped titanium dioxide with respect to selected variables: radiation type (UV+ visible and visible), catalyst concentration (0.0, 0.10, 0.25 and 0.5 mg mL–1) and pH (6.0, 6.5, 7.0, 7.5. 8.0 and 8.5). Inactivation process exhibited a clear dependence on radiation type, pH value, and catalyst concentration. In their first experiment, they have tested inactivation of *E. coli* using nitrogen-doped TiO_2 at different catalyst concentration (e.g., 0.00, 0.10, 0.25 and 0.50 mg L−1 and complete (UV + visible) solar radiation at pH = 7.0. At this pH bacteria were capable to show higher resistance to the photocatalytic inactivation than the rest of the pH values tested. They have also compared the inactivation process with and without nitrogen-doped titanium dioxide.

According to their report inactivation process considerable improved by adding 0.10 mg m/L of nitrogen-doped titanium dioxide.

2.5. Types of photoreactor system configuration

Different researchers have been applied TiO_2 photocatalyst for degradation of many hazardous organic compounds as well as inactivation of pathogenic microorganisms. So far, this photocatalyst have been utilized either in the form of suspended powder or immobilizing in other support material [109]. The selection of appropriate types of photoreactor system configuration in terms of total irradiated surface area of catalyst per unit volume, reaction kinetics and light distribution within the reactor for activation of the catalysts are the most important factors [17], [33]. In this regard, suspended type photoreactor offer relatively high surface area for better mass transfer [109]. However, the difficulty in downstream catalyst separation and higher recovery cost are the main drawbacks on this type photoreactor in practical applications [114], [152]. Immobilization of the catalyst through coating in other supporting materials overcome this disadvantaged and permits a continuous operation [17], [111].

Several immobilized type photoreactor design have been proposed in different applications, this includes rotating corrugated drum reactor [30], fixed-bed reactor [31], tubular photoreactor [32], multi tubular photoreactor [33], hollow sphere in a Vis-LED photoreactor [153]. However, most of them have applied in degradation of hazardous organic compounds and there is only limited type photoreactors have proposed for application of pathogenic microorganism inactivation.

Some of previous works regard to microbial disinfection photoreactor systems are presented as follow.

Acevedo *et al.* [154] have investigated the disinfection of natural water using TiO_2 as the fixed catalyst incorporated in a homemade photoreactor. The catalyst was

immobilized on the external surface of a cylinder of frosted glass situated in the longitudinal axis of a tubular glass reactor (Figure 2.6). Two alternative methods of immobilizing the catalyst on glass were studied: in the first, a commercial titanium oxide powder (Aeroxide TiO_2 P25) was mounted on a polymeric support; and in the second, it was applied by sol-gel deposition. Illumination was effected by installing the glass reactor in the irradiation chamber of a solar simulator. The authors investigate this work under laboratory conditions, groundwater contaminated with cultured and wild bacteria was treated photocatalytically, and the influence of the photolysis, the pumping, and the catalyst was studied.

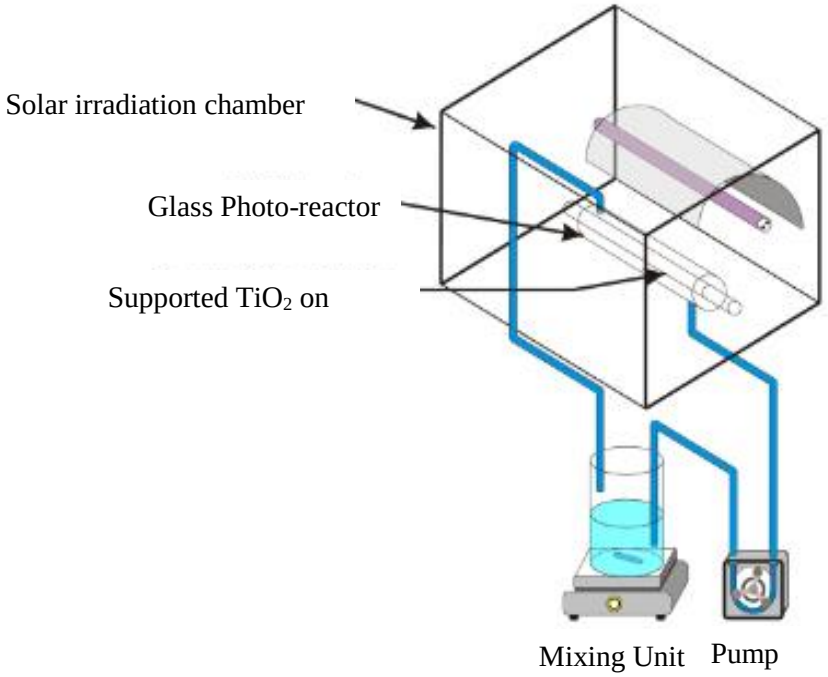

Figure 2. 6 Experimental device employed in the disinfection [154].

The results obtained have demonstrated that the catalyst immobilized in the interior of the photoreactor presents similar results, in the disinfection of *E.coli*, as 0.5 g/l of TiO_2 P25; and that, in 1.5 h approximately of simulated solar illumination (167 kW_{UVA} s/m^2) on the sol-gel deposit of TiO_2, it is possible to eliminate 100% of the

bacteria covered by international regulations in respect of water for human consumption. With regard to the aging assay of the system, they are observed at 250 h of operation a reduction in the effectiveness of the disinfection process. At 0 and 250 h of operation, the percentages of elimination of *E. coli* after 50 min of illumination were 100% and 99.5%, respectively. They have concluded that the reduction in the effectiveness of the process was due to the formation of a film of calcium carbonate adhering to the internal glass wall of the photoreactor, which is in contact with the liquid being treated, and to the presence of calcium carbonate precipitates on catalyst surface.

Belapurkar *et al.* [155] have studied two photoreactor configuration on bactericidal effect using with *Escherichia coli*. They have designed and prepared the two reactors through immobilizing highly porous TiO_2 photocatalysts supported glass tube and a stainless-steel plate (23cm x 28cm) and configured placed in a plastic tray (23cm x 28cm). The reactor was covered with 5 mm thick glass plate and has used 350 nm light and solar light (Figure 2.7). They have also includes quartz cell having 2.5 cm internal diameter and 35 cm in length their study to uses as photoreactor.

According to their result *E. coli* concentration decreased to a safe level from initial concentration of 500–100,000 bacteria/mL during 4 h of photolysis using 350 nm light and solar light. They have also observed that the time required for disinfection of water was found to increase with increase in the concentration of bacteria.

They have also tried to analyze the effect of inorganic impurities (1 wt% NaCl) and organic impurities (10 ppm nutrient agar) on the performance of the photoreactor. They have observed, the efficiency of the reactor decreased by 40% for the case of organic impurities. But the inorganic impurities have not any adverse effect on bactericidal activity.

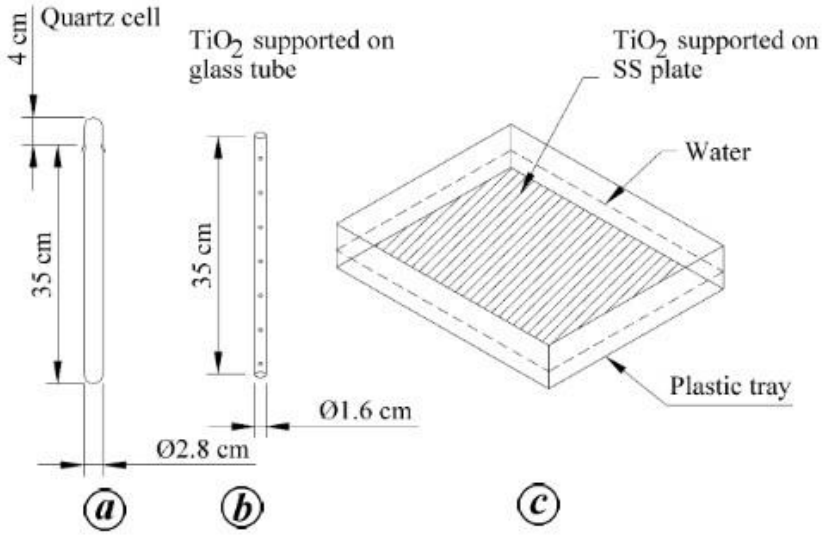

Figure 2. 7 Schematic diagram of quartz cell (a), TiO_2 photocatalyst supported on a glass tube (b) and TiO_2 photocatalyst supported on a stainless steel plate kept in a plastic tray (c) [155].

The system was found to be effective when 1 litter of water was photolysed by solar light in a plastic tray containing TiO_2 photocatalyst coated on a stainless plate. They have also indicated that the technique can be used for disinfection of approximately 20 litter of water daily using solar light.

Guimarães and Barretto [156] has proposed a cylindrical reactor impregnated with titanium dioxide and irradiated with ultraviolet light (15 W). The reactor was constructed with a borosilicate glass cylinder with an internal diameter of 3.8 cm and a length of 42.5 cm. A germicide lamp (15 W, λmax = 254 nm) was fixed at the centre of the reactor. The inside of the reactor had a working volume of 273 mL. The photoreactors were operated in a one-way ascending passage mode. The photocatalytic reactor was internally coated with a fixed bed of TiO_2 (Degussa P-25, $30 m^2/g$, mainly anatase). The TiO_2 catalyst in its immobilized form was supported on the inner surface of the glass cylinder (Figure 2.8).

They have examined the photocatalytic inactivation of two groups of micro-organisms: spores of the anaerobic bacterium *Clostridium perfringens* and *coliphage*.

Parameters such as color, turbidity, hydraulic detention time (HDT) and initial concentration of micro-organisms were evaluated in relation to the efficiency of the inactivation process. They have reported 98% reduction in number of *C. perfringens* after an irradiation time of 152 seconds, independent of color and turbidity. For solutions with low turbidity efficiency of the coliphage inactivation reached approximately 100% between 89 and 104 HDT, while this value was 98% for solutions with higher turbidity.

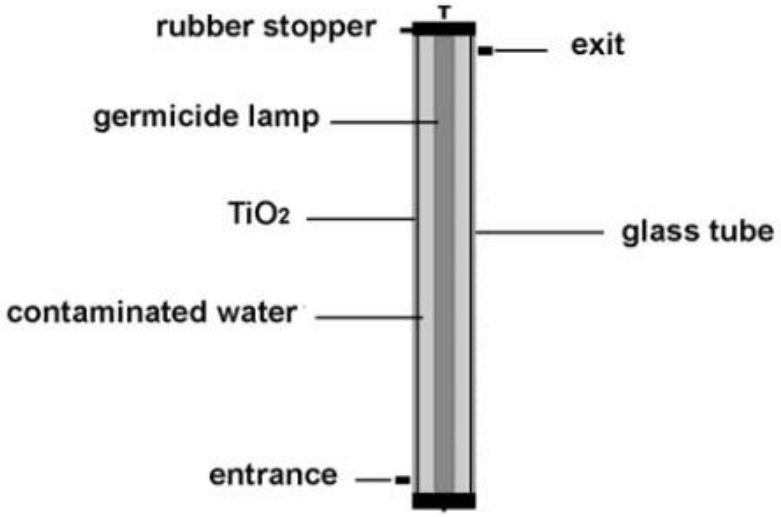

Figure 2. 8 Photocatalytic Reactor Design [156].

Chai *et al.* [157] have evaluated the photocatalytic disinfection of *E. coli* in a suspended TiO_2/UV reactor. They have used P-25 TiO_2 photocatalyst in a batch-type slurry reactor. A 100 W high- pressure mercury lamp was used as a UV light source (Figure 2.9). In order to investigate the effect of UV intensity on the disinfection capabilities, UV was irradiated onto the cell suspensions including *E.coli* in a 1-litter slurry reactor at 10, 20, 30, 40, 50, and 70 W /m^2. They have reported the 100% reduction lime at a UV intensity of 10W/m^2 with 0.1 g TiO_2 process takes only 8 min, while the time at 10 W/m^2 without TiO_2 existence takes 220 min. This indicates that disinfection capability in the aspect of time using both TiO_2 and UV light was more than 27 times as that by using only the UV light. They have achieved 100 % disinfection efficiency

at optimum values of 0.1 g/l titanium dioxide concentration, 50 W/m^2 UV light intensity and 2-3 min contact time.

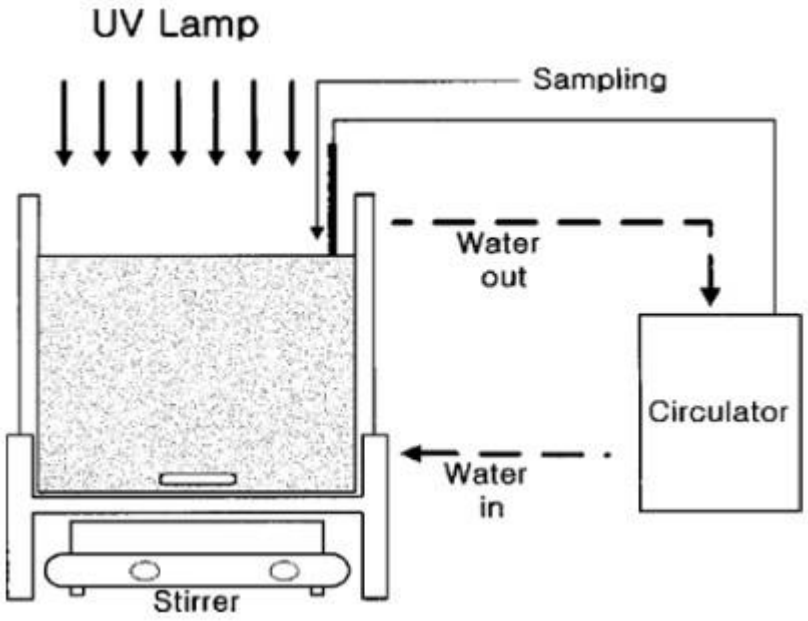

Figure 2. 9 Schematic diagram of a suspended TiO_2/UV reactor [157].

In this reactor configuration, the authors have raised the need of downstream separation process as main disadvantages.

2.6. Factors affecting the photoreactor

After the integration of the semiconductor catalyst with a photoreactor, the oxidation rates and efficiency of the photocatalytic system are highly dependent on a number of the operation parameters that govern the kinetics of photo- mineralization and photo-disinfection. This section will discuss the significance of each operation parameters on the inactivation performance of the photoreactor system.

2.6.1. TiO_2 concentration

Concentration of TiO_2 in the photocatalytic water treatment system affects the overall photocatalysis reaction rate in a true heterogeneous catalytic regime, where

the amount of TiO_2 is directly proportional to the overall photocatalytic reaction rate [158]. A linear dependency holds until certain extent when the reaction rate starts to aggravate and becomes independent of TiO2 concentration [159]. This is attributed to the geometry and working conditions of the photoreactor where the surface reaction is initiated upon light photon absorption [160]. When the amount of TiO_2 increases above a saturation level (leading to a high turbidity state), the light photon absorption coefficient usually decreases radially [17]. Other factors that contribute to the rate independence of TiO: concentration include the reactor configuration and the light reflection [157]. Generally, an optimum amount of TiO_2 is mainly depend on geometrical dimension of the reactor.

2.6.2. pH

In heterogeneous photocatalytic water systems, pH is one of the most important factors that affect the charge on the catalyst particles, size of catalyst aggregates and the positions of conductance and valence bands. The metal such as TiO_2 are presumed to have a tendency of changing their surface charge by a pH variation and their photocatalytic reactivities change at the same time [161]. Moreover, the pH of the solution affects the formation of hydroxyl radicals by the reaction between hydroxide ions and photo-induced holes on the TiO_2 surface [19]. The positive holes were considered as the major oxidation species at low pH whereas hydroxyl radicals were considered as the predominant species at neutral or higher pH levels [162]. Any variation in the operating pH is known to affect the isoelectric point or the surface charge of the photocatalyst used [17]. The point of zero charge (PZC) is a condition where the surface charge of TiO_2 is zero or neutral that lies in the pH range of 4.5-7.0.

Different pH will affect the surface charge density of the TiO_2 catalyst according to the following water equilibrium equations [163];

$$\text{At pH} < \text{PZC:} TiOH + H^+ \leftrightarrow TiOH_2^+$$

At pH > PZC:$TiOH + OH^- \leftrightarrow TiO^- + H_2O$

The surface charge density distribution for these TiO_2 catalyst clusters is highly dependent on the operating pH. It was reported that the distribution of TiOH is ≥ 80% at 3 < pH < 10; TiO^- ≥ 20% at pH > 10 and $TiOH_2^+$ ≥ 20% at pH < 3. The equilibrium constants for these reactions at different pH are pH $_{TiOH2}{}^+$ = 2.4 and pK $_{TiOH}$ = 8.0 [164].

During photocatalytic reaction, the initial operating pH usually drops slightly from the formation of multitude intermediate by-products that may possess different chemical functional groups that affect the water pH [17].

A similar electrostatic interaction enhancement for photo-disinfection of micro-organisms was observed during the photocatalytic process. At increased density of d $TiOH_2^+$ (low pH) the catalyst can form electrostatic links with the bacteria through their negatively charged surfaces, resulting in increasing rates of photo-disinfection. Herrera Melián et al. [165] observed that the bacterial inactivation rate was enhanced at pH 5.0. It should be noted that the enhanced bactericidal activity of TiO_2 at a low pH is due solely to the TiO2 mediated photo-killing and not acidification of the cell.

2.6.3. Temperature

For photo-disinfection using TiO_2 photocatalysis, the increase in reaction temperature will increase the inactivation rate of micro-organisms [163]. This is consistent with the Van't Hoff-Arrhenius equation below, where the rate constant k is linearly proportional to the exponential (-1/T);

$$\ln (k_1/k_2) = - (E_a/R) ((1/T_2) - (1/T_1)$$

In which k_1 and k_2 are the constants for temperatures T_1 and T_2, E is the energy of activation and R is the universal gas constant. The sensitivity of a microbe to the catalyst activity depends on its incubation temperature, type and resistance of the

microorganism to temperature change. The order of resistance of micro-organisms to conventional disinfection treatment is: Non-spore forming bacteria < Viruses < Spore forming bacteria < Helminths < Protozoa (oocysts). To date, there is no comprehensive study conducted to compare the effect of TiO_2 photo-disinfection of each microorganism type under different operating temperatures. However, some studies show that the gram-positive bacteria (such as enterococci), increasing the temperature from 23 to 45 ^oC photocatalytic disinfection rate, whereas for gram-negative bacteria, the resistance to the photocatalytic treatment is enhanced by heating. The opposite response of gram negative bacteria is mainly due to morphological difference from gram-positive bacteria leading to a difference in resistance to photocatalytic treatment [163]. Catalyst is usually conducted below temperature of 80^oC. Thus, the photo-disinfection using TiO_2 to prevent high water heating costs (high heat capacity) [166].

2.6.4. Dissolved oxygen (DO)

Since oxygen serves as a trap for the photogenerated electrons, thus inhibiting the recombination of the electron/hole pair, the concentration of dissolved molecular oxygen also affects the photocatalytic efficiency [167]. The oxygen does not affect the adsorption onto the TiO_2 catalyst surface as the reduction reaction takes place at a different location from where oxidation occurs [168]. Other roles for (DO) may involve the formation of other ROS and the stabilization of radical intermediates, mineralization and direct photocatalytic reactions. The total amount of DO in a reactor depends on a few technical considerations. For a photoreactor, the total delivered DO not only acts as an electron sink but also provides sufficient buoyant force for complete suspension of TiO_2 particles. Photoreactor sparging with pure oxygen in TiO_2 slurry reactor is usually a cost-ineffective solution, as the amount of DO being held-up is a function of the photoreactor geometry [160].

To date, the effect of DO on the efficiency of photo-disinfection rate has been paid little attention. The formation of various ROS under the series of redox reactions on the catalysts surface was assumed to be similar in both photomineralization and photo-disinfection reaction. If sufficient nutrients are available, the constant sparging of DO will generally promote microbial growth and offset the photo-disinfection rate [17]. This indirectly prolongs the irradiation time necessary to achieve the desired inactivation level. It is thus, recommended that the effect of DO on microbial inactivation should be investigated thoroughly in a particular photoreactor system before improvising DO sparging strategy.

2.6.5. Light intensity

Light intensity determines the extent of light absorption by the semiconductor catalyst at a given wavelength. The overall pollutant conversion and degradation efficiency of a given photoreactor relies on this factor [19]. Photocatalytic reaction rate increases with increase in light intensity. However, the initiation of TiO_2 photocatalysis reaction rates is not highly dependent on light intensity, where a few photons of energy (i.e. as low as 1 $\mu W\ cm^{-1}$) can sufficiently induce the surface reaction [169]. To achieve a high photocatalytic reaction rate, particularly in water treatment, a relatively high light intensity is required to adequately provide each TiO_2 surface active sites with sufficient photons energy required [17]. In other word, higher light intensity provides higher energy for more TiO_2 nanoparticles to produce electron–hole pairs [170].

Zhang et al. [171] have demonstrated the effects of varying the light intensity on the photocatalytic inactivation of *E. coli*. The result shown the rate of cell inactivation increases with increases in the incident light intensity. This is due to a higher light intensity produces a higher concentration of active oxygen species such as $OH\cdot$ and results in improved photocatalytic disinfection.

2.6.6. Contaminant loading

As TiO_2 photocatalytic reaction is surface contact dependent, it is dependent on initial contaminant load. Under similar operating conditions, a variation in the initial concentration of the water contaminants will result in different irradiation time necessary to achieve complete mineralization or disinfection [17]. In addition, at excessive higher concentration of organic load the TiO_2 surface became saturate as result the photocatalyst deactivate [172]. In the case of photocatalytic disinfection, some of researchers indicated that photocatalytic efficiency decrease with a lower initial concentration of bacteria. The explanation of this process is based on direct contact between photocatalyst and bacterial outer surface membrane and its potential to transfer the free radicals directly without intermediaries. As more bacteria, will come in contact with TiO_2 nano-particles, with enough effective irradiation upon TiO_2 particles, more bacteria will be oxidized, damaged or killed during the process. Another explanation could be that under high bacterial load, more bacteria will be present within the reactor zone, close to water-air or water-solid interfaces, where irradiation is the most effective [173].

2.7. Light emitting diodes (LEDs)

The efficient use of solar light based photocatalytic reactors is sanitary and sustainable to environment but it needs large area and high cost for installation. Also, the efficiency of reactors depends upon the direction, intensity and availability of solar light [135]. To prevail over these disadvantages, the usage of energy efficient ultra-violet or visible light emitting diode (UV/Vis-LED) source in designing the compact photocatalytic reactor.

Light emitting diodes (LEDs) are semiconductor devices that emit light of a single wavelength which is produced by a form of electroluminescence [174], [175] . It is solid-state technology based entirely on p-n junction devices made of semiconductor

materials [174]. they are made of aluminum nitride (AlN) or gallium and aluminum nitride (AlGaN) that are not toxic [176].

LED light sources, beyond being a reliable and continuous source (unlike solar), are inexpensive and promise high current-to-light conversion efficiency, with little heating (more efficient than many conventional mercury discharge lamps) [177]. They can emit light of different wave- length (infrared, visible, or near-ultraviolet) based on the composition and condition of the semiconducting materials [174].

They are having high robustness, long life time (hundred thousands of hours compared to thousands of hours in the case of classical lamps) [178], little heat production, good linearity of the emitted light intensity with current, suitability for operation in a pulsed regime at high frequencies [135], fast- responding (nanosecond scale) artificial light sources emitting nearly monochromatic light at various wavelengths. Moreover LEDs are driven by direct current, can accommodate rapid "on" and "off" toggling, and do not contain toxic mercury [179]. In comparison with incandescent lamps and fluorescent tubes, their advantages include higher luminosity, energy efficiency [180].

Chapter 3

MATERIALS AND METHODS

3.1. Preparation of N-doped TiO_2

Nitrogen-doped titanium dioxide (N-doped TiO_2) was synthesized through sol-gel method using ammonium hydroxide solution (28 %) as a nitrogen source. 20 mL of a precursor solution titanium (IV) isopropoxide (TTIP) was slowly added to 100 mL of absolute ethanol, and the solution was adjusted to pH = 1 with nitric acid (60%). After 10 minutes of vigorous stirring in ice bath, a different amount of ammonia solution was added to the prepared nano colloid solution to facilitate incorporation of nitrogen into TiO_2 crystal. The amounts of ammonia solution were adjusted to give N/Ti molar ratios of 2, 4 and 6 with vigorous stirring for 2 h. Subsequently, the mixtures were aged at room temperature for 24 h, to remove the solvent and then oven dried at 90°C for 16 h. The produced powder was then ground and calcined in a muffle furnace at a heating rate of 5°C/min under air. Three calcination temperatures (400, 500, and 600°C), and three calcination times (3, 4, and 5 h) were used. The undoped titanium dioxide with optimum synthesis parameters was synthesized with the same method except that water was added instead of ammonia solution. The N-doped TiO_2, and the undoped TiO_2 were designated as xNTyz, where x, y and z respectively denote the N/Ti molar ratio, the calcination temperature and time.

3.2. Photocatalytic activity of N-doped TiO_2

The photoactivity of N-doped TiO_2 nanoparticles was investigated using methylene blue (MB) as a model chemical in batch photoreactor under visible-light irradiation (Figure 3.1). 300 mL beaker was used as photoreactor for all experiments in which visible light was provided by Osram lamp (50 PARA30) with a wavelength of 400 – 700 nm. During this process, 1.0 g L^{-1} of the prepared powder was suspended in 100

mL of 10 ppm methylene blue solution. The solution was continuously stirred with a magnetic stirrer to ensure homogenous mixing during 3 h irradiation period. Prior to proceeding to photoactivity test, the solution was stirred further for additional 30 minutes in dark environment to create adsorption-desorption equilibrium. After which, 10 mL of aliquots were taken from the reactor and filtered using 45 μm syringe filter. The MB concentration of supernatant was then analyzed with a portable spectrometer (DR 2700, Hach) at 664 nm wavelength absorbance. The MB decolorization efficiency (R) was calculated using the following equation:

$$R\ (\%) = (C_o - C_f)/C_o * 100 \quad 3.1$$

Where, C_o and C_f are the concentrations of methylene blue before and after visible light irradiation.

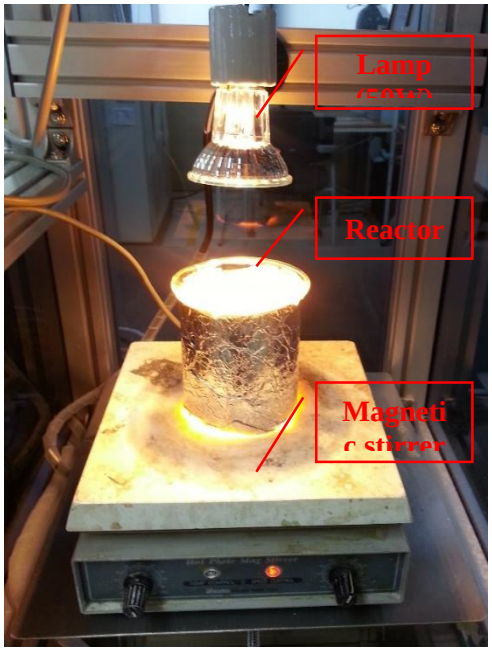

Figure 3. 1 Photoreactor used in decolorization of methylene blue with N-doped TiO_2.

3.3. Box-Behnken experimental design

The experiments were designed according to the Box-Behnken method with the selected three important sol-gel synthesis parameters: nitrogen to titanium molar ratio (N/Ti), calcination temperature and calcination time. The required responses such as anatase weight fraction (W_A), Brunauer-Emmett-Teller (BET) specific surface area (S_{BET}) and photoactivity (methylene blue decolorization efficiency (R)) under visible-light sources were optimized after studying the influences of these independent parameters and their interaction effects.

Table 3. 1 Experimental levels of selected variables for Box-Behnken design.

Abbreviation	**Variables**	**Units**	**levels**		
			- 1 (Low)	0 (medium)	+1 (High)
A	N/Ti	Molar ratio	2	4	6
B	Calcination temperature	^oC	400	500	600
C	Calcination time	h.	3	4	5

The factors and levels are given in Table 3.1. The factors, i.e., N/Ti molar ratio, calcination temperature, and calcination time were designated as A, B, and C, respectively. According to BBD the total number of experiment can be calculated as:

$$N = k^2 + k + Cp \qquad 3.2$$

where k is a number of factors, and *Cp* is a central replication point [181]. Table 3.2 shows the 15 experimental runs which are arranged according to BBD.

Table 3. 2 Box-Behnken design with actual and predicted values of anatase weight fraction (WA), BET specific area (SBET), and MB decolorization efficiency (R).

Run	A[1]	B[2]	C[3]	W_A (%)		S_{BET} ($m^2 g^{-1}$)		R (%)	
				Actual value	Predicted value	Actual value	Predicted value	Actual value	Predicted value
12	2 (-1)	400 (-1)	4 (0)	100.00	100.31	80.18	80.60	59.01	60.12
5	6 (1)	400 (-1)	4 (0)	100.00	99.62	77.07	78.17	74.77	73.52
15	2 (-1)	600 (1)	4 (0)	91.67	92.05	30.81	29.71	34.92	36.18
13	6 (1)	600 (1)	4 (0)	94.43	94.12	27.97	27.55	36.66	35.55
4	2 (-1)	500 (0)	3 (-1)	100.00	99.73	63.32	61.88	56.71	55.61
10	6 (1)	500 (0)	3 (-1)	100.00	100.42	62.51	60.39	60.55	61.81
14	2 (-1)	500 (0)	5 (1)	100.00	99.57	51.15	53.27	54.74	53.48
11	6 (1)	500 (0)	5 (1)	100.00	100.26	48.73	50.17	58.94	60.04
8	4 (0)	400 (-1)	3 (-1)	100.00	99.96	87.58	88.60	68.32	68.31
7	4 (0)	600 (1)	3 (-1)	93.52	93.40	37.99	40.53	36.10	35.95
1	4 (0)	400 (-1)	5(1)	100.00	100.12	84.39	81.86	64.80	64.95
6	4 (0)	600 (1)	5 (1)	92.88	92.92	29.46	28.44	35.40	35.41
3	4 (0)	500 (0)	4 (0)	100.00	100.00	45.20	47.91	55.56	56.69
9	4 (0)	500 (0)	4 (0)	100.00	100.00	47.24	47.91	57.37	56.69
2	4 (0)	500 (0)	4 (0)	100.00	100.00	45.30	45.95	57.14	56.69

[1] N/Ti (Molar ratio)
[2] Calcination temperature (°C)
[3] Calcination time (h)

A second-order polynomial equation was used to find the relationship between the independent variables and the response. For the three chosen factors, the equation can be written as:

$$Y = \beta_o + \beta_1 A + \beta_2 B + \beta_3 C + \beta_{12} AB + \beta_{13} AC + \beta_{23} BC + \beta_{11} A^2 + \beta_{22} B^2 + \beta_{33} C^2 + \varepsilon \qquad 3.3$$

Where β_o is a constant, A, B, and C are the independent variables, β_is are the coefficients for linear interaction effect, β_{ii}s are the coefficients for cross-product interaction effect, β_{ij}s are the coefficients for quadratic interaction effect and ε is the

random error. The regression analysis and estimation of these coefficients were performed with a statistical software package Design-Expert® version 7.0.0 (Stat-Ease, Inc.). The adequacy of the model equations was evaluated using analysis of variance (ANOVA). Quality of fit of the model equations and their statistical significance were expressed using F-test, coefficient of determination (R^2), prediction coefficients of determination (Pred R^2), adjusted coefficients of determination (adj-R^2), and coefficients of variation (CV).

3.4. Immobilization of N-doped TiO_2

Immobilization of TiO_2 on glass support was done using TEOS as a binder according to the methods described by Kete *et.al* with minor modification [182]. A suspension containing N-doped TiO_2 (10 g/L) was prepared from an equal amount of ethyl alcohol (99.9 %) and distilled water using different volume percentages of TEOS (5, 10, 20, and 30%). Prior to introduce N-doped TiO2 powder, the solution was adjusted to pH = 2 with HCl (35%) and vigorously stirred for 30 min. After addition of N-doped TiO_2 particles, the suspension was stirred for 2 h and sonicated for 1 h until a homogenous suspension was obtained. The samples prepared with this method are designated as SiO_2/N-TiO_2-x, where x denotes the percentage of TEOS added. The N-doped TiO_2 immobilizations were done on a substrate (Ø 5 mm sodium glass beads) through immersion. Prior to coating, the glass beads were washed with distilled water and soaked in hydrofluoric acid (5% v/v) for 24 h to create a rugged surface. After washing several times with distilled water the glass beads were oven dried at 120 ^oC for 30 minutes. Then, the glass beads were immersed in the prepared sol–gel using stainless steel wire mesh for 10 min. Finally, the glass beads were treated at a temperature of 120 ^oC for 2 h to obtain strong substrate and coated TiO_2 attachment. The coating and heating processes were repeated five times to get the required thickness for higher photocatalytic activity.

3.5. Catalyst characterization

The crystal phase compositions were obtained from the X-ray diffraction (XRD) measurement on PANalytical X'Pert PRO-MPD diffractometer with Cu-Kα radiation (λ=0.15406), accelerating voltage (40 kV) and current (25 mA) at scan rate of 0.017 degree per minute in the range of $2\theta = 20^{o}$ to 85^{o}. The average crystallite sizes of anatase and rutile phases were determined with the Scherrer equation $D= k\lambda/\beta\cos\theta$, where D is the crystallite size, k is a constant (shape factor, about 0.9), λ is the X-ray wavelength (0.154059 nm), β is the full width at half maximum (FWHM, in radian) of the diffraction peak at $2\theta = 25.3^{o}$ [183]. The weight fractions of the two phases were calculated using Spurr and Myers equation $W_A=1-W_R = 1/[1+0.8(I_R/I_A)]$,where W_A and W_B are weight fractions of anatase and rutile, I_R and I_A are relative intensity of rutile peak (110) (at ~27.5^{o}) and anatase peak (101) (at ~ 25.3^{o}) [184], respectively. The specific surface area, pore volume and pore diameter were obtained from N_2 adsorption-desorption isotherm by using Brunauer Emmett Teller (BET) and Barett–Joyner–Halenda (BJH) methods with Micromertics, Tristar II 3020. The structural properties were investigated by High-resolution micro-Raman spectroscopy (Horiba/Jobin-Yvon, LabRAM HR800) with spectra resolution of 0.54 cm^{-1} in the range of 0-1000 cm^{-1} Raman shift. Analysis of functional groups was performed using Fourier Transformed Infrared (Varian 640-IR) FT-IR spectrometer, from 4000 – 400 cm^{-1} wavenumbers. The binding energy and nitrogen content were estimated with X-ray photoelectron spectroscopy (XPS) (VG Microtech ESCA 2000) with Mg-Kα X-ray source (hv=1253.6) equipped with CALM 4 hemispherical electron energy analyzers (fixed pass energy of 23.4 eV). The binding energy of carbon (C 1s: 284.8 eV) was used as an internal standard for the correction of charging shift, and the spectra was analyzed using CasaXPS software (version 2.3.17PR1.1). UV-Vis spectra of the samples were scanned using UV/Vis/NIR Spectrophotometer (Hitachi, U-4100) in the range of 200–800nm. High-resolution transmission electron microscopy, HR-TEM (TECHNAI G^2 F30 S-TWIN) operating at 300kV and equipped with X- ray energy-

dispersive analyses (EDX) (BRUKER) was also used to investigate the average crystals size, morphology and structure of the prepared nanoparticles as well as elemental mapping. The surface morphologies and chemical composition of the syntheses samples were examined using field emission scanning electron microscope, (FE-SEM (JEOL JSM-7610F). Photoluminescence (PL) was obtained at room temperature by fluorescence spectrophotometer (HITACHI, F-7000) with an excitation wavelength of 340 nm by 150 W Xe lamp. To study the thermal stability of N-doped TiO_2 xerogel, the thermo gravimetric analysis (TGA) and differential scanning calorimeter (DSC) were performed using TA instrument (SDT-Q600) at heating rate of 10 ^oC/min in air.

3.6. Photocatalytic investigation of immobilized catalyst

The photocatalytic performance of immobilized N-doped TiO_2 was performed under visible light and the photoreactor set up was adopted from the works of Daneshvar *et.al* (Figure 3.2) [185]. For this test, known number of TiO_2 coated glass beads (80) were attached with plastic plate and immersed to a known amount of methylene blue solution (10ppm) at 2 cm height above the bottom of a 300mL beaker. This arrangement gives enough space for continuous stirring using magnetic stirrer. After 3 h of irradiation with Osram lamp (75PAR30) the sample was taken and analyzed with a portable spectrometer (DR 2700, Hach) at an absorbance of 664 nm. The MB decolorization efficiency (E) was calculated using the following equation:

$$E\ (\%) = (C_o - C_f)/\ C_O * 100 \quad 3.4$$

Where, C_o and C_f are the concentrations of methylene blue before and after visible light irradiation.

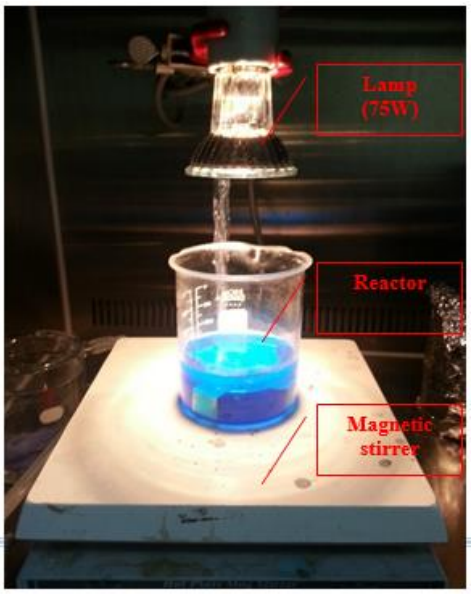

Figure 3. 2 Photoreactor used in decolorization of methylene blue with immobilized N-doped TiO_2.

3.7. Adhesion properties of the coating

The adherence strength of the coated particles was investigated with sonication test according to the procedure described by Nawi and Zain with minor modification [186]. For this particular test, TiO_2 coated soda-lime slide glass plates (75mm X 25mm X 1.5mm) were prepared in three cycles at different TEOS concentration (5,10,20 and 30 %) using similar methods as described earlier for glass beads. Each sample was placed in a 100 mL beaker filled with distilled water and sonicated in an ultrasonic bath (Bransonic 5510) for different times (1, 2, 3, 4, and 5 minutes). After each sonication, the samples were washed with distilled water and oven dried at 120 ^{o}C for 30 minutes. Finally, the adherence strength was determined from percentage mass loss of the sample at each test using the following equation:

$$\% \text{ of mass loss} = (m_i - m_o)/m_o * 100 \qquad 3.5$$

Where, m_i and m_o are mass of coated TiO_2 before and after sonication test.

3.8. Reactor setup for photocatalytic bacterial inactivation

The photoreactor setup used for bacterial inactivation consisted of four rectangular containers (height 15mm, width 50mm and length 100mm) made from 5 mm thick acrylic sheet. The containers were placed similar to a stair-case as shown in Figure 3.3(a) and 3.3(b). The water inlet and outlet points were arranged in such a way that water flow short-cut was minimized and the residence time of the water in each container was increased. The bottom surface of each container was filled with N-doped TiO_2 coated glass beads. The water with test microorganisms was stirred continuously with magnetic stirrer in 1000 mL beaker and introduced into the first container at 40 mL min^{-1} using peristaltic pump. Flow was gravitational afterwards and the process was continuous at a given irradiation time. The whole reactor setup was covered with a rectangular acrylic box and the catalyst was irradiated using Samsung LED (SMD 5050, 3LED Module light, 1 W/Module) with a total of 60 W (wavelength λ = 450 nm) from five sides (from top, and other four sides). The incident photon flux in the reactor was measured by potassium ferrioxalate actinometer.

For sunlight experiment, the reactor setup covered with a rectangular acrylic box was exposed to sunlight at the rooftop of microbiology laboratory building 352 (Gyeongsang National University, Jinju, South Korea). The experiments were performed in a good sunny day between 12:00-13:00 in June 2016. The average solar and UV irradiance were approximately 71.2 mWcm-2 and 4.6 mWcm-2, respectively.

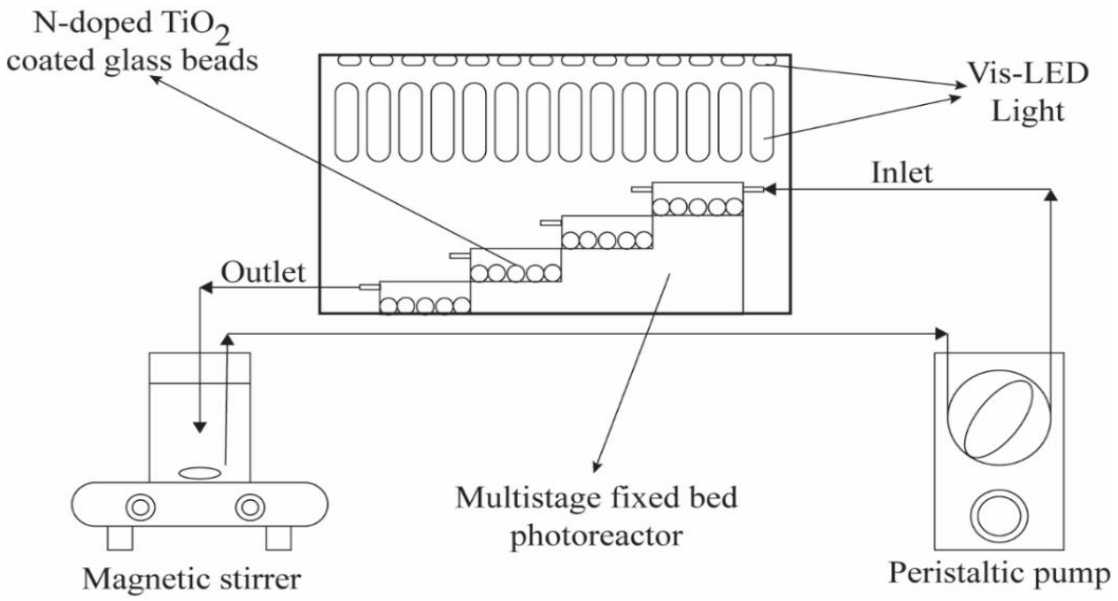

(a)

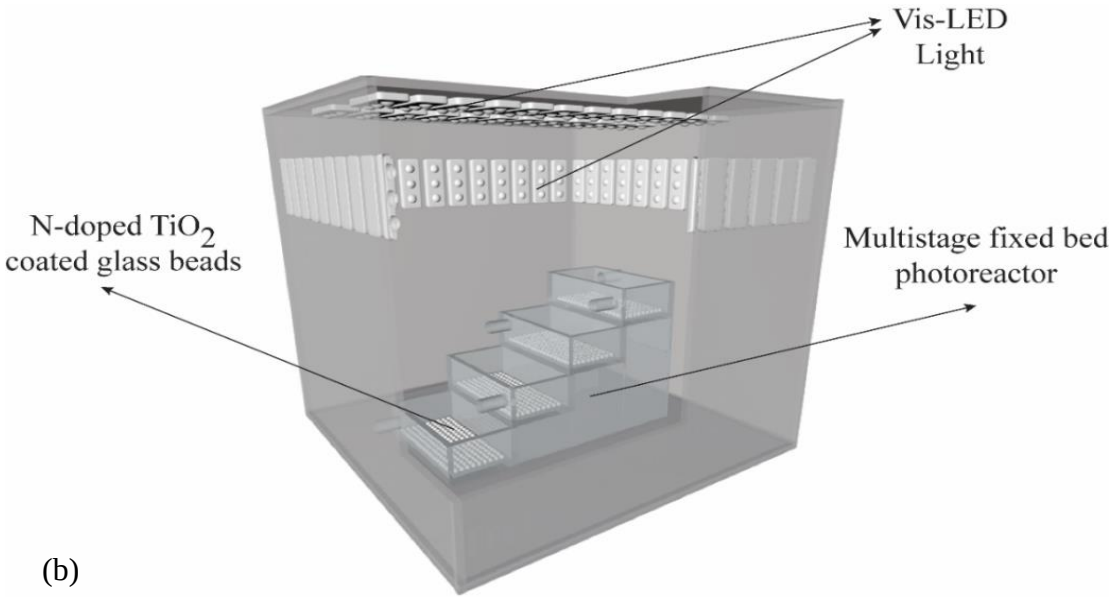

(b)

Figure 3. 3 Schematic diagram of the photoreactor system (a) 3D representation of multistage fixed bed photoreactor (b).

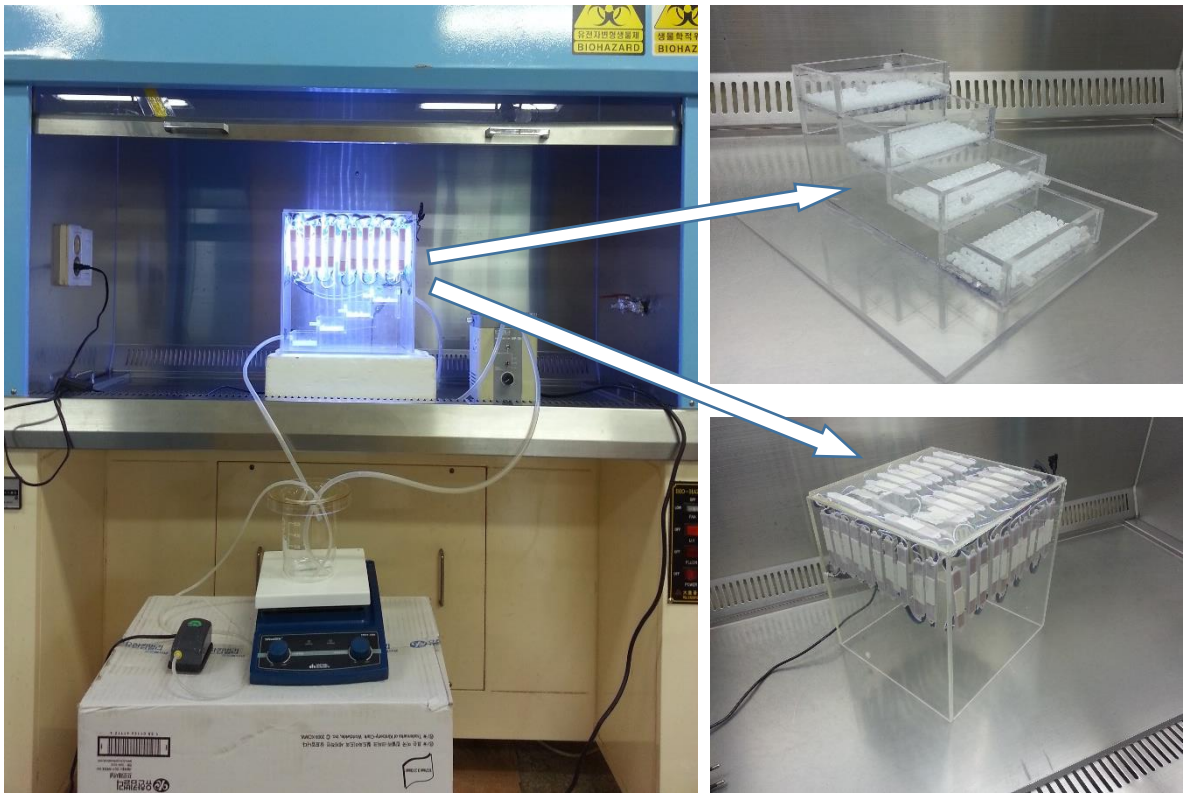

Figure 3. 4 Photograph of multi-stage fixed bed photoreactor set up.

3.9. Bacteria strain and growth media

Five different strains of bacteria, *E. coli* K-12 (KCTC 2443), *S. flexneri* (KCTC 2517), *S. typhimurium* (ATCC 14028), *S. aureus* (KCTC 1916), and *B. subtilis* (ATCC 6633) were used as test organisms for inactivation experiments.

E. coli and *S. aureus* were, respectively grown in Luria-Bertani broth (LB, Difco™) and tryptic soy broth (TSB, Bacto™), in a shaking incubator at 160 rpm and 37 °C. *S. flexneri*, *S. typhimurium*, and *B. subtilis* were also grown in nutrient broth (NB, Difco™) with the same condition. After 18 h, the bacteria cells were collected by centrifugation at 3000 rpm for 15 min at 4°C and the bacteria pellet was then washed three times with phosphate buffer solution (1X) (PBS, iNtRON Biotechnology). Finally, the initial bacterial suspensions were prepared at different concentration in

colony-forming units (CFU mL^{-1}) in sterile 1X PBS solution by observing from their optical density readings at 600nm (OD_{600}) using spectrophotometer (X-ma 1200).

3.10. Detection of viable bacteria

The viable bacteria were determined immediately on appropriated medium using standard plate counting techniques. At each bacterial inactivation experiment, the samples of 100 µL were withdrawn from the reactor. Serial dilutions were performed in 900 µm of sterile 1X PBS solution in decimal steps (10^{-1} to 10^{-7}) and 100 µm of diluted samples from each step were plated on Agar medium. The plates were incubated at 37 ^{o}C for 24 h prior to counting. All the experiments were performed in three trials and each point on the graphs represents an average value together with standard deviation of three replicate trials error bars. The photocatalytic inactivation efficiencies were calculated as bacterial log unit reduction (L_r):

$$Lr = Log10\ (N/No) \qquad 3.6$$

Where, N_o and N are the number of viable bacteria at initial and at a given duration of treatment, respectively.

The statistical significance of differences in the mean values among the treatment groups were calculated from One way analysis of variance. A P value of less than 0.05 was considered as significant. The statistical analysis was carried out using Sigma Plot V. 12.0 software.

3.11. Effects of operational parameters of the photocatalytic reactor

The effects of different operational parameters of the photoreactor (such as TiO_2 concentration, initial bacterial concentration, flow rate, and incident photon flux) was investigated from the photocatalytic inactivation efficiency on *E. coli* as model bacteria. The experiment was repeated three times for each condition, and the average of the three trials was determined. The error bars are standard deviations

from the average values of triplicate experiment. The statistical significance of differences in the mean values among the treatment groups were calculated from One way analysis of variance. A P-value of less than 0.05 was considered significant. The statistical analysis was carried using SigmaPlot V. 12.0 software.

3.12. Photocatalytic bacterial inactivation efficiency and rate of disinfection

The photocatalytic bacterial inactivation efficiency of immobilized TiO_2 were further investigated on Gram-negative (*E. coli, S. typhimurium and S. flexneri*) and Gram-positive bacteria (*B. subtilis and S. aureus*) using the same operational conditions selected in section 3.11.

Furthermore, the rate of photocatalytic inactivation of each bacterial strain for the experiment under vis-LED and Sun light was calculated using the most common Chick-Watson disinfection kinetic Model (equation 3.7) [187].

$$\mathrm{Log}(N/N_o) = kt \qquad 3.7$$

Where N_o and N are the initial and final number of viable bacteria ($CFU\,mL^{-1}$), k disinfection kinetic constant and inactivation time (min). k was determined from a slop of a plot of $\mathrm{Log}(N/N_o)$ as a function of time.

3.13. SEM analysis

To examine the photocatalytic effect of TiO_2 nanoparticle on bacterial cell membrane, before and after inactivation, the bacterial cells were collected and centrifuged. The cell pellet was resuspended with PBS (1x) solution and separated from the supernatant with centrifuge. The cells were prefixed by 2.5 % glutaraldehyde solution (diluted in PBS buffer), washed three times in PBS solution and postfixed in 1% osmium tetroxide at 4 ^oC for 30 min. Subsequently, the cells were dehydrated by series of ethanol solutions (60, 70, 80, 90 and 100 %) and 100 % acetone. The cells were then resuspended in hexamethyl-disilazane at 4 ^oC for 20 min and centrifuged.

Finally, the cells were subjected to sputter-coating with gold and examined using a field emission scanning electron microscope (FE-SEM, JEOL JSM-7610F).

Chapter 4

RESULTS AND DISCUSSION

4.1.N-doped TiO_2 nanomaterial

4.1.1. Optimization of sol-gel synthesis parameters

Based on BBD and using the relationships in Table 3.1, a total of 15 runs were performed including the central point which measures process stability and inherent variability.

Powder X-ray diffraction (XRD) was used for crystal phase identification and estimation of the anatase to rutile ratio and the crystallite size of each phase present. The specific surface area of the prepared sample also examines based BET analysis. Figures 4.1 and 4.2 show X-ray diffraction (XRD) patterns and nitrogen adsorption-desorption isotherms of the as prepared N-doped TiO_2 samples according to BBD. The results from these two characterizations, W_A and $S_{BET,}$ were used as experimental response together with R (Table 3.2).

The analysis of the models indicates that they are highly significant with F-values of 77.57 for (W_A), 94.95 for (S_{BET}) and 92.23 for (R) with their corresponding P value < 0.0001. The ANOVA for the three selected responses is shown in (Table 4.1, 4.2, and 4.3). The mutual interaction between the test variables can be revealed using P-values [188].

The model adequacy was further investigated using R^2 for the three responses (W_A, S_{BET} and R), which were found to be 0.9929, 0.9942, and 0.994, respectively. These imply that the models are adequate enough to predict the response in the experimental range with 99.29 %, 99.42 %, and 99.40% variability, respectively. The experimentally found and the predicted values were in good agreement as depicted

in Table 4.1. The Pred R^2 show that the model equations for W_A, S_{BET} and R give good predictions with 88.62 %, 91.30 %, and 91.63 % variability, respectively. In addition, the adj-R^2 of W_A (98.01 %), S_{BET} (98.37 %) and R (98.32 %) were in a reasonable agreement with Pred R^2 values. The degree of precision and reliability can be explained by the low values of CV which were 0.46 for W_A, 4.73 for S_{BET} and 3.01 for R. Furthermore, adequacy precision for each response (W_A, S_{BET} and R) was found to be 22.76, 28.961, and 28.701. All the above values can be changed when only the significant terms are considered (see Table 4.4). The values of "Prob > F" less than 0.05 indicate model terms are significant.

Furthermore, the adequacy of the model was checked by constructing different diagnostic plots for anatase weight fraction, BET surface area and MB decolorization efficiency shown in Figures 4.3, 4.4 and 4.5. The normal % probability plots of residuals for response was normally distributed, as they lie reasonably close to the straight line and show no deviation of the variance (Fig. 4.3a, 4.4a and 4.5a). Internally studentized residuals plots were constructed to facilitate the satisfactory fit of the developed model and the plots (Fig. 4.3b, 4.4b and 4.5b) show that, all the data points lie within the limits (±3). The predicted values obtained from the developed models were quite close to the experimental values and lie reasonably close to the straight line and indicate the adequate agreement with real data (Fig. 4.3c, 4.4c and 4.5c).

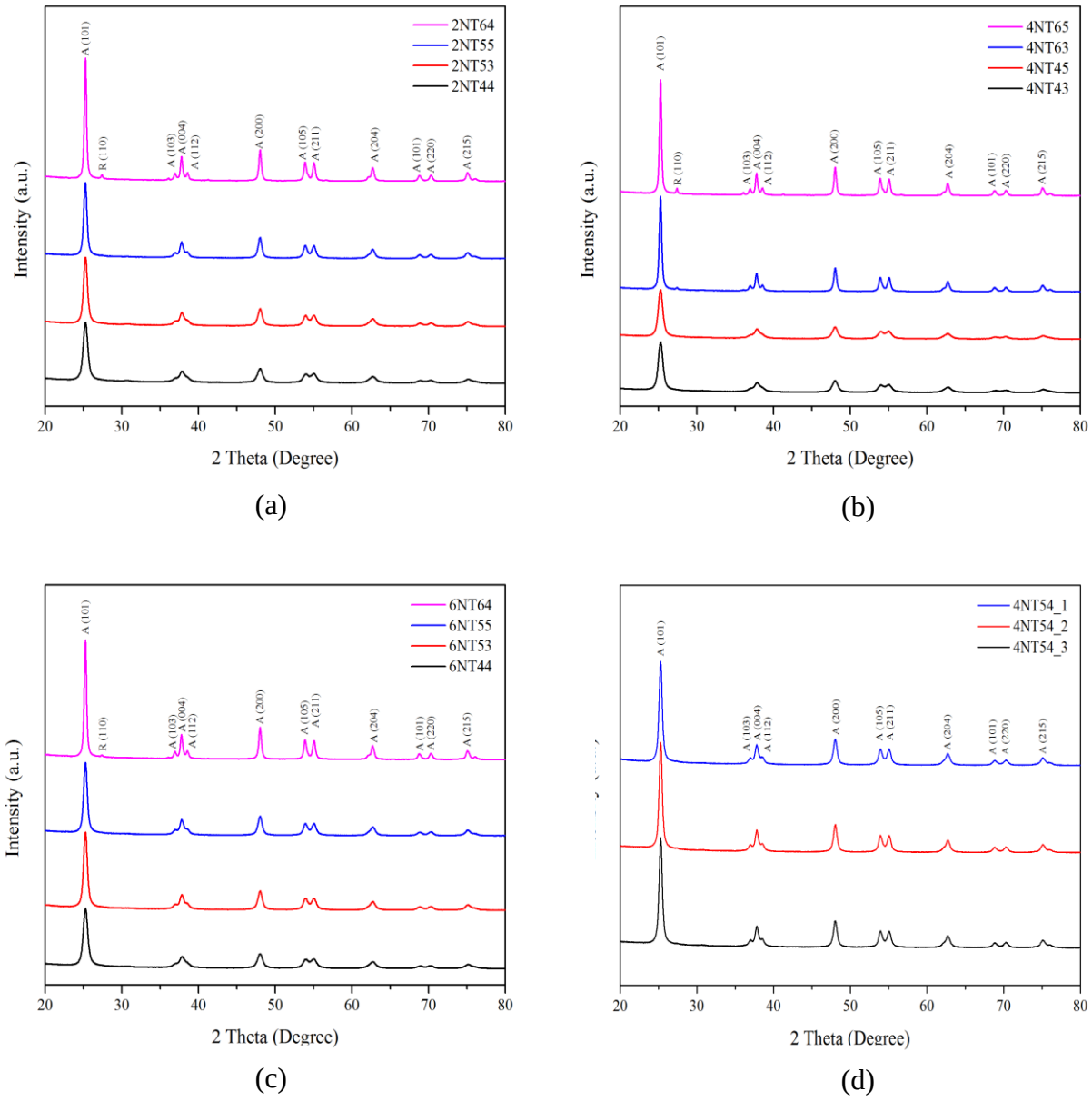

Figure 4. 1 X-ray diffraction patterns of (a) N/Ti molar ratio of 2, (b) N/Ti molar ratio of 4, (c) N/Ti molar ratio of 6, and (d) N/Ti molar ratio of 4 for central replication point.

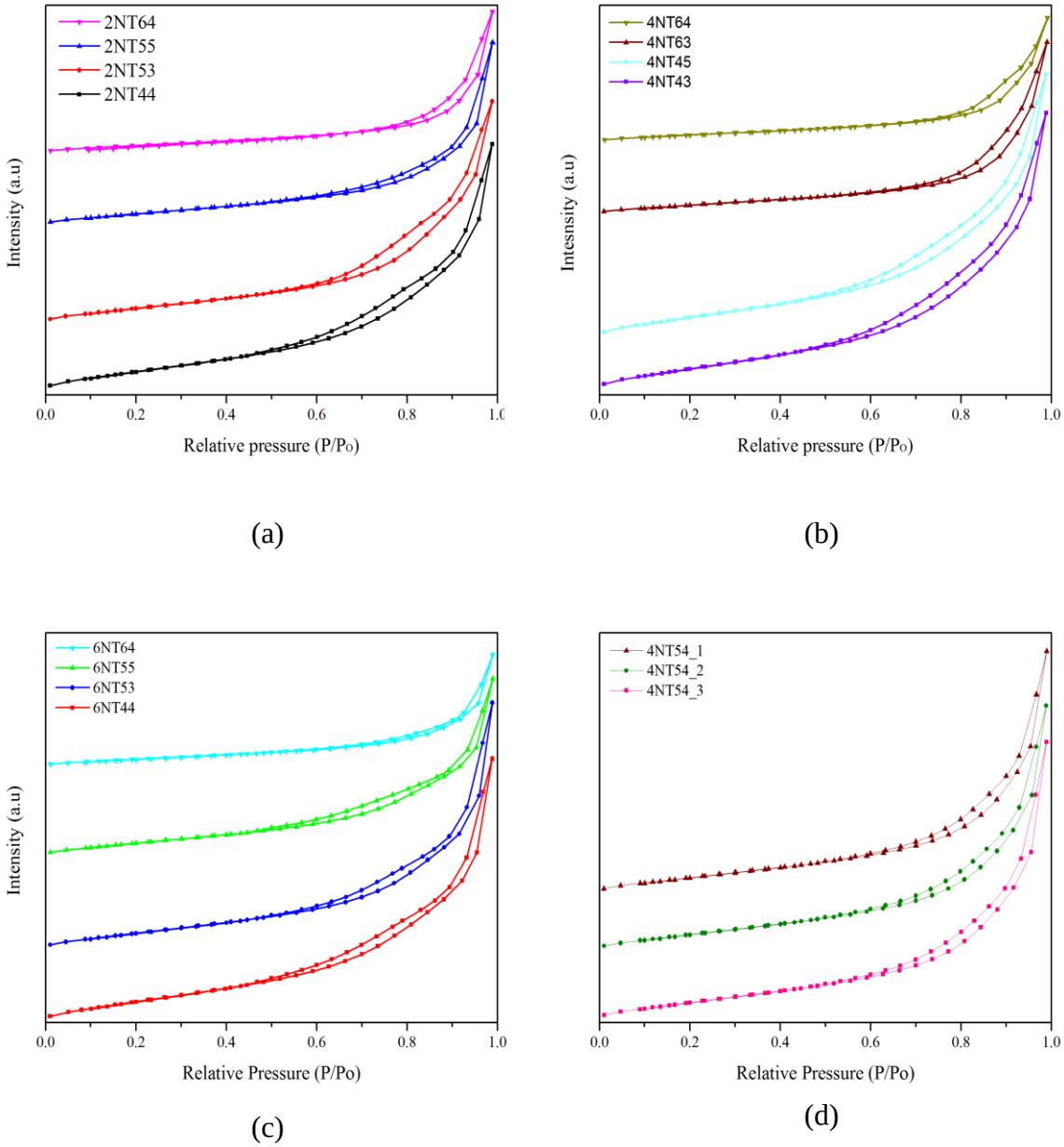

Figure 4. 2 Nitrogen adsorption-desorption isotherms of (a) N/Ti molar ratio of 2, (b) N/Ti molar ratio of 4, (c) N/Ti molar of 6 and (d) N/Ti molar ratio of 4 for central replication point.

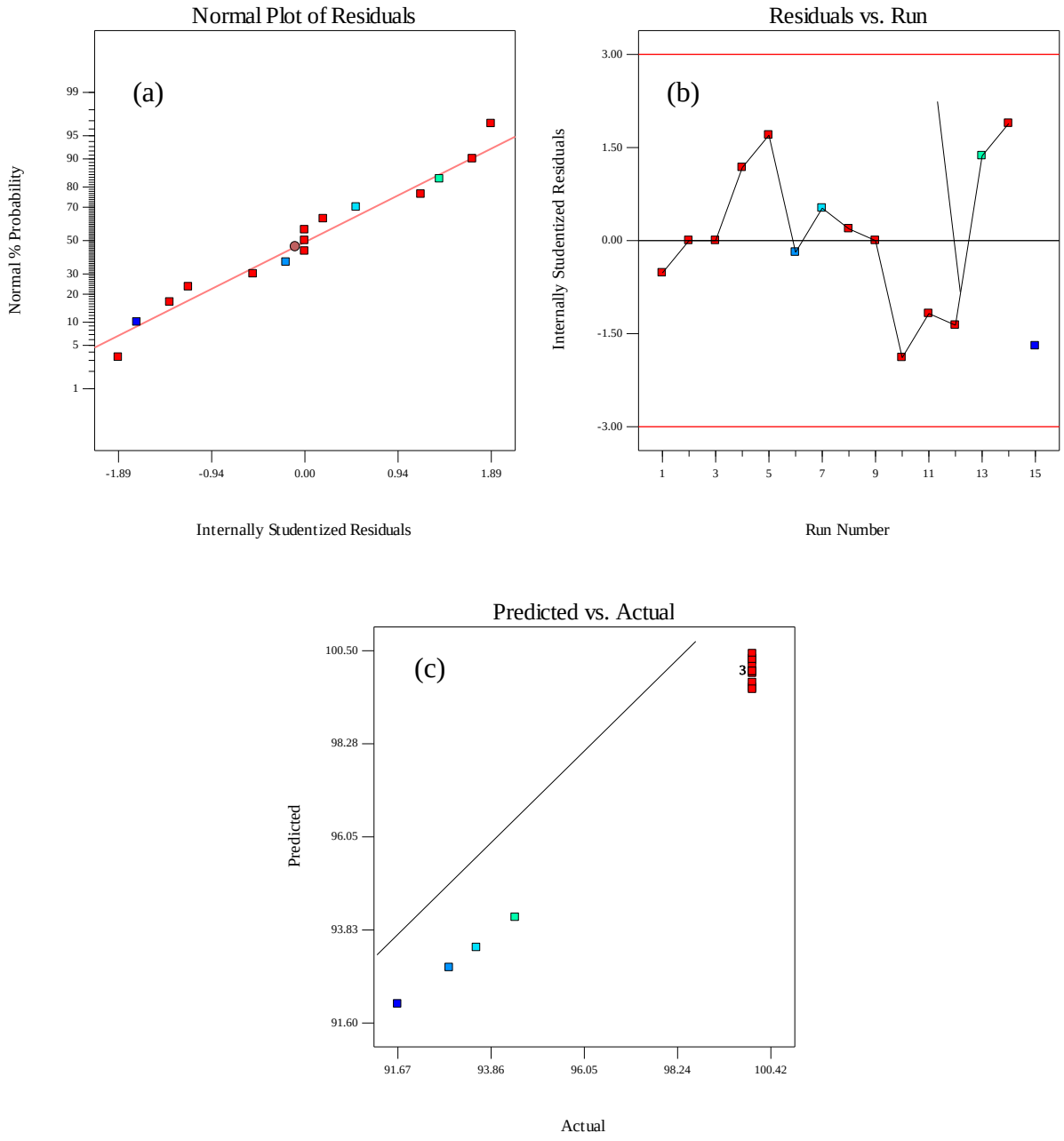

Figure 4. 3 Diagnostic plots for the adequacy of proposed model for anatase weight fraction.

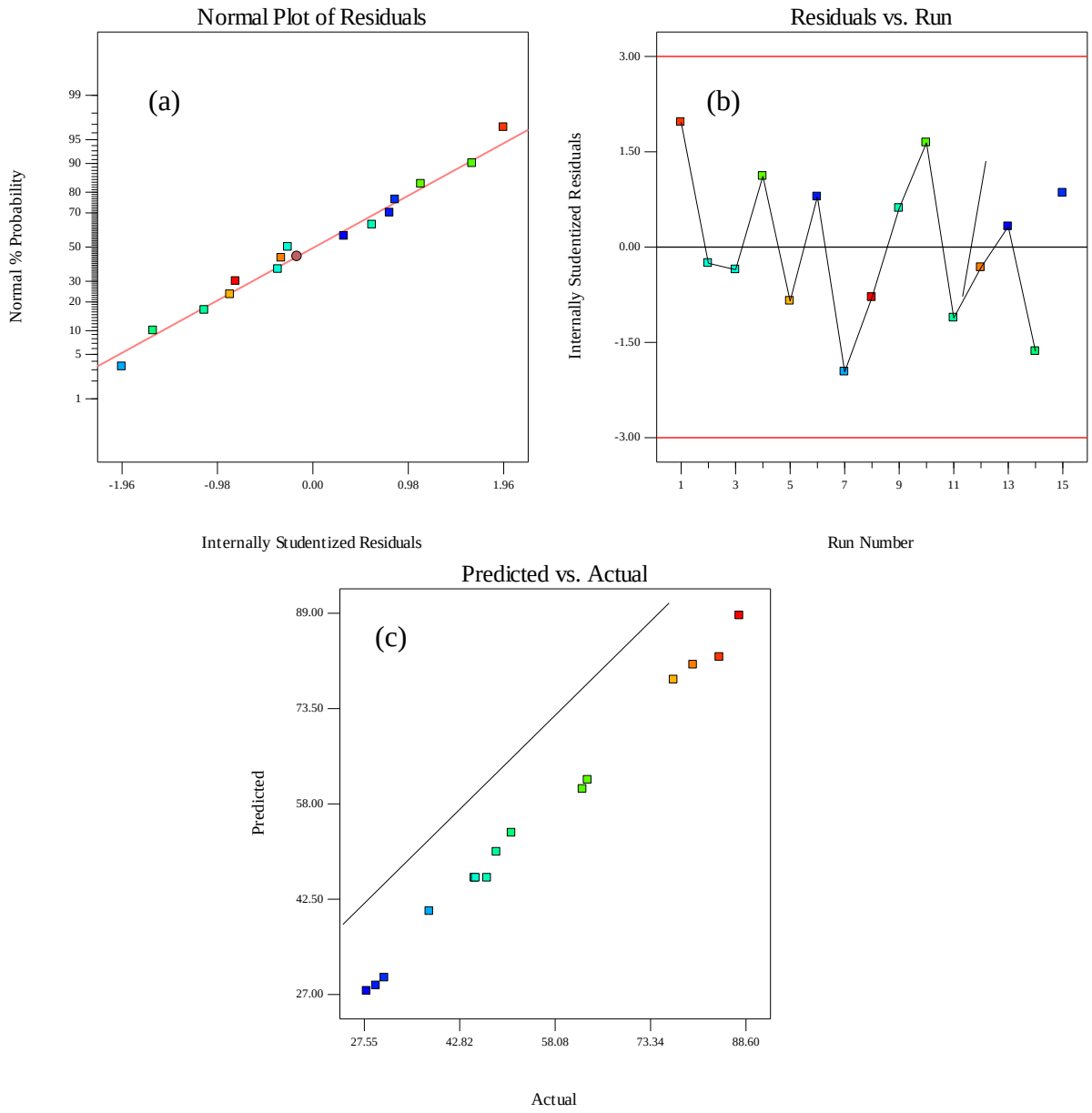

Figure 4. 4 Diagnostic plots for the adequacy of proposed model for BET surface area.

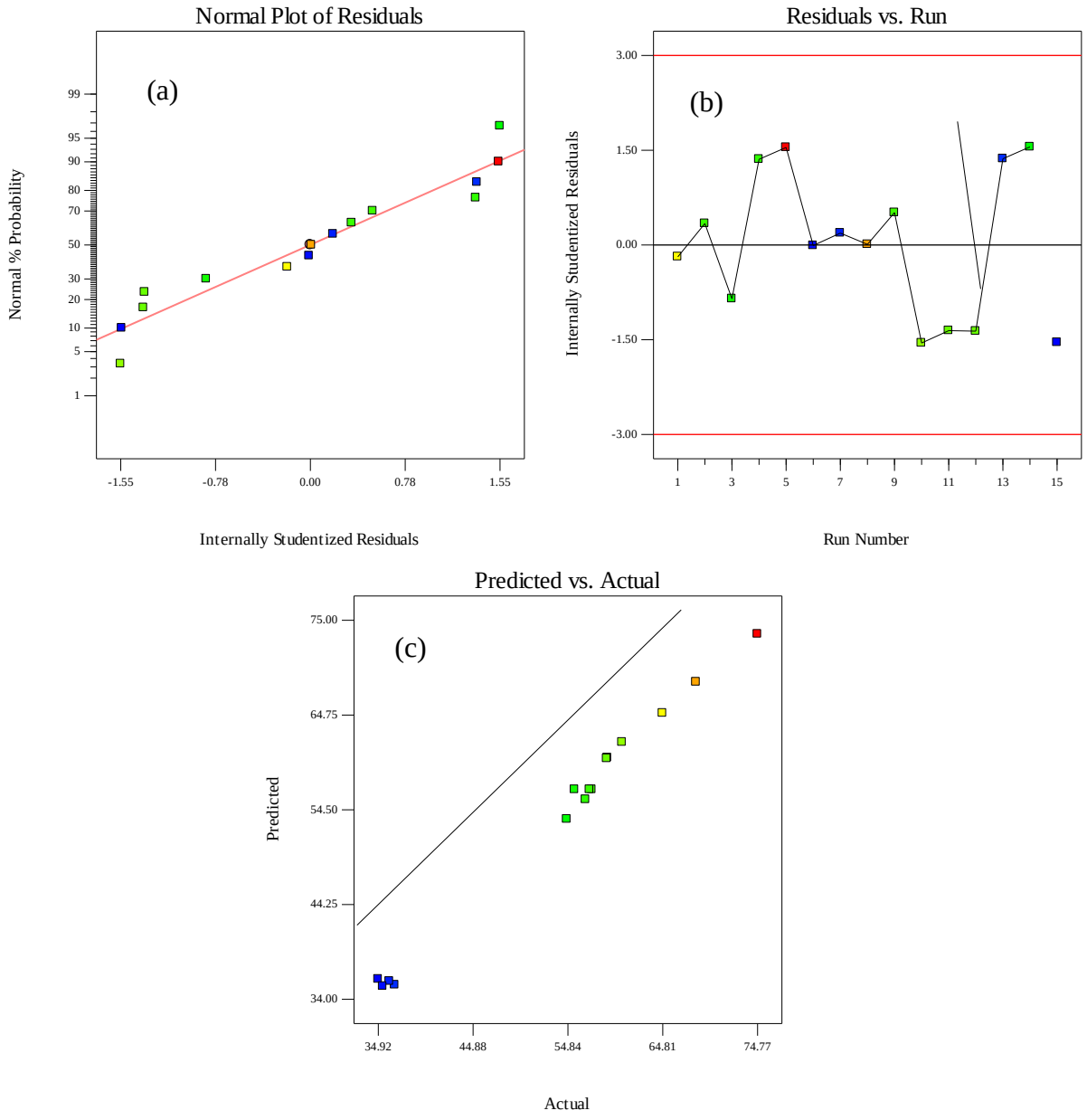

Figure 4. 5 Diagnostic plots for the adequacy of proposed model for MB decolorization efficiency.

Based on regression analysis the quadratic model equations for the three responses, W_A, S_{BET}, and R, in terms of actual values can be written by considering the significant terms as follows:

$$W_A(\%) = 37.46 - 1.553A + 0.296B + 0.334AB - 0.000343B^2 \quad 4.1$$

$$S_{BET}\ (m^2g^{-1}) = 477.343 - 5.202A - 70.0034C + 0.576A^2 + 0.000574B^2 + 8016183C^3 \quad 4.2$$

$$R\ (\%) = -\ 53.8514 + 10.359A + 0.519B\ 0.975C - 0.01753AB - 0.000604B^2 \quad 4.3$$

Table 4. 1 Analysis of variance (ANOVA) Box-Behnken quadratic model for anatase weight fraction.

Source	Sum of squares	df	Mean square	F Value	p-value Prob > F	
Model	141.67	9	15.74	77.57	< 0.0001	significant
A-N/Ti (Molar ratio)	0.95	1	0.95	4.69	0.0825	
B-Calcination temperature (^oC)	94.53	1	94.53	465.83	< 0.0001	
C-Calcination time (h)	0.051	1	0.051	0.25	0.6368	
AB	1.9	1	1.9	9.38	0.028	
AC	0	1	0	0	1	
BC	0.1	1	0.1	0.5	0.5092	
A^2	5.19E-03	1	5.19E-03	0.026	0.8792	
B^2	43.63	1	43.63	215	< 0.0001	
C^2	5.19E-03	1	5.19E-03	0.026	0.8792	
Residual	1.01	5	0.2			
Lack of Fit	1.01	3	0.34			
Pure Error	0	2	0			
Cor Total	142.68	14				

Table 4. 2 Analysis of variance (ANOVA) Box-Behnken quadratic model for BET surface area.

Source	Sum of Squares	df	Mean Square	F Value	p-value Prob > F	
Model	5695.95	9	632.88	94.95	< 0.0001	significant
A-N/Ti (Molar ratio)	10.53	1	10.53	1.58	0.2642	
B-Calcination temperature (^oC)	5150.62	1	5150.62	772.77	< 0.0001	
C-Calcination time (h)	177.38	1	177.38	26.61	0.0036	
AB	0.02	1	0.02	0.00	0.9603	
AC	0.65	1	0.65	0.10	0.7678	
BC	7.13	1	7.13	1.07	0.3484	
A^2	19.78	1	19.78	2.97	0.1456	
B^2	121.73	1	121.73	18.26	0.0079	
C^2	245.97	1	245.97	36.90	0.0017	
Residual	33.33	5	6.67			
Lack of Fit	30.81	3	10.27	8.17	0.1110	not significant
Pure Error	2.51	2	1.26			
Cor Total	5729.27	14				

Table 4. 3 Analysis of variance (ANOVA) Box-Behnken quadratic model for methylene blue decolorization efficiency.

Source	Sum of squares	df	Mean square	F Value	p-value Prob > F	
Model	2194.85	9	243.87	92.23	< 0.0001	significant
A-N/Ti (Molar ratio)	81.54	1	81.54	30.83	0.0026	
B-Calcination Temperature (^oC)	1916.42	1	1916.42	724.74	< 0.0001	
C-Calcination Time (h)	7.61	1	7.61	2.88	0.1507	
AB	49.14	1	49.14	18.58	0.0076	
AC	0.032	1	0.032	0.012	0.9162	
BC	1.99	1	1.99	0.75	0.4255	
A^2	1.4	1	1.4	0.53	0.5	
B^2	131.38	1	131.38	49.68	0.0009	
C^2	0.68	1	0.68	0.26	0.633	
Residual	13.22	5	2.64			
Lack of Fit	11.28	3	3.76	3.87	0.212	not significant
Pure Error	1.94	2	0.97			
Cor Total	2208.07	14				

Table 4. 4 Model adequacy test values after only significant model terms are considered.

Response	F values	R^2	Adj-R^2	Pred R^2	CV	Adeq Precision
Anatase wt. fraction	229.92	0.9917	0.9884	0.9668	0.35	41.632
BET surface area	184.44	0.9928	0.9874	0.9721	4.15	40.323
MB decolorization efficiency	229.51	0.9922	0.9879	0.9696	2.56	44.202

From these results we can conclude that response surface methodology can be potentially used to analyze the relative significance of various sol-gel synthesis parameters in the preparation of N-doped TiO_2. As demonstrated here Box-Behnken design was properly predict the sol-gel parameters with in the selected experimental range as well as outside these rang.

4.1.2. Crystal phase composition

Figure 4.1 shows the XRD patterns for the N-doped TiO_2 (W_A) samples prepared under different calcination temperatures, calcination times, and nitrogen to titanium molar ratios. The crystal phases well much with (JCPDS) Card No 21-1272 and 21-1276 for anatase and rutile, respectively. It can be observed that no peak associated with nitrogen was revealed in all of the XRD patterns in this figure. This might due to the dopant is uniformLy distributed either in the TiO_2 crystal structure occupying interstitial or substitutional sites [189]–[191]. However, Figure 4.1 indicates that the two crystal phases (anatase and rutile) appear at different sol-gel operational parameters with the anatase phase being dominant at calcination temperatures below 600^{o}C. Similarly, as can be observed from Figure 19a, at high calcination temperature (600^{o}C), the phase transformation process is seen to be slightly retarded with increasing nitrogen concentration from 2 to 6 N/Ti molar ratio. This result suggests that the thermal stability of the catalyst can be improved by the addition of nitrogen [192]. The effect of the presence of nitrogen on phase composition of TiO_2 can be further evidenced from Figure 4.7 where the XRD pattern of the undoped TiO_2 catalyst prepared at the optimum condition (400 ^{o}C, 3 h) is presented. As can be observed from this figure, the presence of rutile is quite evident and its amount is estimated to be about 12.87 %. However, comparison with Figure 14 shows that rutile phase was not detected in the N-doped TiO_2 samples prepared below 600 ^{o}C. This is may be due to the presence of higher concentration of nitric acid which favors the formation of rutile. Therefore, the presence of rutile at lower temperature (400 ^{o}C) in the undoped sample can be related to the highly acidic media of the solution as reported in previous studies [193]–[197]. This is mainly because in such an acidic medium, with the dissolution of the precursor, the grain growth is more rapid [194]. In addition, Figure 4.1 depicts that as the calcination temperature increased from 400 ^{o}C to 600 ^{o}C, the anatase peak became sharper and more intense. The average crystal size of all samples increased with the calcination temperature which is due to

the formation of bigger crystallite aggregation of the catalyst at higher temperature [190]. As compared to the effect calcination temperature, the effect of nitrogen on crystal structure and particle size was minimum in all samples. The effect of calcination time was also found to be insignificant in this study (Figure 4.6b). The crystallite size of each sample was calculated according to Scherrer formula and presented in Table 4.5.

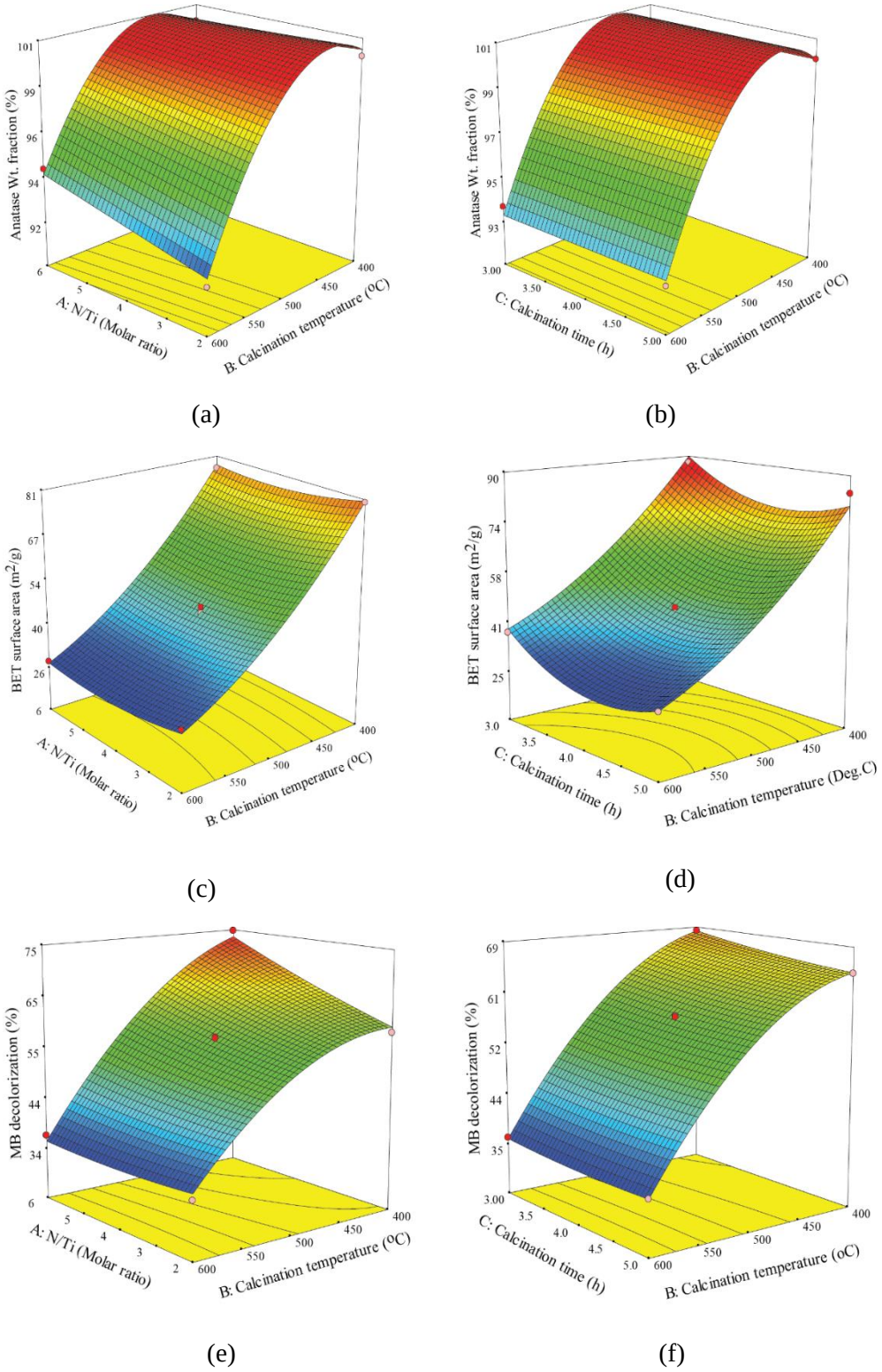

Figure 4. 6 Three-dimensional response plots showing interaction effects of N/Ti molar ratio, calcination temperature and time on anatase wt. fraction (a) and (b), on BET surface area (c) and (d), on MB decolorization (e) and (f).

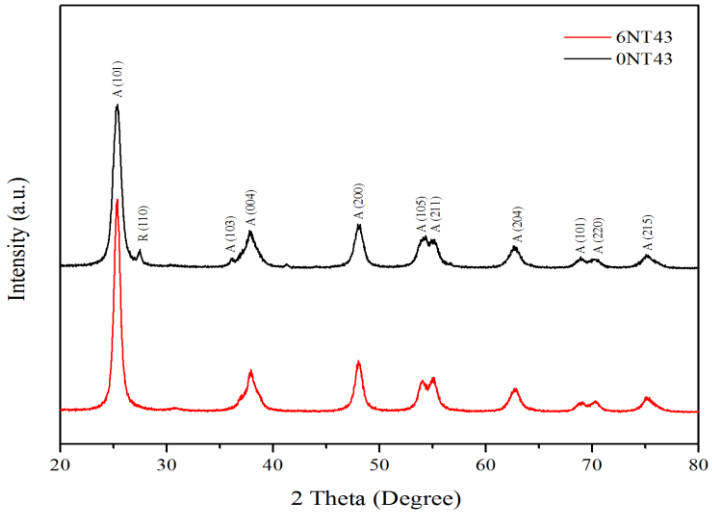

Figure 4. 7 XRD patterns of undoped and doped TiO_2 prepared under optimum condition.

Table 4. 5 Crystal phase composition and size of all N-doped TiO_2 samples.

Samples	Crystal phase composition		Crystal size	
	Anatase weight fraction (W_A) (%)	Rutile weight fraction (W_R) (%)	Anatase (nm)	Rutile (nm)
2NT44	100	-	10.05	-
2NT53	100	-	12.01	-
2NT55	100	-	12.84	-
2NT64	91.67	8.33	22.78	55.08
4NT43	100	-	9.94	-
4NT45	100	-	10.11	-
4NT63	93.52	6.48	18.84	44.78
4NT65	92.88	7.12	21.82	52.60
6NT44	100	-	10.28	-
6NT53	100	-	12.13	-
6NT55	100	-	13.35	-
6NT64	94.43	5.57	23.84	58.26
4NT54	100	-	14.89	-
4NT54	100	-	14.35	-
4NT54	100	-	14.07	-

4.1.3. Specific surface area

The N_2 adsorption-desorption isotherms for different N-doped TiO_2 are given in Figure 4.2. The specific surface areas of the synthesized samples are found to be more dependent on calcination temperature than on calcination time and N/Ti molar ratio as shown in Table 3.2 (see section 3.3). All N-doped TiO_2 samples prepared at 400 and 500 ^oC and calcined for 3 and 4 h showed a classification of type IV adsorption isotherms with narrow H2 hysteresis loop at around medium relative pressure. On the other hand, for calcination temperatures of 500 and 600 ^oC and calcination times of 4 and 5 h, the adsorption isotherm shifted to type V and H3 hysteresis loop at higher relative pressure (Figure 4.2). The two hysteresis loops at lower and higher relative pressure are raised from smaller and larger mesopore characteristics, respectively. A plausible explanation can be at higher calcination temperature and extended calcination time, there is an expansion of mesopores and consequently the formation of bigger pores [198]. The specific surface areas also indicated a decreasing trend with increase in calcination temperature and time (Figure 4.6c and 4.6d). Decreased specific surface area is due to catalyst aggregation at the higher temperature [27]. In addition, the specific surface area and crystal size of the undoped sample was found to be higher than that of the doped TiO_2, although the total pore size of the N-doped TiO_2 sample was higher as compared to that of the undoped TiO_2 sample (Figure 4.8). This can be attributed to the three-dimensional network microstructure which was formed between N-doped TiO_2 catalyst particles [25], [130], [199], [200].

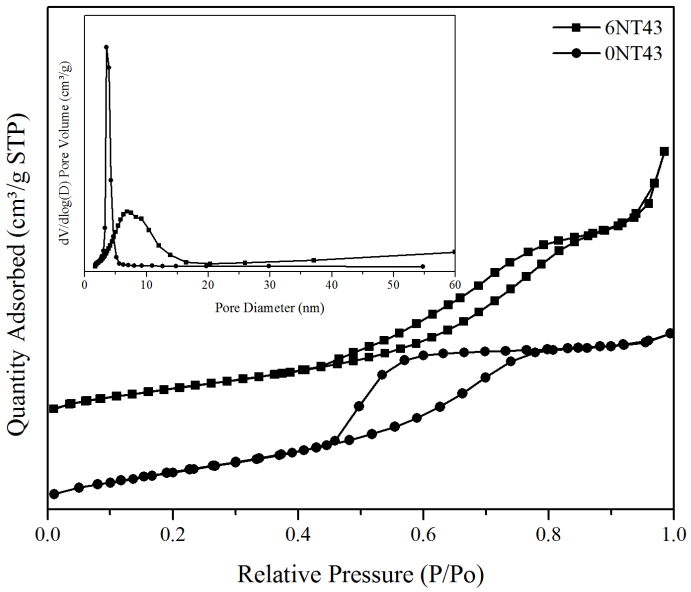

Figure 4. 8 Nitrogen adsorption-desorption isotherms and pore size distribution of doped TiO_2 (6NT43) and undoped TiO_2 (0NT43) prepared under optimum condition.

4.1.4. Photoactivity test

The photocatalytic performance of all synthesized N-doped TiO_2 samples was examined by decolorization of methylene blue in the liquid solution with visible light (λ>400nm). The samples at higher calcination temperature exhibited the lowest percentage of decolorization of methylene blue as shown in Figure 4.6e and 4.6f. Significant specific surface area reduction and larger particle size at elevated calcination temperature and time might have led to lowest decolorization. It was also observed that the decolorization efficiency increased remarkably when the amount of N dopants increased from 2 to 6 N/Ti molar ratio and at lower calcination temperature (Figure 4.6e). A possible explanation for this condition is that a higher concentration of N dopant facilitated proper incorporation of nitrogen into the TiO_2 structure and consequently increased the visible light-activity of TiO_2. All samples that were prepared at lower calcination temperatures and higher N concentrations

have larger surface area, which provided better adsorption of reactive molecules as the most active sites are those on the surface [82]. Furthermore, these also helped to improve the light harvesting on the larger surface area but with fewer degrees [201]. Though, the nitrogen dopant amount, and the higher specific surface area were the main factors for high photoactivity in the present study, particle size and crystallinity also played important role. Lower photoactivity can be caused by the charge recombination which is associated with low crystallinity and larger particle size [202], [203]. As a matter of fact, the highest photocatalytic activity shown by the N-doped TiO_2 sample prepared at N/Ti molar ratio of 6 and calcined at 400°C for 4 h, can be related to its high specific surface area, nitrogen content, and improved anatase crystallinity.

4.1.5. Model optimization and verification

Based on Derringer's desirability function approach for multiple response processes, the desired set of sol-gel synthesis parameters were determined through optimization of the responses from the three quadratic models (Equation 4.1,4.2, and 4.3). Accordingly, N/Ti molar ratio of 6, calcination temperature of 400°C, and calcination time of 3 h (6NT43) were selected with 0.987 desirability to predict anatase weight fraction of 100 %, BET surface area of 90.99 m^2g^{-1}, and MB decolorization efficiency of 74 %.

Table 4. 6 Model validation results of doped and undoped TiO2 prepared under optimized condition.

Sample	Crystal phase composition (%)		Crystal size (nm)		S_{BET} (m^2g^{-1})	R (%)
	(W_A)	(W_R)	Anatase	Rutile		
6NT43	100	-	10.14	-	87.12	72.7 ± 1.54
0NT43	87.13	12.87	8.27	19.96	92.84	11.8 ± 0.56

W_A: Anatase weight fraction, W_R: Rutile weight fraction, S_{BET}: BET surface area, R: Methylene blue decolonization efficiency.

The predicted values were also validated on sample prepared under the optimum condition (Table 4.6). The results show that with the given Pred R^2 for each response, the model equations can be potentially used to predict sol-gel synthesis parameters in the same preparation routes. For further investigation doped and undoped samples were then synthesized at these optimum conditions (N/Ti molar ratio of 6, calcination temperature of 400 ^{O}C and calcination time of 3 h) and their chemical and physical properties were characterized and compared. These analyses are presented as follow:

4.1.6. XPS analysis

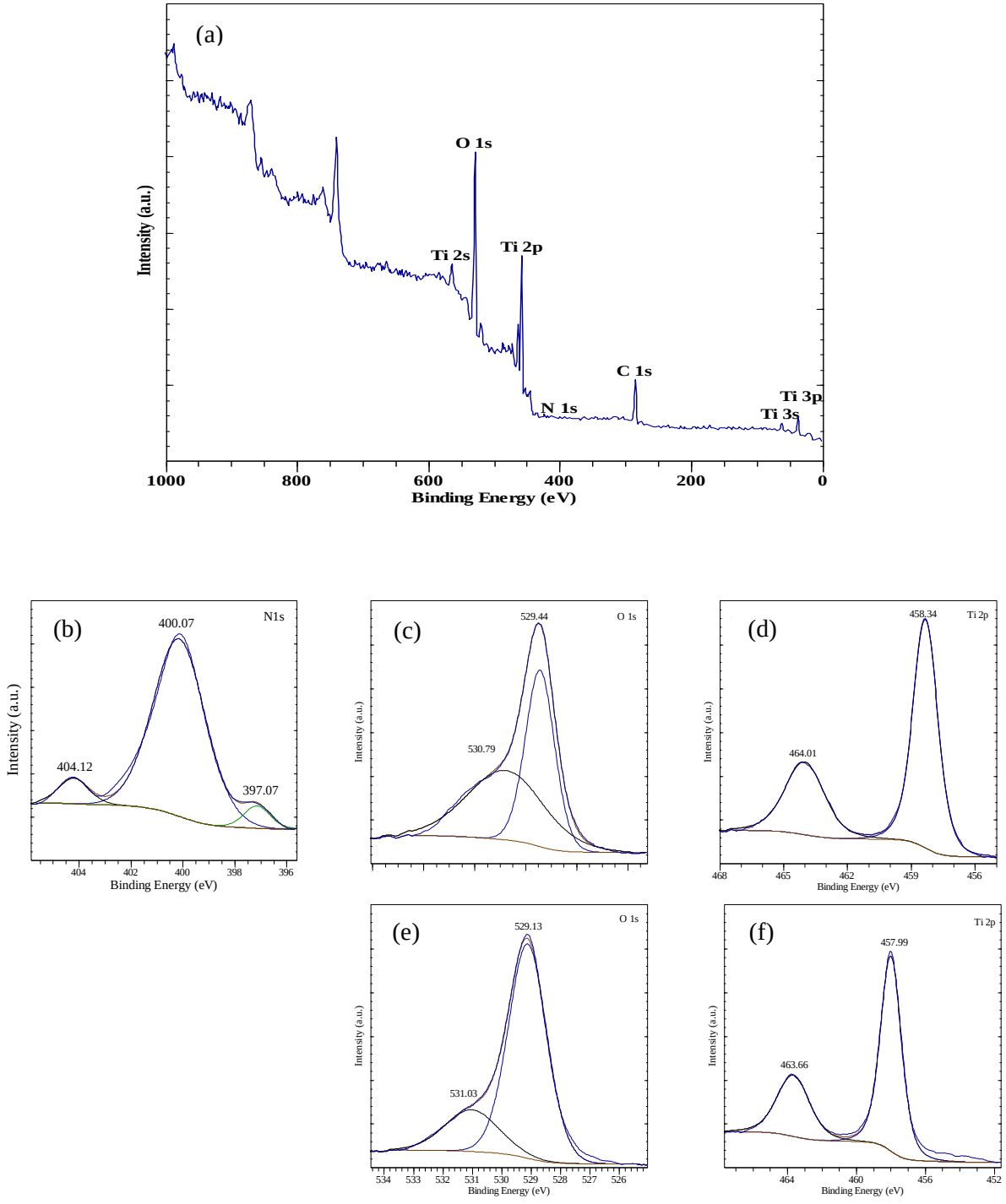

Figure 4. 9 Wide XPS spectra of (a) N-doped TiO_2 and High resolution XPS spectra of doped TiO_2 (b), (c) and (d) and undoped TiO2 (e) and (f), prepared under optimum condition.

The elemental analysis and chemical binding energy of the prepared N-doped TiO_2 sample was determined using X-ray photoelectron spectroscopy (XPS). Figure 4.9 shows the high-resolution spectra of N-doped TiO_2 and undoped samples which were prepared under the optimum condition. From the deconvolution of the N 1s peaks of high-resolution spectra, the atomic concentration of N was found to be around 2.79 % for N-doped TiO_2 (6NT43). The three peaks were detected at 397.06, 400.03 and 404.13 eV binding energies. The exact positions of N atoms are still unclear and under debates. Many previously done studies assigned the position at the various locations from 395-404 eV binding energy based on their preparation routes and nitrogen source. However, in some of the well-known articles, the binding energy of N at 396 eV was surely assigned for atomic ß-N [141], [204], [205]. This binding energy can be further extended to around 397.5 eV [206], [207]. At this site, a substitutional replacement of oxygen by nitrogen takes place within TiO_2 crystal lattice in the form of Ti-N-Ti entity and may act, for visible light, as active site [208]. On the other hand, for interstitial N-doped TiO_2 such as Ti-N-O and/or Ti-O-N oxynitride, there is no common agreement. Generally, the peak approximate to 400 eV is assigned for interstitial N-doping [204], [209]. The binding energy around 397 eV has also as been assigned for interstitial N-doping by some authors [205], [210]. In the present study, N is assigned at 397.07 eV and 400.07 eV for substitutional and interstitial doping, respectively (Figure 22 (b)). Whereas, the other peak at 404.12 was assigned to nitrite (NO_2^-). The peaks for O 1s core level of the N-doped TiO_2 are located at 529.44eV (Figure 22 (c)) and it appears at 529.13 eV for undoped TiO_2 (Figure 22 (e)). In comparison, the undoped O 1s core level decreased by 0.31 eV. Furthermore, Ti $2p_{3/2}$ and $2p_{1/2}$ core level peaks appear at 458.34 and 464.01 eV and 457.99 and 463.66 eV for doped and undoped TiO_2 respectively (Figure 4.9 (d) and Figure (f)). These results indicated that, the binding energy of undoped TiO_2 shift towards lower binding energy by 0.35 eV from doped TiO_2. The binding energy shifts in both cases are implied that the TiO_2 crystal lattice was modified by addition of nitrogen.

4.1.7. UV/Vis analysis

UV/Vis/NIR spectrophotometer was used to evaluate optical properties of both undoped and doped TiO_2 samples (Figure 4.10). For comparison, the maximum optical absorption edge (λ_g) of N-doped TiO_2 which was prepared with optimized parameters (6NT43) and undoped sample (0NT43) are shown in Table 4.7.

Table 4. 7 Maximum adsorption edge and corresponding band gap energy of N doped and undoped TiO_2.

Sample	$\lambda_{g,1}$ (nm)	$E_{g,1}$ (eV)	$\lambda_{g,2}$ (nm)	$E_{g,2}$ (eV)
6NT43	395	3.13	475	2.61
0NT43	388	3.19	-	-

The band gap energy (E_g) of each sample was calculated using the formula:

$$E_g \text{ (eV)} = 1240/\lambda_g \qquad 4.4$$

Many researchers pointed out that the preparation of N-doped TiO_2 shows spectra shift towards the visible light region [130], [201]. Asahi et al. claim that its visible light photoactivity can be related to narrowed band gap by mixing of nitrogen 2p and oxygen 2p state in the valence band caused by substitutional doping [141].

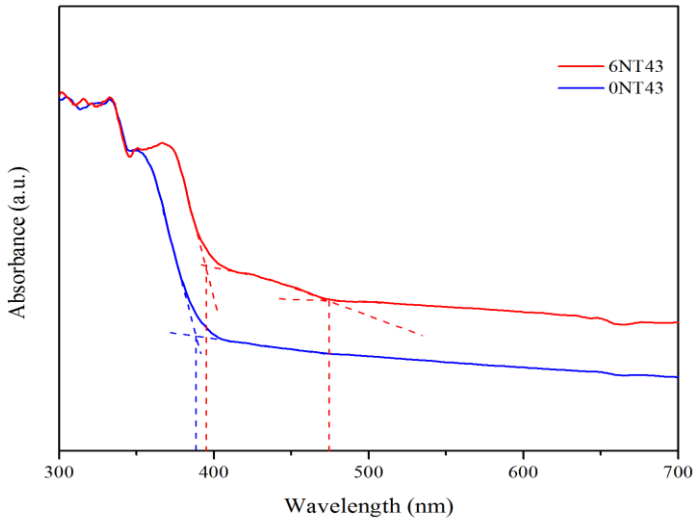

Figure 4. 10 UV-vis spectra of undoped and doped TiO_2 prepared under optimum condition.

In contrast, Burda and his coworker have stated that the extra electronic states just above the valence band edge were the main reasons behind this phenomenon [211]. On the other hand, other reports state that either isolated N impurity energy level (N 2p localized states) forms above the O 2p valence band (0.14 eV) in the case of substitutional doping or JI* character generated by NO bond slightly above the valence band (0.73) in the case of interstitial doping which caused a visible light active N-doped TiO_2 photocatalyst (Figure 4.11) [191], [207], [212], [213]. Furthermore, the formation of oxygen vacancies between the valence and conduction bands during thermal treatment enhance the photocatalysis in the visible range above 500 nm [190], [191], [214]–[216]. In this study, in contrast with undoped TiO_2, the N-doped sample (6NT43) provides two absorption edges; one at 395 nm due to intrinsic band gap absorption typical for anatase in UV region (<400 nm) (charge transition corresponding to the excitation of electrons from the valence band (O 2p) to the conduction band (Ti 3d)) and other additional edge at 475 nm which can be attributed to extrinsic electronic levels (excitation of electrons from N 2p located above valence band O 2p to conduction band Ti 3d) due to substitutional nitrogen doping. This result exhibited the successful doping of nitrogen in TiO_2 lattice.

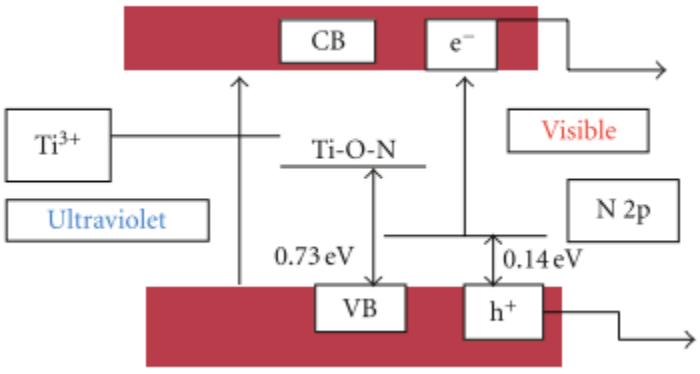

Figure 4. 11 Schematic energy level diagram for nitrogen substituted TiO_2 [Bare semiconductor absorbs UV radiation while the localized energy levels of nitrogen above valence band facilitate the visible light absorption][252].

4.1.8. FT-IR analysis

The FT-IR spectra of N-doped and undoped TiO_2 samples is presented in Figure 4.12. For N-doped TiO_2 FT-IR characterization, the absorption peaks which are located at around 3100-3500 cm^{-1} and 1630-1645 cm^{-1} assigned to stretching and bending vibrations of O-H bond in hydroxyls group and adsorbed water on the surface of TiO_2 [98], [217]. In the present study, these peak intensities were presented at 3344 cm^{-1} and 1637cm^{-1} and were stronger than those of the undoped TiO_2. The adsorbed OH groups are helpful to improve photocatalytic activity of N-doped TiO_2 by serving as an oxidizer for degradation of organic pollutant and giving better charge transfer by interacting the photogenerated holes [217], [218]. Furthermore, on N-doped TiO_2 sample, multi-peaks were shown on the spectra range from 1000 to 1600 cm^{-1} which could be ascribed to different nitrogen species [219]. Especially the strong peak at around 1110 – 1020 cm^{-1} may be due to the formation of hyponitrite species [207], [220]. The appearance of these peaks gives additional evidence and further confirmation for the successful doping of N into the TiO_2 crystal. The other strong peaks in the region 480 -700 cm^{-1} correspond to Ti-O stretching vibration [217], [221], [222].

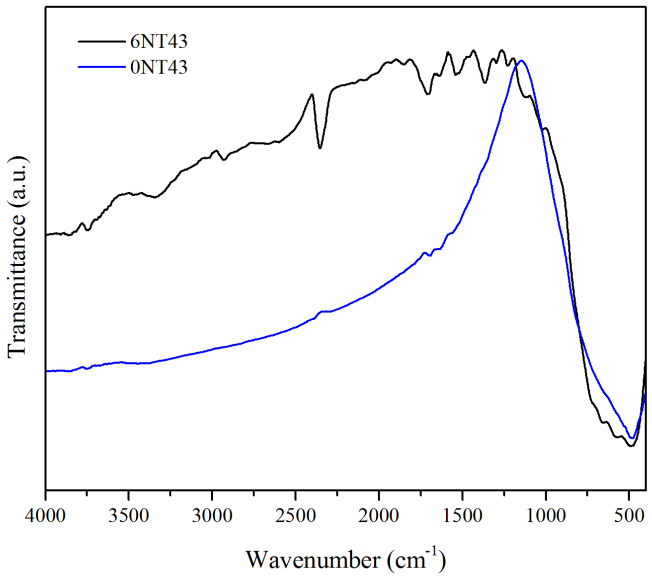

Figure 4. 12 FT-IR spectra of undoped and doped TiO_2 prepared under optimum condition.

4.1.9. Raman analysis

The crystalline structure of the TiO_2 nanoparticles was determined by Raman spectroscopy. Raman spectra of nitrogen doped and undoped TiO_2 samples are shown in Figure 4.13. Both samples show typical anatase crystalline phase with major bands at 144 cm^{-1}, 196 cm^{-1}, 397cm^{-1}, 519 cm^{-1} and 639 cm^{-1}. Moreover, the doped sample did not indicate the presence of nitrogen, which may be because nitrogen is incorporated in the form of substitutional doping. In contrast to the XRD analysis, Raman analysis did not show the presence of rutile phase. This is because at the low rutile mass fraction, Raman spectroscopy can be used only to detect the presence of TiO_2 but not for phase identification [192]. Moreover, the Raman shift can help to identify the particle size difference between doped and undoped TiO_2. Noticeably, the peak at 144 cm^{-1} slightly shifts towards the lower band for doped TiO_2 indicating slightly higher crystal size. This observation is in agreement with the results of the XRD analysis which showed that the addition of nitrogen can enhance the growth of crystals.

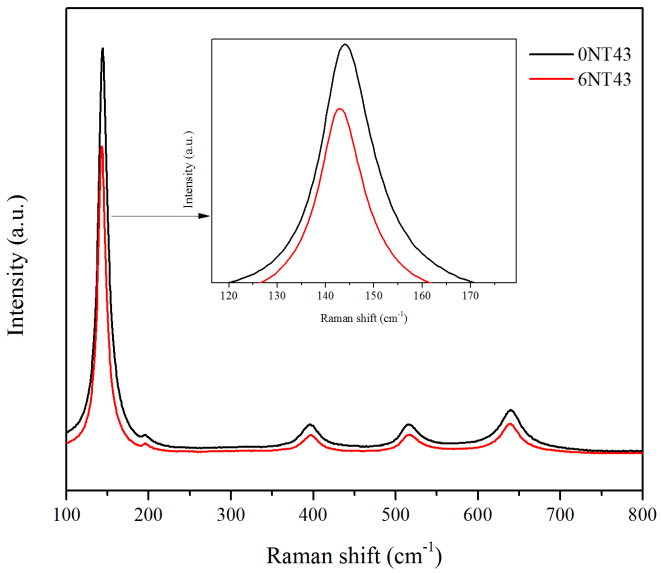

Figure 4. 13 Raman spectra of undoped and doped TiO_2 prepared under optimum condition.

4.1.10. FE-SEM analysis

Analysis of TiO_2 morphology was useful since the photocatalyst oxidation mechanism is explained in terms of surface-oriented adsorption of substrates and of hydroxyl radicals. FE-SEM images of N-doped and undoped TiO_2 are shown in Figure 4.14. As it can be clearly observed from the figure, the nanoparticles in both samples appeared to be agglomerated. However, the N-doped TiO_2 sample exhibited well dispersed particles and a large number of pores. This may be a result of decomposition of ammonia into different gases during heating process. This result is consistent with the BET analysis, which revealed a mesoporous structure.

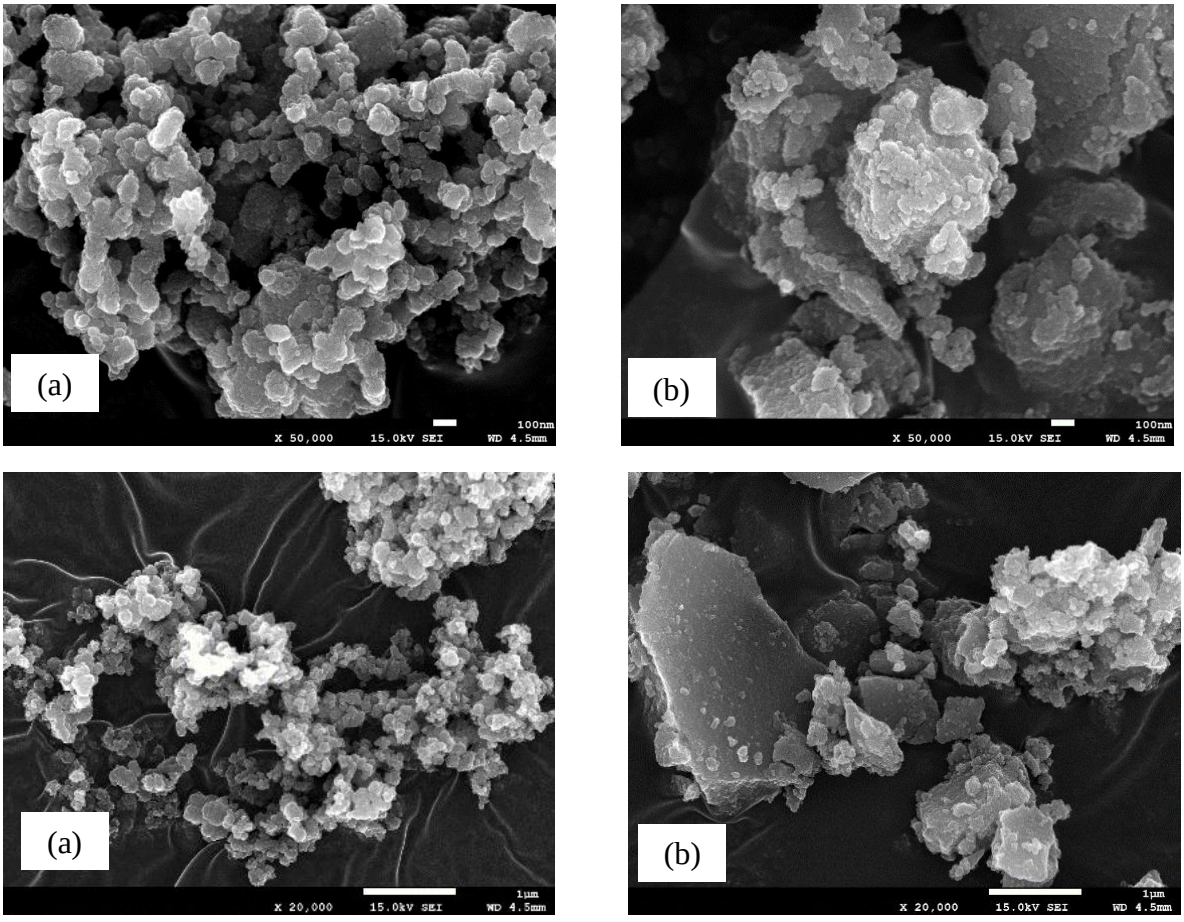

Figure 4. 14 Different resolution of FE-SEM images of doped TiO_2 (a), and undoped TiO2 (b), prepared under optimum condition.

Generally, with this structure, it is possible to achieve enhanced photocatalytic activity as it promotes diffusion and access to reactive sites on the surface of the catalyst [223]. Furthermore, the particles in N-doped TiO_2 sample have also shown irregular spherical shape.

4.1.11. HR-TEM analysis

The morphology and crystal size of nitrogen doped and undoped catalysts are shown in Figure 4.15.

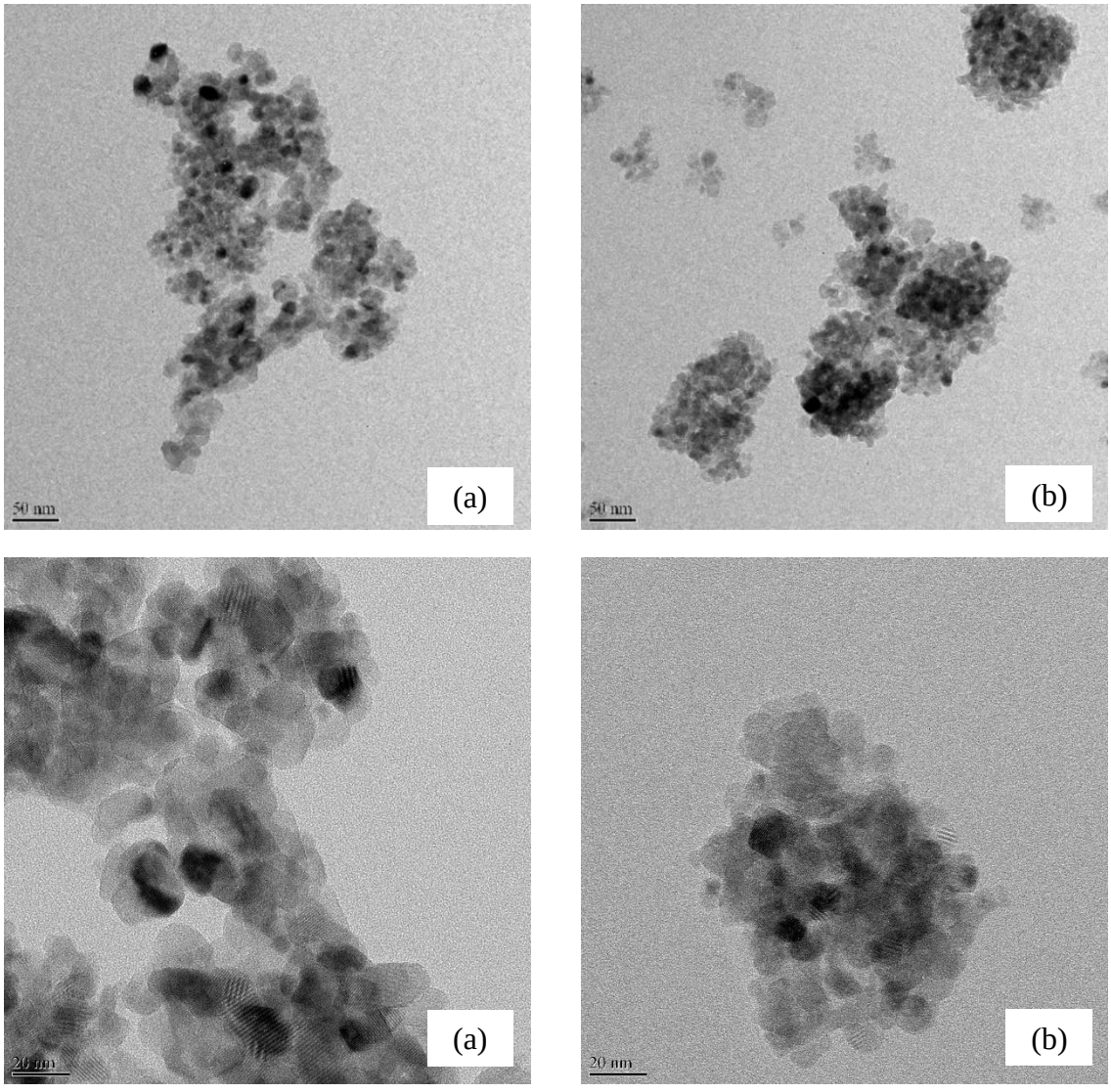

Figure 4. 15 Different resolution of TEM images of doped TiO_2 (a) and (b) undoped TiO_2 prepared under optimum condition.

The TiO_2 particles are seen to be more dispersed in the N-doped sample while more agglomerated in the undoped sample. The average crystallite size was estimated from HR-TEM image analysis using imageJ V 1.50i software, and was found to be in the range of 10-21 nm and 8-16 nm for the N-doped and undoped TiO_2 samples, respectively.

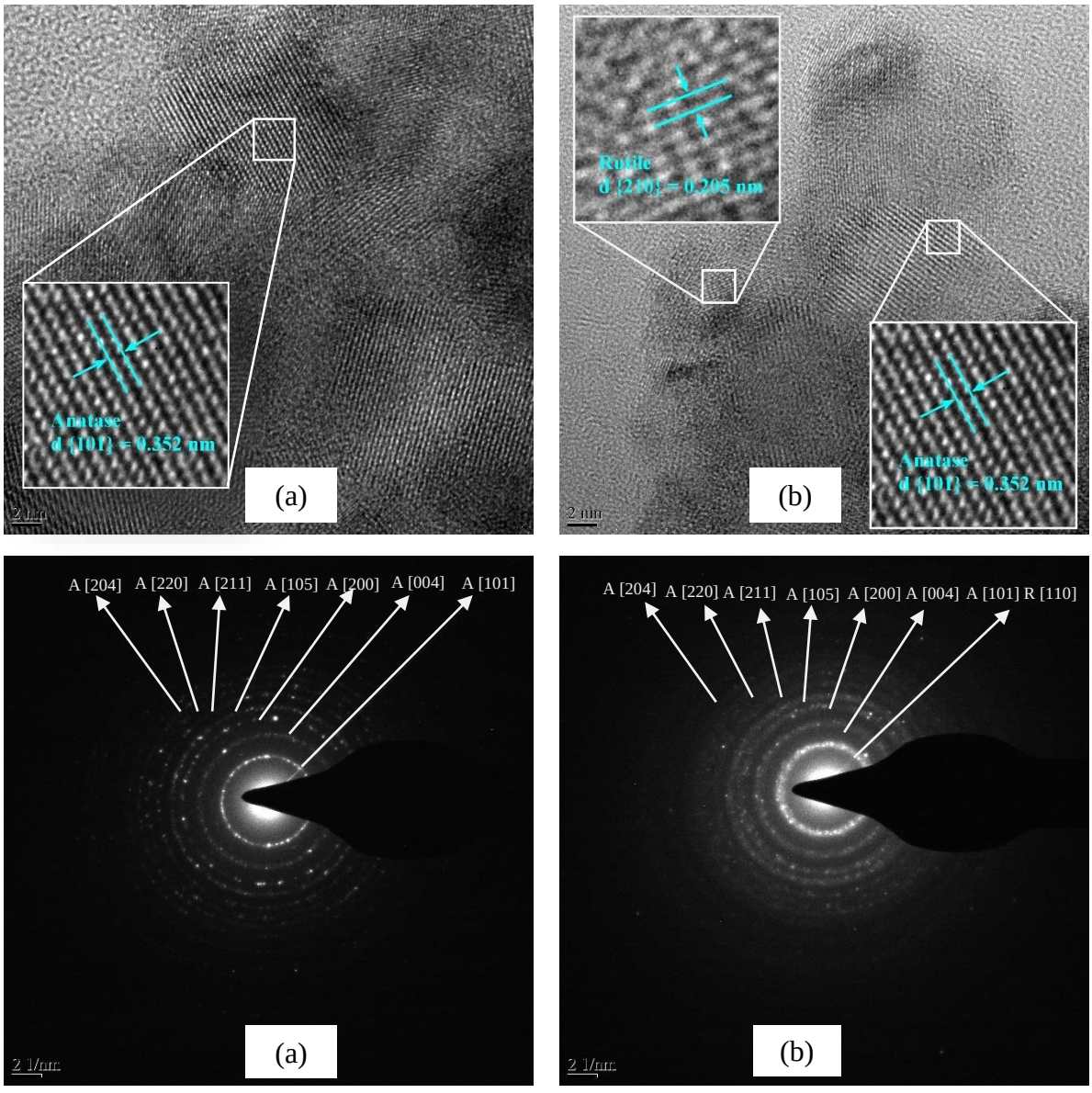

Figure 4. 16 HR-TEM images and corresponding interplanar space and selected area electron diffraction of the (a) doped TiO_2 and (b) undoped TiO_2, prepared under optimum condition.

The fact that larger crystal size was observed for N-doped TiO_2 in both HR-TEM and XRD analysis suggests that the addition of nitrogen can improve the crystal size growth of TiO_2 [23], [192], [224].

Furthermore, the interplanar distances d=0.205 nm for rutile and d=0.352 nm for anatase at (210) and (101) planes indicate good crystallinity (Figure 4.16). In the case of N-doped sample, there was no significant change in lattice space due to the addition of nitrogen. The well-defined selected area electron diffraction (SAED) rings for doped and undoped samples are in good agreement with (JCPDS) Card No 21-1272 and 21-1276 for anatase and rutile phase of TiO_2 nanocrystals in their respective SAED patterns. These well-defined diffraction rings are attributed to the polycrystalline nature of the nanoparticles.

4.1.12. TGA-DSC analysis

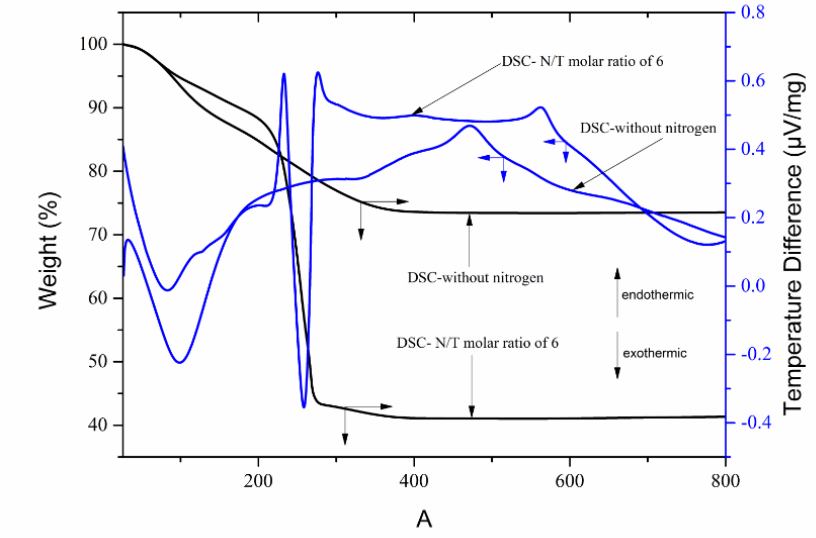

Figure 4. 17 TGA-DSC diagram of TiO_2 xerogel sample prepared with and without addition of nitrogen.

Figure 4.17 shows the TGA-DSC analysis of the TiO_2 xerogel sample prepared with and without addition of nitrogen. The sample prepared with addition of nitrogen shows larger weight loss (59 %). This mainly happened at three steps: (between 26-

210 °C, 210-275 °C, and 275-360 °C). The first step showed approximately 12 % weight lost, due to the evaporation of physically absorbed water and organic solvent such as ethanol in the xerogel. The 46 % weight loss observed in the second step can be associated with the decomposition of organic matters as well as nitrogen species. The weight loss at the third step (about 1 %) could be due to the loss of chemically adsorbed water or non-reactive titanium precursor. This phenomenon was further confirmed by three endothermic peaks at approximately 90 °C, 210 °C and 260 °C on DSC curve. Furthermore, a minor exothermic peak at around 400 °C and a major peak at around 560 °C are associated with a crystallization of amorphous TiO_2 to anatase and a phase transformation of anatase to rutile, respectively. Furthermore, as previously shown from XPS analysis, the presence of nitrogen in the TiO_2 crystal lattice at 400 °C due to strong bond, like Ti-N.

In the case of TiO_2 xerogel sample prepared without addition of nitrogen, a total weight loss of approximately 26 % was observed, which took place in two steps (26-150 °C and 150-400 °C) which may be attributed, respectively to the loss of weakly absorbed water molecule and organic solvent at 150 °C and loss of organic matters at 400 °C. In contrast with TiO_2 xerogel sample prepared with addition of nitrogen, the DSC curve shows a phase transformation of anatase to rutile at 450 °C for sample prepared without addition of nitrogen. These results further confirm the XRD analysis that the addition of nitrogen retarded the formation of rutile and stabilized the anatase phase as previously observed by different researchers [190], [225].

4.1.13. PL analysis

Photoluminescence (PL) emission spectra mainly results from the recombination of excited carriers and have been widely used to investigate the efficiency of charge carrier trapping, migration, and transfer in order to understand the fate of electron–hole pairs in semiconductor particles [216], [226]. Generally, the recombination rate of electron–hole is lower at lower PL intensity [216], [227]. Figure 4.18 shows PL

spectra of undoped and doped TiO_2. A lower PL intensity in the case of N-doped TiO_2 indicates a greater separation of electron–hole pairs as a result of nitrogen doping, which may also imply a higher photocatalytic activity. This, due to an optimum doping concentration, can enhance the photocatalytic performance due to increased separation efficiency of photogenerated electron–hole pairs in the impurity energy levels with an adequate gap so as to inhibit their recombination [201]. This phenomenon is further explained by the two PL possible pathways: (1) the excited electrons are trapped by the oxygen vacancies, while the holes are trapped by the doped nitrogen, thus the recombination rate of electron-holes is reduced; (2) the excited electrons can transfer from the valence band to the new defect levels introduced by nitrogen doping that exist near the minimum of conduction band [201]. At higher concentration of nitrogen doped in TiO_2 may become the recombination site [216].

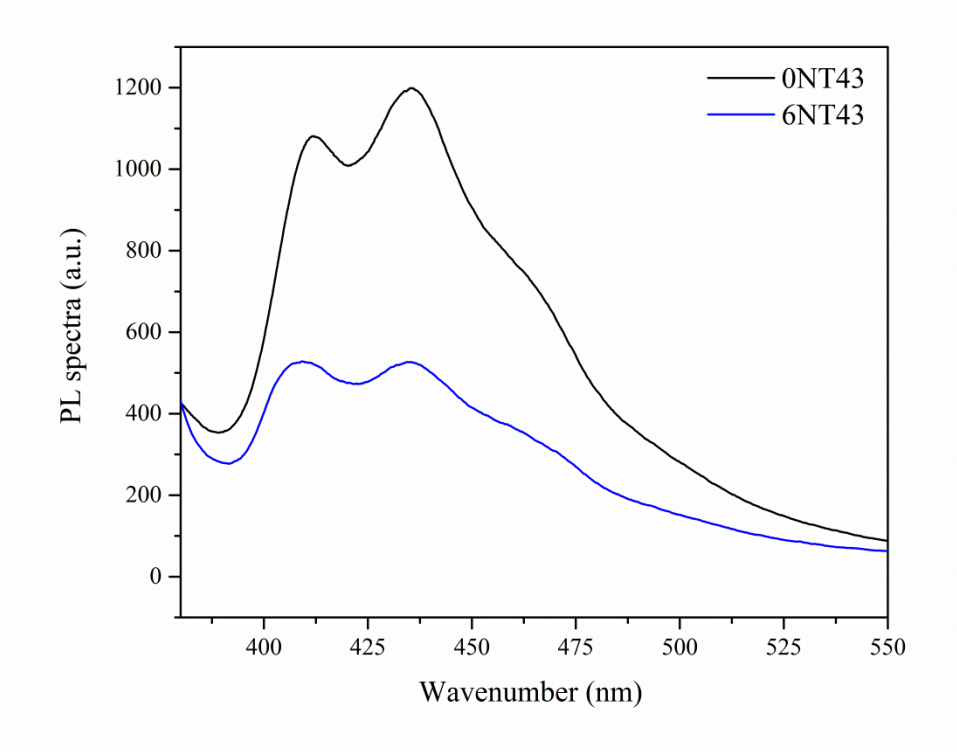

Figure 4. 18 PL spectra of undoped and doped TiO_2 prepared under optimum condition.

4.2. Immobilization of N-doped TiO_2

4.2.1. BET analysis

The specific surface area and pore size distribution of the samples prepared for immobilization were investigated using nitrogen adsorption-desorption analysis. The adsorption-desorption isotherm and pore size distribution are presented in Figures 4.19 and 4.20, respectively. According to IUPAC physisorption isotherms classification, all of the samples show typical type IV and H2 hysteresis loops, indicating a mesoporous material characteristic [228], [229]. However, the sample prepared with TEOS exhibited narrow hysteresis loop and larger surface area compared with pure N-doped TiO_2. This is due to the presence of Si-O-Ti bonds and a larger amount small void spaces between SiO_2/N-doped TiO_2 particles [200], [230]. Furthermore, the pore size in SiO_2/N-TiO_2 sample showed decreasing trend with increase in TEOS concentration. `

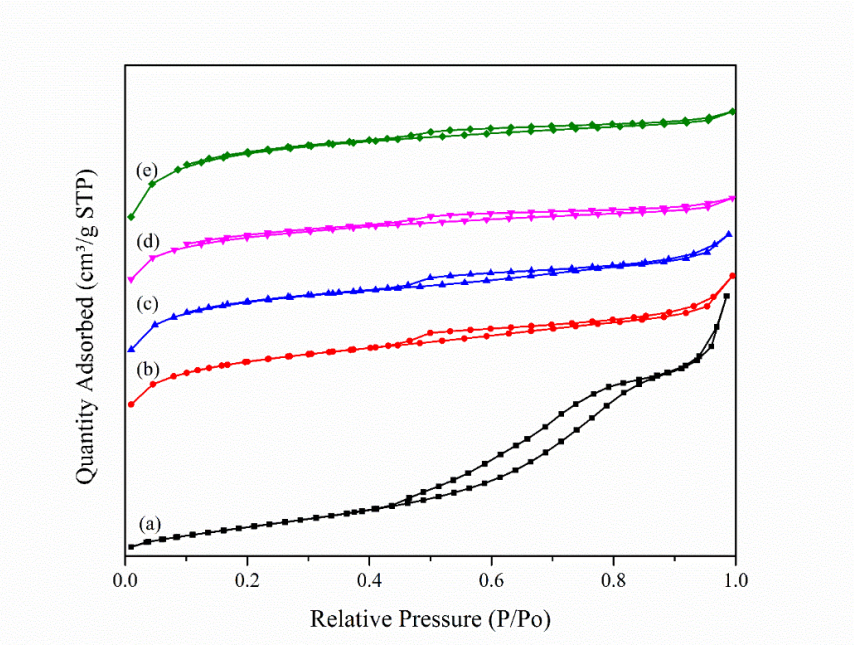

Figure 4. 19 Nitrogen adsorption-desorption isotherms of pure and different concentration of TEOS of N-doped TiO_2.

It is understood that, a larger surface area can improve the photocatalytic activity due to the more available active site on the surface of the catalyst and better mass transfer [24], [27].

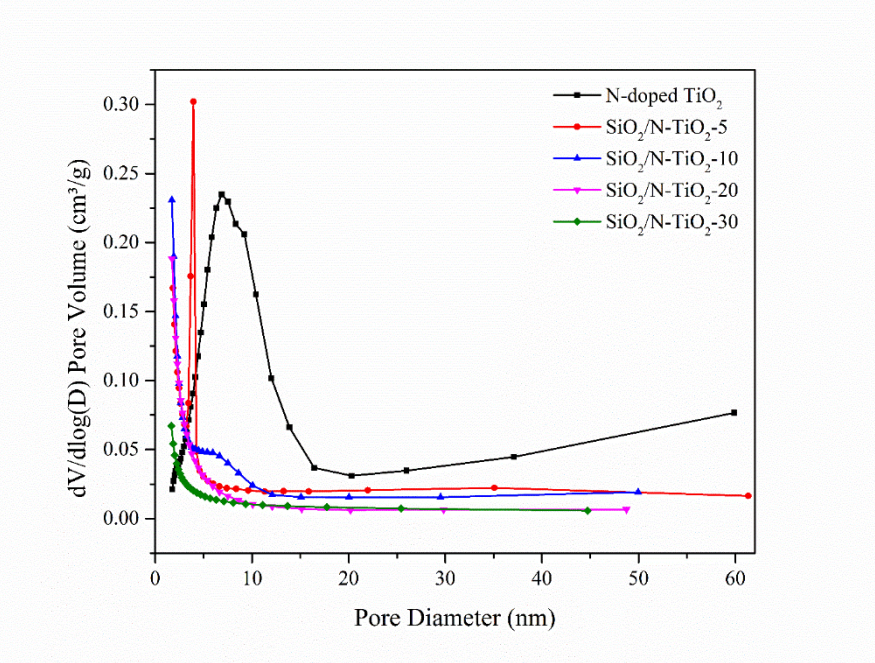

Figure 4. 20 Pore size distribution curve of pure and different concentration of TEOS of N-doped TiO_2.

4.2.2. FT-IR analysis

A FT-IR spectrum of each sample was investigated to see the change in chemical composition due to the addition of TEOS (SiO_2) (Figure 4.21). For all samples, the peaks at about 3325 and 1635 cm^{-1} were assigned to a surface hydroxyl group and adsorbed water molecule respectively [217], [222]. Noticeably, the peak became more intense at these two bands when the amounts of TEOS increased from 0 % for pure N-doped TiO_2 to 30 % for SiO_2/N-TiO_2. This may be due to, either absorbed water molecules from air increasing with the addition of TEOS (SiO_2) or to a higher water holding capacity related to the larger surface area in the case of SiO_2/N-TiO_2 [230]. The presence of OH group on the surface of TiO_2 improves the photoactivity of the

catalyst [218]. The other peaks between 1100 and 1600 cm^{-1} could be related to the presence of nitrogen atom in TiO_2 crystal structure [98], [231], [232]. For the N-doped TiO_2 samples prepared with TEOS solutions (5, 10, 20, 30 %), the figure also shows the presence of adsorption bands at about 1070 cm^{-1} and 940 cm^{-1} related with Si-O-Si asymmetric stretching vibration mode and Si-O-Ti vibration mode, respectively [227], [233]–[235]. The absorption band at about 940 cm^{-1} might be due to Si-OH mode [230]. Furthermore, the peaks at about 500 to 700 were associated with Ti-O stretching vibration [221], [236].

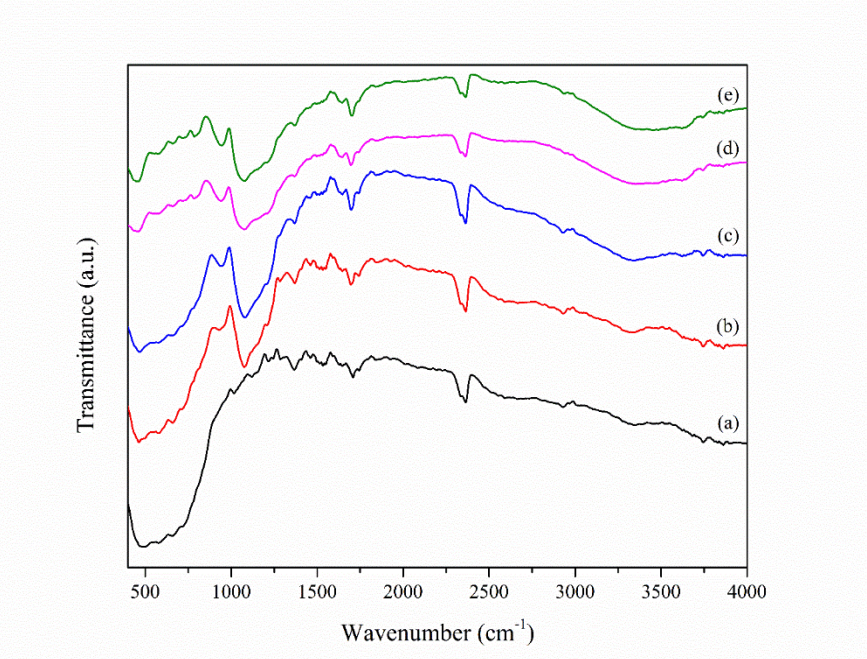

Figure 4. 21 FT-IR spectra of (a) N-doped TiO_2, (b) SiO_2/N-TiO_2-5, (c) SiO_2/N- TiO_2-10, (d) SiO_2/N-TiO_2-20, (e) SiO_2/N-TiO_2-30.

4.2.3. SEM analysis

The FE-SEM images of powder pure N-doped TiO_2 and SiO_2/N-TiO_2 are presented in `Figure 4.22. The particles in both samples tend to aggregate and form a three-dimensional network. However, in the case of SiO_2/N-TiO_2, a high amount of void spaces between the clustered particles was observed. This observation is in agreement with the BET analysis which showed the formation of higher surface area

and smaller pore size with the addition of TEOS as a binder as well as a SiO_2 source [229].

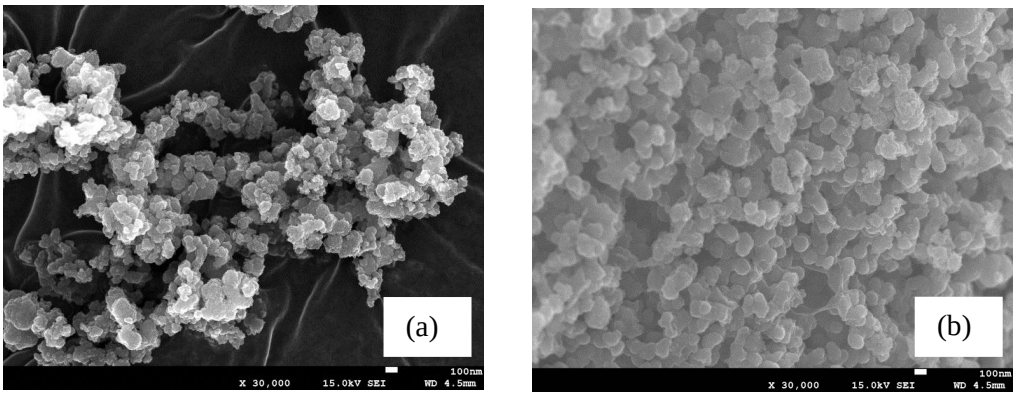

Figure 4. 22 FE-SEM images of (a) N-doped TiO_2, (b) SiO_2/N-TiO_2-5.

Figure 4.23 shows the particle morphology and the film thickness of immobilized SiO2/ N-TiO_2 on a glass surface at first and fifth coating cycle.

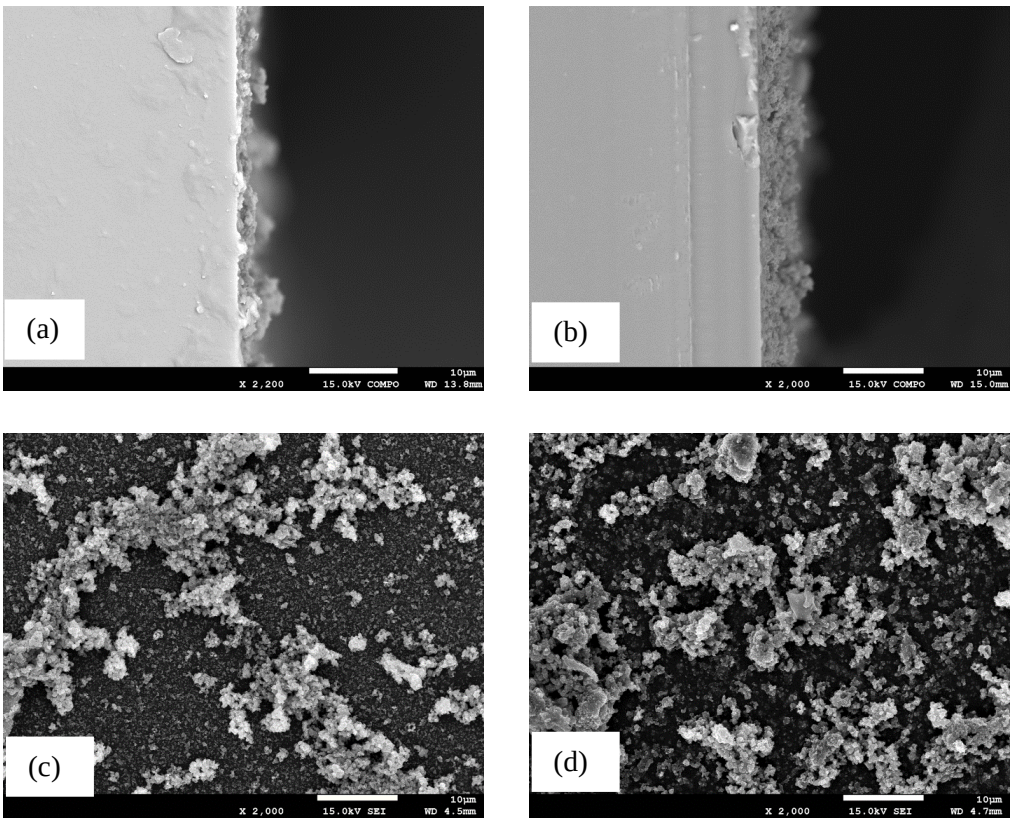

Figure 4. 23 FE-SEM images of films and surface coatings of SiO_2/N-TiO_2-5 of first cycle (a) and (c), SiO_2/N-TiO_2-5 of fifth cycle (b) and (d).

It can be observed from the FE-SEM images, high amount of SiO_2/N-TiO_2 was accumulated on the glass surface at fifth coating cycle as compared with the first coating cycle. This helps to increase the availability of the active site for better photoactivity.

The final average film thickness of immobilized TiO_2 on the glass beads was found to be around 4.5 μm after five repeated coating cycle. Higher amount of immobilized TiO_2 helps to increase the availability of the active site for better photoactivity.

4.2.4. TEM analysis

Figure 4.24 shows the transmission electrons microscopy (TEM) images of powder pure N-doped TiO_2 and the sample prepared with 5 % TEOS (SiO_2/N-TiO_2-5). Noticeably, the crystal morphologies of nanoparticles in SiO_2/N-TiO_2 samples demonstrate highly integrated mesoporous characteristics compared with pure N-doped TiO_2 [228]. The crystal size in both cases was found to be the same. This might be due to the insignificant effects of temperature since low calcination temperature was used for the sample preparation.

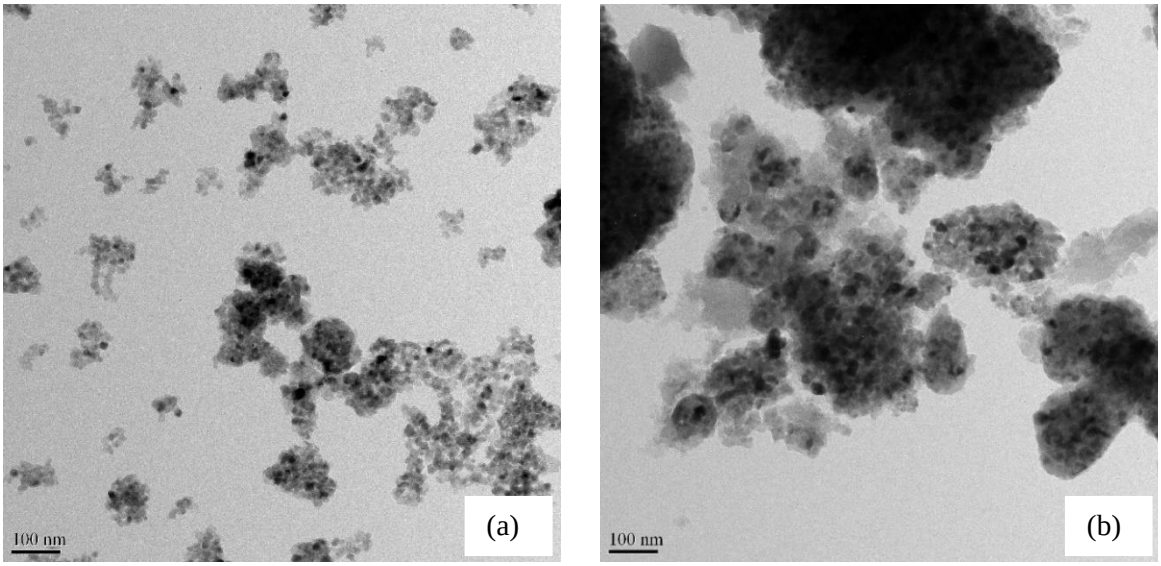

Figure 4. 24 TEM images (a) N-doped TiO_2, (b) SiO_2/N-TiO_2-5.

4.2.5. Adherence test

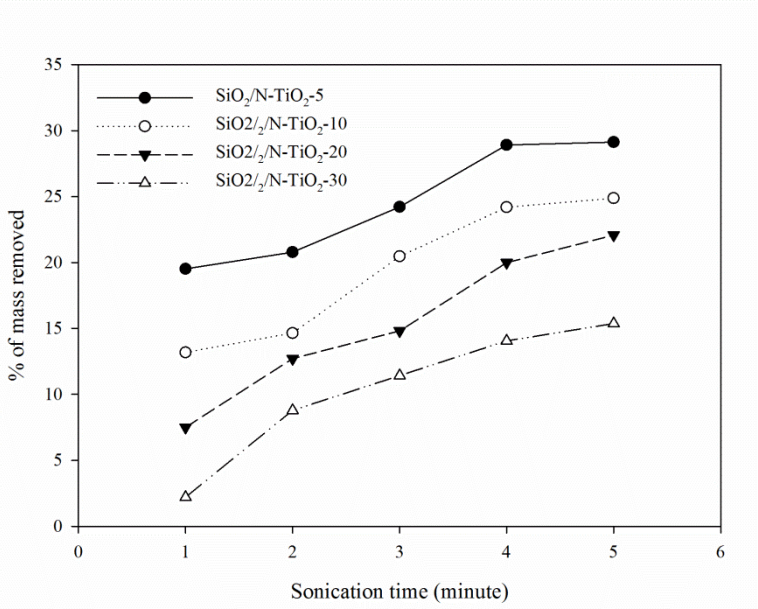

Figure 4. 25 Sonication test of coated N-doped TiO_2 at different TEOS concentration.

The characteristic of adherence to glass support is one of the most important factors for immobilized TiO_2 catalyst since repeated utilization of the catalyst without loss of its photoactivity is highly reliant on this property. The sonication tests were aimed to investigate this property. As shown in Figure 4.25, at each test the mass loss decreased as the percentage of TEOS increased from 5% to 30%. After 5 minutes of sonication test, the amount of mass loss was estimated to be 29.13, 24.88, 22.08, and 15.37 % for 5, 10, 20, and 30% of TEOS added, respectively. Glass coated sample with higher content of TEOS (30%), seemed to exhibit better adherence to the glass beads which may be due to the presence of larger amount of SiO_2 in TEOS for binding the glass and the catalyst. On the other hand, the immobilization of the catalyst without the addition of TEOS was completely lost from the glass surface after 30 second sonication test.

4.2.6. Photoactivity test

Furthermore, the photoactivity of the coated glass bead was also investigated as a function of TEOS content at 3 coating cycle. As can be seen in Figure 4.26 the activity was found to show slight increase when the percentage of TEOS increased from 5 to 10 %. However, further increase in the percentage of TEOS (20 and 30%) showed a decreasing trend in decolorization of methylene blue indicating that higher TEOS content tend to suppress the activity of the catalyst [237]. On the other hand, there was no significant photoactivity for the control run under the same irradiation time.

As the demonstrated in the above analyses (photoactivity and adherence test) the sample with 10 % TEOS seems to have better photoactivity and mechanical stability. However, this difference is only marginal when compared to the sample prepared with 5 % of TEOS. The marginal improvement in photoactivity between 10 % of TEOS and 5 % of TEOS may not be justify the extra cost associated with the higher concentration TEOS.

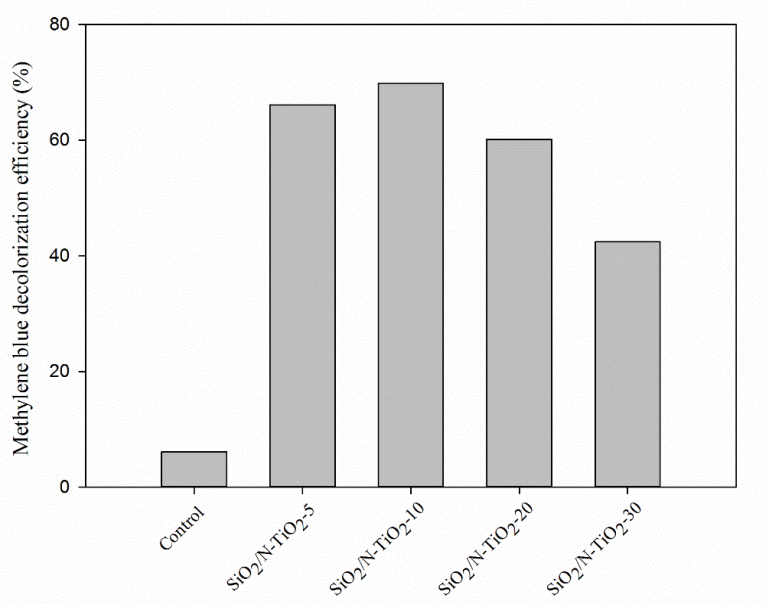

Figure 4. 26 Photocatalytic decolorization of methylene blue of coated N-doped TiO_2 at different TEOS concentration.

Figure 4.27 shows the photodecolorization efficiency of methylene blue on SiO_2/N-TiO_2-5% coated glass beads for different coating cycles. The figure demonstrates that the photodecolorization efficiencies increased as the coating cycles increased. This is obviously related to the increase in the amount of TiO_2 particles on the surface of the glass beads and consequently the increase in film thickness from 1st to 5th coating cycle as observed from FE-SEM analysis (Figure 4.23). The observed efficiencies as calculated using equation 2.1, were about 22, 39, 69, 77 and 98 % for 1st, 2nd, 3rd, 4th and 5th coating cycles, respectively.

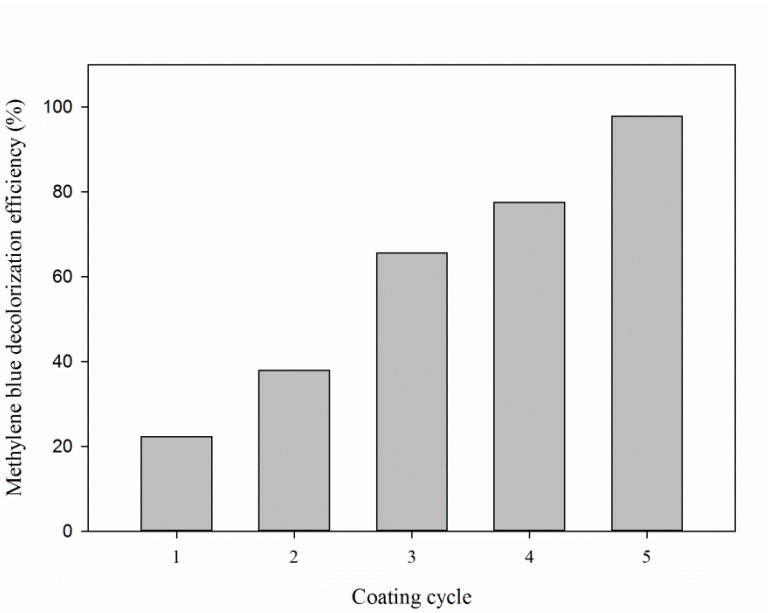

Figure 4. 27 Photocatalytic decolorization of methylene blue of SiO_2/N-TiO_2-5 at different coating cycle.

4.2.7. EDX analysis

An energy dispersive analyzer (EDX) was applied for the qualitative analysis of elements and its distribution in the nanocomposites by mapping each element. As shown in Figure 4.28 the EDX elemental mapping revealed that the uniformLy distributed nitrogen and silicon with in all particles.

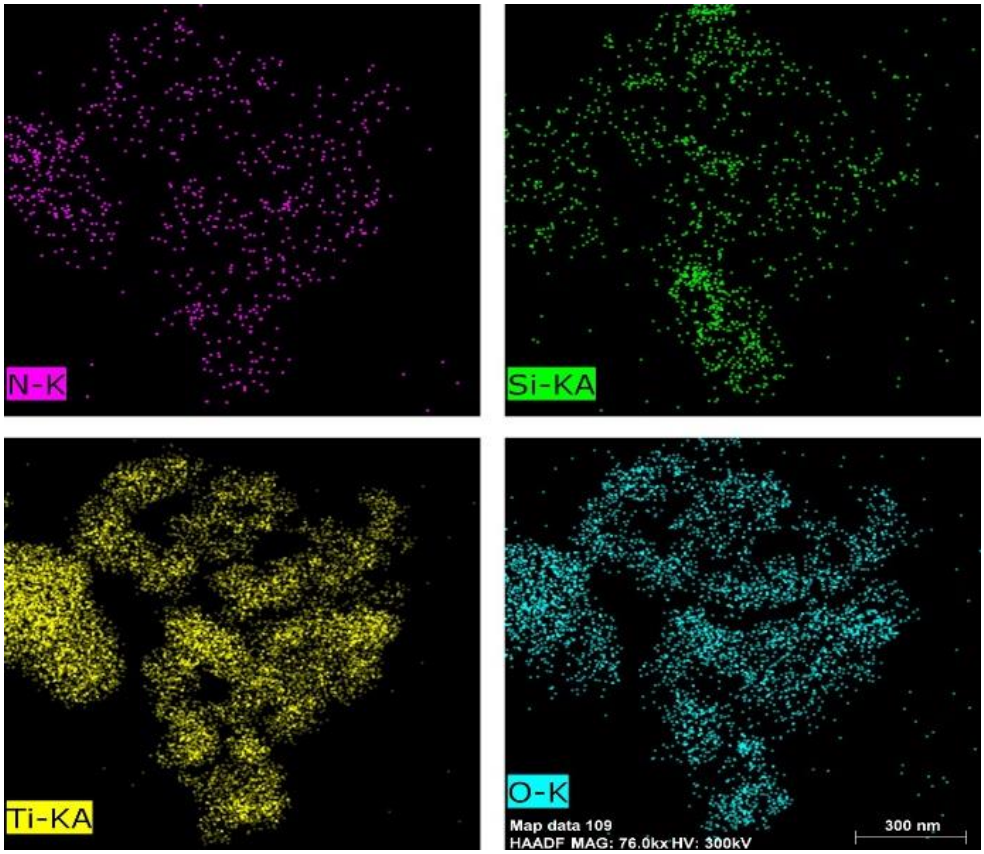

Figure 4. 28 EDX elemental mapping of SiO_2/N-TiO_2-5 %.

4.2.8. Photoactivity of the recycled immobilized TiO_2

The importance of immobilization is to repeatedly use the catalyst without losing its catalytic activity for an extended period of time in practical application. In this respect, the capability of the coated glass beads (5 cycles) was tested several times by probing its photoactivity on decolorization of methylene blue. The results show that the efficiency slightly decreased at each step with only about 6 % reduction after 5 cycles test (Figure 4.29) suggesting that the immobilization has been effective and the catalyst can now be used many times (more than 5 times) without significantly compromising the efficiency.

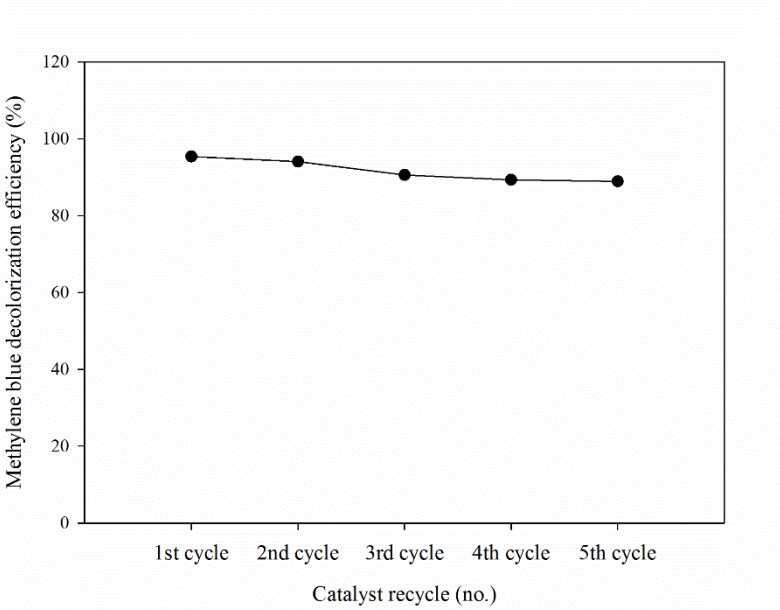

Figure 4. 29 The photocatalytic efficiency of immobilized TiO_2 on decolorization of methylene blue at different catalyst recycles.

4.3. Bacterial photocatalytic inactivation

4.3.1. Effects of operational parameters of the photoreactor

i) Effect of TiO_2 Load

The photocatalytic inactivation of *E. coli* was investigated using different TiO_2 load. The load was controlled by increasing the number of stages in the reactor. The amount of TiO_2 load at each stage was around 0.15 gm. Figure 4.30 illustrates the effects of TiO_2 load on photocatalytic inactivation efficiency. As shown on the figure the inactivation efficiency is highly dependent on the amount of TiO_2 in the reactor. The log unit reduction of *E. coli* was significantly decreased to 3.0 from 5.36 after 2 h when the concentration was increased from 0.3 g (stage 1 and 2) to 0.6 g (stage 1, 2, 3 and 4). This is due to a higher amount of immobilized TiO_2 particle exposed to available light illumination which generates more reactive species and consequently increases the photocatalytic inactivation of *E. coli*.

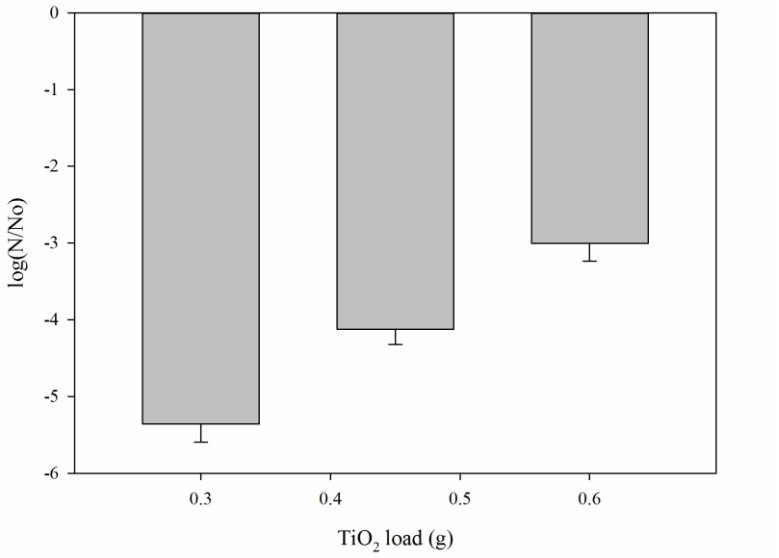

Figure 4. 30 Effects of TiO_2 load on photocatalytic E. coli inactivation (initial E. coli concentration 10^6 CFU mL-1, flow rate 40 mL min^{-1}, incident photon flux 5.23 x 1016 photons/s) ($P<0.05$).

ii) Effect of initial *E. coli* concentration

Figure 4.31 shows the photocatalytic inactivation efficiency of TiO_2 for different initial *E. coli* concentrations. Where a TiO_2 load of 0.6 g (all four stages) and initial *E. coli* concentrations of from 10^3, 10^6 and 10^9 CFU mL^{-1} were subjected to inactivation experiments in a given reactor. The inactivation efficiency was found to be statistically significant between *E. coli* concentrations of 10^3, 10^6 and 10^9. However, at low *E. coli* concentration of 10^3 CFU mL^{-1}, the log unit reduction of *E. coli* was found to be -1.20 while at the initial concentrations of 10^6 and 10^9 CFU mL^{-1} the percentages of surviving *E. coli* were found to be much lower: 5.19 and 2.89, respectively. The observed low photocatalytic inactivation at the lower initial *E. coli* concentration of 10^3 CFU mL^{-1} may be due to a possible minimum close proximity of bacteria surface to immobilized N-doped TiO_2 nanoparticles as previously reported [173], [238]. Furthermore, some researches pointed out at higher bacterial concentration (>10^7) the inactivation efficiency can decrease by competition between internal components (which result from cell disintegration, many dead cell and bacteria) for OH radicals [239].

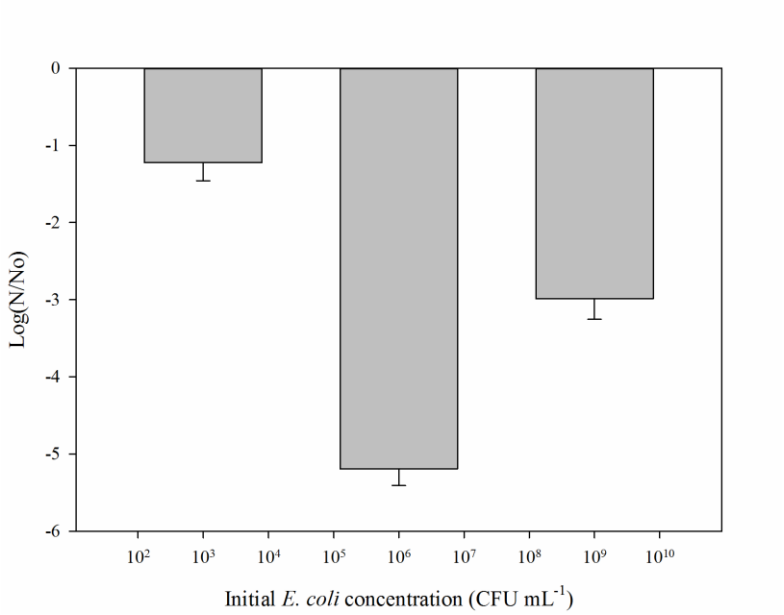

Figure 4. 31 Effects of initial E. coli concentration on photocatalytic E. coli inactivation (TiO_2 concentration 0.6 g, flow rate 40 mL min^{-1}, incident photon flux 5.23 x 10^{16} photons/s) (P<0.05).

iii) Effect of flow rate

Figure 4.32 shows effects of flow rate (range from 40 to 60 mL min^{-1}) under 10^6 CFU mL^{-1} of initial *E. coli* concentration, TiO_2 load of 0.6 g, incident photon flux 5.23 x 10^{16} photons/s, and 2 h of treatment. As demonstrated on the figure the log unit reduction of *E. coli* decreased from 5.54 to 3.08 with increasing flow rate. The effect of flow rate on inactivation efficiency was found statistically significant. This can be explained by the decrease in residence time of the bacterial solution associated with increase in flow rate which lead to insufficient contact between bacteria surface and immobilized TiO_2 at each stage.

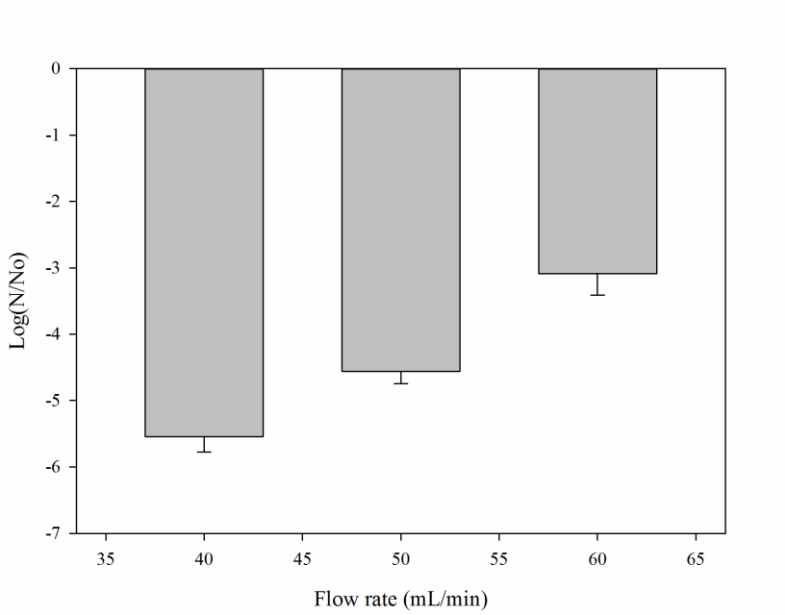

Figure 4. 32 Effects of flow rate on photocatalytic E. coli inactivation (initial E. coli concentration 10^6 CFU mL^{-1}, TiO_2 concentration 0.6 g, incident photon flux 5.23 x 10^{16} photons/s) ($P<0.05$).

iv) Effect of light intensity

The effect of light intensity on photocatalytic *E. coli* inactivation is shown in Figure 4.33. Results show that inactivation efficiency is directly proportional to the light intensity and exhibited a significant effect. The log unit reduction of *E. coli* was found to be 5.69, 4.01, and 2.23 for corresponding vis-LED light incident photon flux of 2.24 x 10^{16}, 3.36 x 10^{16}, and 5.23 x 10^{16} photons/s. The higher incident photon flux provides higher energy for more TiO_2 nanoparticles to produce electron–hole pairs and generate a higher concentration of active oxygen species such as OH · and results in improved photocatalytic inactivation [170], [240].

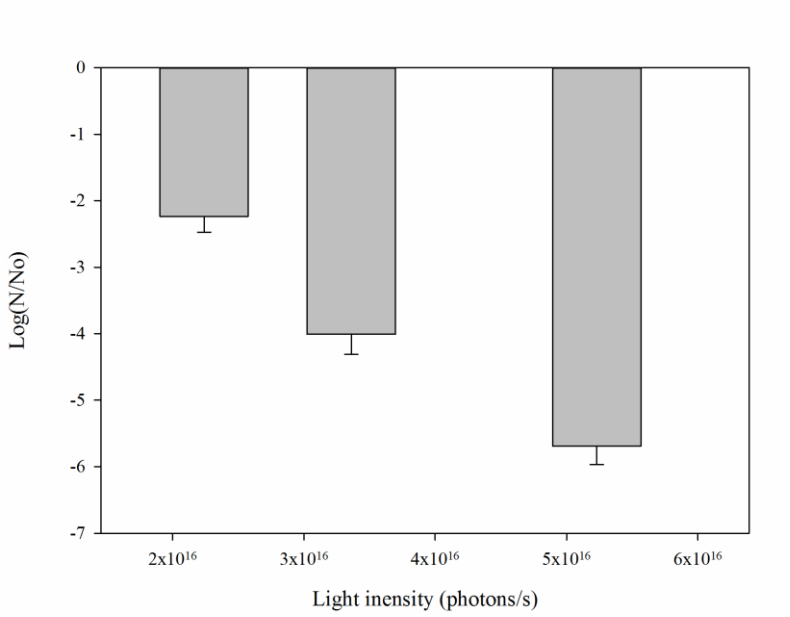

Figure 4. 33 Effects of light intensity on photocatalytic E. coli inactivation (initial E. coli concentration 10^6 CFU mL-1, TiO_2 concentration 0.6 g, flow rate 40 mL min^{-1}) (P<0.05).

From this study, the reactor operational parameters of initial E. coli concentration of 10^6 CFU mL^{-1}, TiO_2 load of 0.6 g, flow rate of 40 mL min^{-1} and incident photon flux of 5.23 x 10^{16} photons/s are selected as an optimum parameter. The following studies of photocatalytic bacterial inactivation efficiency and rate of disinfection was performed on Gram negative and Gram positive bacterial strain using these parameters.

4.3.2. Photocatalytic bacterial inactivation efficiency and rate of disinfection

Figure 4.34, 4.35, 4.36 and 4.37 show the photocatalytic inactivation of Gram-negative bacteria (*E. coli, S. flexneri* and *S. typhimurium) and* Gram-positive bacteria (*B. subtilis, S. aureus)* using N-doped TiO_2 immobilized on glass beads in the proposed multi-stage fixed bed photoreactor under vis-LED and sunlight irradiation. The photocatalytic inactivation on both experiments was investigated under similar conditions but at different irradiation times. There was no bacterial inactivation

under dark control with immobilized N-doped TiO_2 and under sunlight without N-doped TiO_2 for 120 and 40 min irradiation time, respectively.

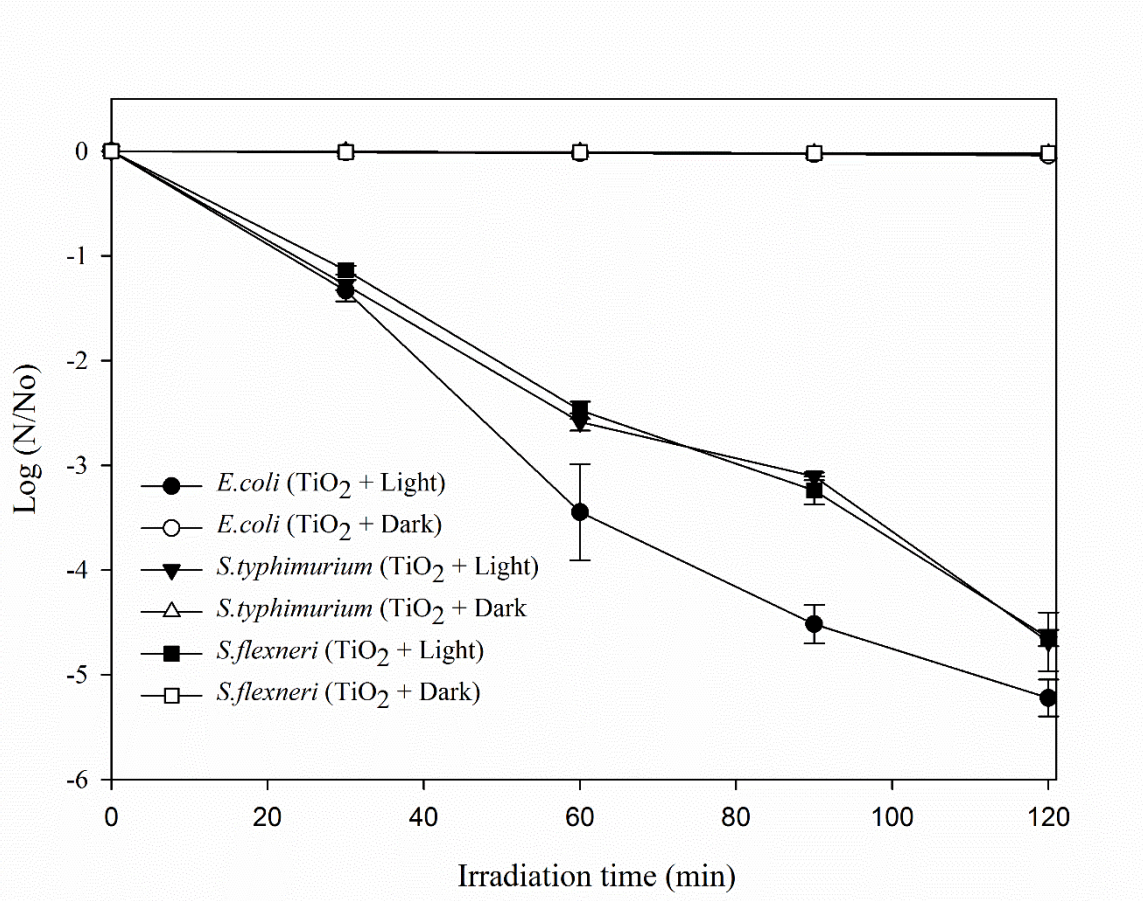

Figure 4. 34 Photocatalytic inactivation of Gram-negative bacteria under vis-LED irradiation.

However, in 120 min visible light irradiation in presence of N-doped TiO_2, log unit reductions of 5.22, 4.69, 4.65, 4.03, and 3.08 were achieved for *E. coli, S. typhimurium S. flexneri, S. aureus* and *B. subtilis,* respectively (Figure 4.34 and 4.35). Comparing the bacterial inactivation among Gram negative strains, statistically significant differences were exhibited between the log unit reduction of *E. coli* and *S. flexneri* as well as *S. flexneri* and *S. typhimurium* ($p \leq 0.001$).

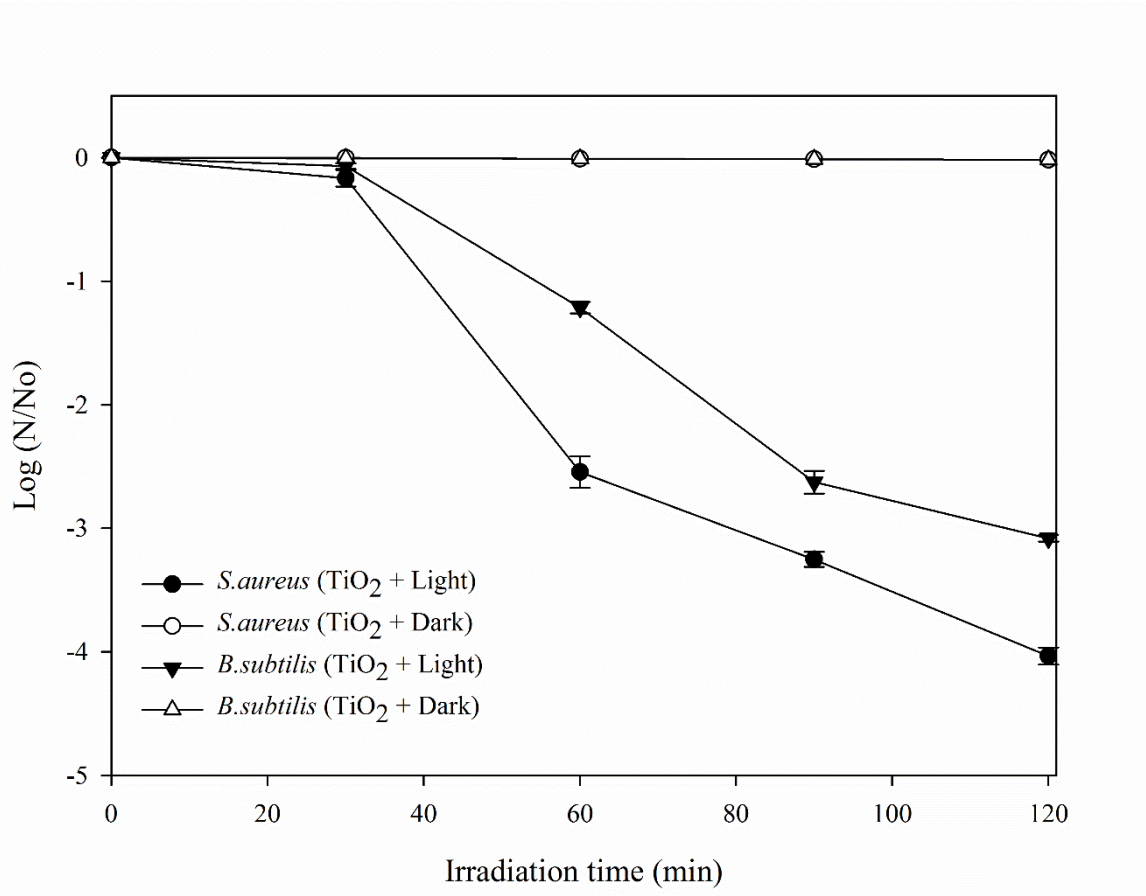

Figure 4. 35 Photocatalytic inactivation of Gram-positive bacteria under vis-LED

However, the difference between of *E. coli* and *S. typhimurium* was not significant. It is worth to note that, *Escherichia coli* demonstrated higher inactivation efficiency as compared to the other selected bacteria strains. Other studies have also pointed out that *Escherichia coli* is the most sensitive Gram negative bacteria towards photocatalytic disinfection treatment [241]–[244].

Similarly, under 40 min sunlight irradiation, log unit reductions of 5.70, 5.05, 4.97, 4.25 and 3.90 were observed for *E. coli*, S. typhimurium, *S. flexneri*, *S. aureus* and *B. subtilis*, respectively (Figure 4.36 and 4.37). As demonstrated here, the experiments under sunlight required only 40 min irradiation to achieve almost complete *E. coli*

removal. Accelerated bacterial inactivation were also reported previously for copper and nitrogen doped TiO_2 in the presence of sunlight [245], [246]

In the present study, the Gram-positive bacteria strains (*S. aureus* and *B. subtilis*) showed the least log unit reduction and the differences were statistically significant ($p \leq 0.001$) when compared to the Gram-negative bacteria strains.

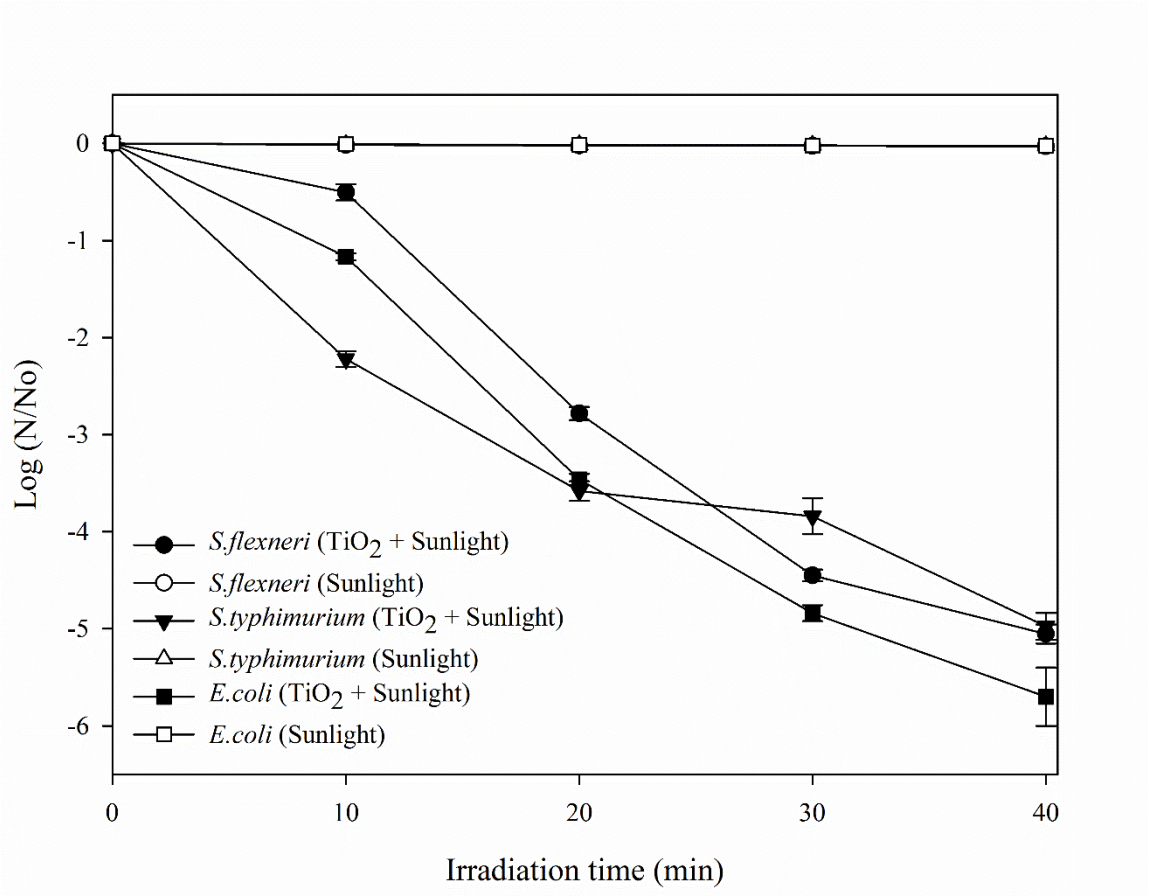

Figure 4. 36 Photocatalytic inactivation of Gram-negative bacteria under sunlight irradiation.

That the Gram-positive bacteria were more resistant to photocatalytic inactivation than the Gram-negative bacteria was also reported elsewhere [239], [247]. This is due to a thick peptidoglycan surface layer structure in the case of Gram-positive bacteria but much thinner peptidoglycan layer and an outer membrane (lipopolysaccharide and phospholipids) in the case of Gram-negative bacteria [248].

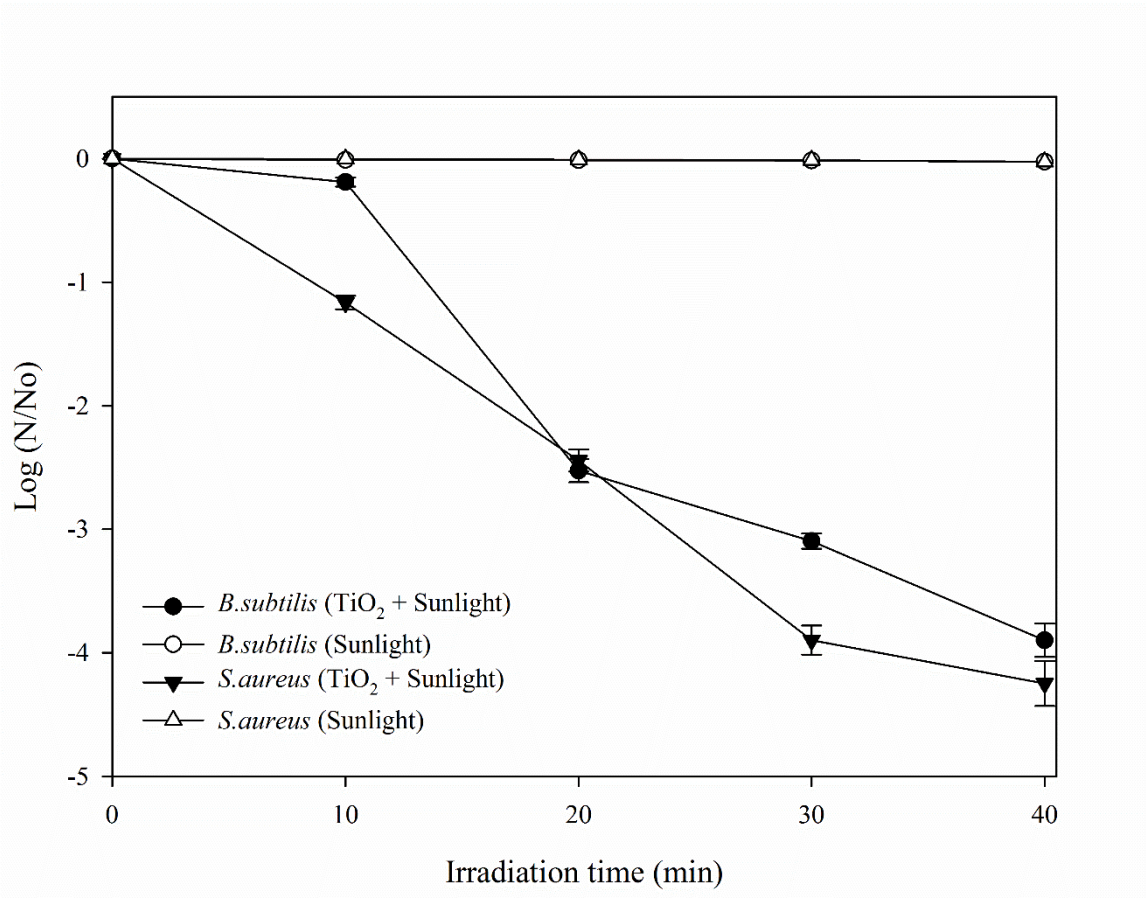

Figure 4. 37 Photocatalytic inactivation of Gram-positive bacteria under sunlight irradiation.

The rate of photocatalytic inactivation of each bacterial strain for both experiments (under Vis-LED and Sunlight) was calculated using the common Chick-Watson disinfection kinetic Model (equation 4.5) [187].

$$\text{Log}(N/No) = kt \qquad 4.5$$

Where No and N are the initial and final number of viable bacteria (CFU mL^{-1}), k is the disinfection kinetic constant (min-1) and t is the inactivation time (min).

As demonstrated in Table 4.8, the inactivation rates under sunlight irradiation were 3 times higher than those under vis-LED irradiation and the differences were statistically significant ($p \leq 0.001$). This can be attributed to the synergetic effects of UV and Vis light spectrum on the activity of the N-doped TiO_2 photocatalyst.

Table 4. 8 Photocatalytic inactivation rate of Gram-negative and Gram-positive bacteria under Vis-LED and sun light irradiation.

Bacteria strain	k (min^{-1}) (Vis-LED)	R^2	k (min^{-1}) (Sunlight	R^2
B.subtilis	0.067	0.971	0.246	0.969
S.aureus	0.086	0.990	0.257	0.974
E.coli	0.104	0.972	0.344	0.982
S.typhimurium	0.085	0.988	0.323	0.975
S.flexneri	0.087	0.993	0.265	0.960

Figure 4.38 (a), (b), (c) and (d) demonstrate scanning electron microscope images of *S. aureus*, *S. flexneri*, *S. typhimurium* and *E. coli* cell surface morphology before and after the photocatalytic inactivation using immobilized N-doped TiO_2. These figures show that the bacteria had intact and normal cell structure before inactivation and damaged cell structures after their contact with immobilized N-doped TiO_2 nanoparticles for 120 min. The damage created on the bacteria as a result of the contact with TiO_2 nanoparticles is usually attributed to the peroxidation of polyunsaturated phospholipid components of the cell structure caused by photo-induced reactive oxygen species (ROS) [17],[249]–[251].

Generally, the photocatalytic bacterial inactivation mechanisms comprises four major steps, these includes the contact between TiO_2 nanoparticle and bacteria cell, oxidative damage on the cell membrane, leakage of intermolecular cell components (such as potassium ion) due to increase in cell permeability, and finally cell death [249]–[251].

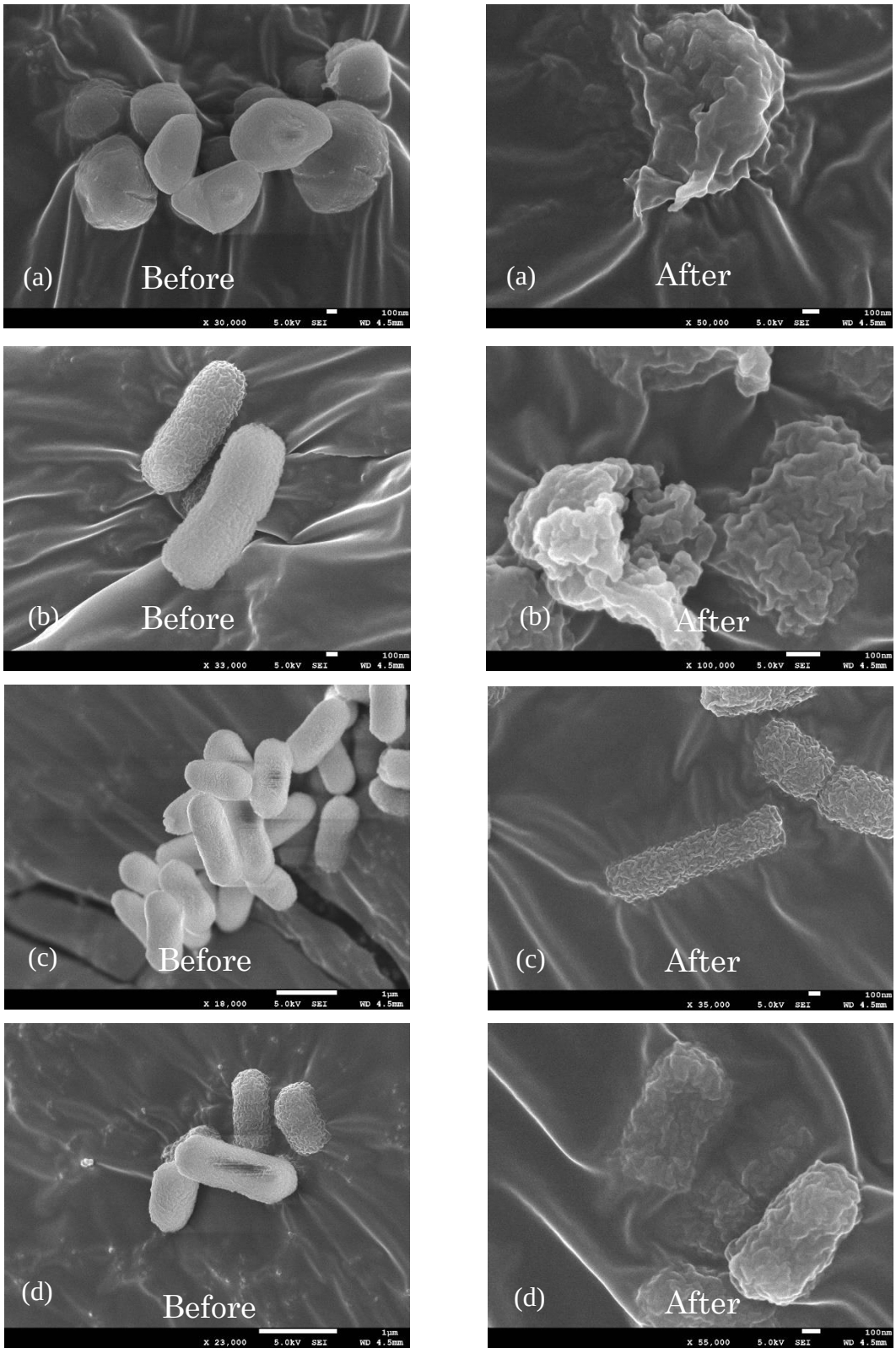

Figure 4. 38 FE-SEM images of cell membrane damage on (a) S. aureus (b) S. flexneri (c) S. typhimurium and (d) E. coli: before and after photocatalytic treatment under vis-LED.

4.3.3. Bacterial inactivation efficiency of the recycled immobilized TiO_2

Recycling of the immobilized TiO_2 is one of the important steps to make this method suitable for sustainable practical use. To this end, immobilized TiO_2 recycling studies were performed using the proposed photoreactor with *E. coli* as test organism. As previously done in section 8.2.8., the catalyst was washed with double distilled water and oven dried at the end of each cycle before the next test. Each cycle was performed in 2 h in a recirculating batch mode with reactor operational parameters of initial *E. coli* concentration of 10^6 CFU mL^{-1}, TiO_2 load of 0.6 g, flow rate of 40 mL, and light intensity of 14 x 10^3 Lux. The photocatalytic bacterial inactivation efficiency was evaluated and compared between the reuse cycles. As demonstrated in Figure 4.39, the log unit reduction of *E. coli* was not significantly decreased with increasing number of cycle. It was observed that the percentage of surviving *E. coli* only reduced by about 0.89 log unit after five-time reuse. This indicates that the immobilized TiO_2 demonstrated good stability after recovery suggesting that the proposed photoreactor can be considered for practical applications.

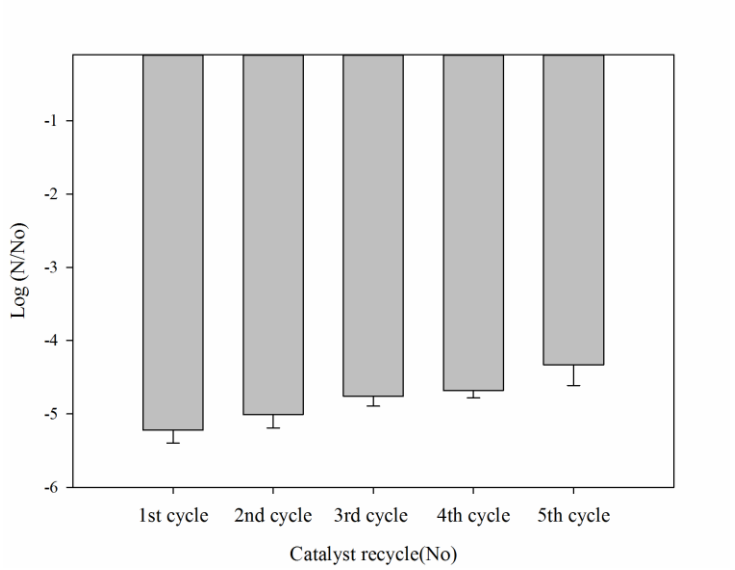

Figure 4.39 the photocatalytic bacterial inactivation efficiency of immobilized TiO_2 catalyst recycles.

Chapter 5

CONCLUSION

In this study, the sol–gel synthesis parameters for the preparation of N-doped TiO_2 were investigated and optimized using the BBD RSM. The study has shown that the experimental method can be used as an excellent tool to identify the interaction effect of the individual sol–gel synthesis parameters. It was also found possible to gather sufficient information about the synthesis method with a limited number of trials. Under optimized process condition, 100 % anatase crystalline phase, BET surface area of 90.99 $m^2 g^{-1}$, and MB decolorization efficiency of 74% were predicted. It is worth to note that all characterization techniques used in the present study have confirmed the successful preparation of visible-light active N-doped TiO_2 with higher specific surface area, larger pore size, smaller crystal size, good crystallinity, and anatase crystal phase.

A simple and low temperature sol-gel method was applied to successfully immobilize visible light active N-doped TiO_2 on the glass beads using TEOS as a binder and SiO_2 source. The effects of TEOS addition was examined on its physical and chemical characteristics, adhesive strength, and photocatalytic activities. The study has shown that the addition of TEOS can significantly improve the mechanical stability of the catalyst on the surface of the glass beads. Better photocatalytic activities were observed at the lower TEOS content (5 and 10 %). 5 % of TEOS which was selected as an optimum TEOS content and gave higher photocatalytic activities and the required adhesive strength for continuous usability.

The effects of different operational parameters of the photoreactor were also studied with the new type of multistage fixed bed photoreactor configured from N-doped TiO_2 in continuous mode. The results exhibited that, the performance of the reactor was

found highly dependent on initial bacterial load, TiO_2 load, flow rate, and light intensity.

Furthermore, photocatalytic inactivation of Gram-positive and Gram-negative bacteria was studied with the new type of multi-stage fixed bed photoreactor configured from N-doped TiO_2 in a recirculating batch mode. It can be seen from the photocatalytic inactivation efficiencies that the proposed photoreactor demonstrated more than 3 log unit reduction of bacterial removal on both under vis-LEDs and sunlight irradiation. Fast inactivation efficiency for all selected bacterial strain was also observed under sunlight irradiation when compared to under vis-LED irradiation. It has been understood that the rate of photocatalytic inactivation on Gram-negative bacteria was found to be higher than the Gram-positive bacteria on both experiments. The bacterial cell membrane damage examined using scanning electron microscope further support the photocatalytic effect of TiO_2 nanoparticles on bacterial cell structure.

Considering the result obtained in the present study, the proposed multi-stage fixed bed photoreactor has a potential in the practical application of bacterial inactivation under either artificial light source such as LEDs or natural sunlight irradiation.

Chapter 6

RECOMMENDATION FOR FURTHER RESEARCH

Visible light activated TiO_2 in drinking water disinfection is an important research topic in practical application of photocatalysis. All experiments were performed under controlled parameters with artificially synthesized bacterial solutions.

Considering the very promising results obtained in this thesis with the above limitations, the following recommendations are suggested for future works:

- ✓ The performance of N-doped TiO_2 in bacterial inactivation should be investigated thoroughly in real wastewater which has variety of minerals composition, basically defined as softness or hardness characteristics which may significantly reduce its performance.
- ✓ The proposed photoreactor should be investigated through modeling and simulation to understand the hydrodynamics nature of the water inside the reactor.
- ✓ The application of N-doped TiO_2 to practical water and wastewater treatment as well as air pollution control are an important research direction in the future.
- ✓ The economic feasibility of this treatment method needs further investigation to confirm its advantages compared to already existing technologies.
- ✓ In practical application of TiO_2 based photocatalysis, there is a lack of researches related with the health impact of TiO_2 and this should be clearly identified before implementing in practical application as disinfectant.

Chapter 7

REFERENCES

[1] UNICEF and World Health Organization, Drinking Water Equity, Safety and Sustainability: Thematic report on drinking water, (2011).

[2] R.K. Sharma, S. Gulati, Water Quality Issues and Solutions in India, Compr. Water Qual. Purif. 1 (2014) 21–39.

[3] The United Nation World Water Development Report, Water for a sustainable world, (2015).

[4] J.K. Mwabi, F.E. Adeyemo, T.O. Mahlangu, B.B. Mamba, B.M. Brouckaert, C.D. Swartz, G. Offringa, L. Mpenyana-Monyatsi, M.N.B. Momba, Household water treatment systems: A solution to the production of safe drinking water by the low-income communities of Southern Africa, Phys. Chem. Earth. 36 (2011) 1120–1128.

[5] J.A. Byrne, P. a. Fernandez-Ibañez, P.S.M. Dunlop, D.M. a Alrousan, J.W.J. Hamilton, Photocatalytic enhancement for solar disinfection of water: A review, Int. J. Photoenergy. 2011 (2011).

[6] J. Ntouda, F. Sikodf, M. Ibrahim, I. Abba, Access to drinking water and health of populations in Sub-Saharan Africa, Comptes Rendus - Biol. 336 (2013) 305–309.

[7] N.F. Gray, Pathogen Control in Drinking Water, Microbiol. Waterborne Dis. Microbiol. Asp. Risks Second Ed. (2013) 537–569.

[8] D. Water, A Snapshot of Drinking Water in Africa Extracted from A Snapshot of Drinking Water and Sanitation in Africa, (2008).

[9] M. African, M.D. Goal, Improving the Quantity, Quality and Use of Africa' s

Water, Africa Environ. Outlook 2 Our Environ. Our Wealth. (2015) 123–174.

[10] Pan African Chemistry Network, Africa' s Water Quality: A chemical Science Perspective, (2010).

[11] Global Development Alliance Safe Drinking Water Alliance, Experiences in Haiti, Ethiopia, and Pakistan: Lessons for future water treatment programs (2008) 34–59.

[12] C. A. Johnson, M. Berg, D. Sabatini, Towards sustainable safe drinking water supply in low- and middle-income countries: The challenges of geogenic contaminants and mitigation measures, Sci. Total Environ. 488–489 (2014) 475–476.

[13] E. Kumpel, K.L. Nelson, Comparing microbial water quality in an intermittent and continuous piped water supply, Water Res. 47 (2013) 5176–5188.

[14] B.H. Rosen, Waterborne Pathogens in, Waterborne Pathog. Detect. Methods Appl. (2000) 1–5.

[15] M.I. Maldonado, J. Blanco, W. Gernjak, S. Malato, P. Ferna, Decontamination and disinfection of water by solar photocatalysis: Recent overview and trends, 147 (2009) 1–59.

[16] M. Muruganandham, R.P.S. Suri, S. Jafari, M. Sillanpää, G. Lee, J.J. Wu, M. Swaminathan, Recent Developments in Homogeneous Advanced Oxidation Processes for Water and Wastewater Treatment, 2014 (2014).

[17] M.N. Chong, B. Jin, C.W.K. Chow, C. Saint, Recent developments in photocatalytic water treatment technology: A review, Water Res. 44 (2010) 2997–3027.

[18] A. Babuponnusami, K. Muthukumar, A review on Fenton and improvements to the Fenton process for wastewater treatment, J. Environ. Chem. Eng. 2 (2014) 557–572.

[19] S. Ahmed, M.G. Rasul, R. Brown, M. A. Hashib, Influence of parameters on the heterogeneous photocatalytic degradation of pesticides and phenolic contaminants in wastewater: A short review, J. Environ. Manage. 92 (2011) 311–330.

[20] J. Ananpattarachai, P. Kajitvichyanukul, S. Seraphin, Visible light absorption ability and photocatalytic oxidation activity of various interstitial N-doped TiO_2 prepared from different nitrogen dopants, J. Hazard. Mater. 168 (2009) 253–261.

[21] C. Dunnill, Z. Ansari, A. Kafizas, S. Perni, D. Morgan, M. Wilson, I. Parkin, Visible light photocatalysts-N-doped TiO_2 by sol-gel, enhanced with surface bound silver nanoparticle islands, (2011) 11854–11861.

[22] X. Huang, Y. Tang, C. Hu, H. Yu, C. Chen, Preparation and characterization of visible-light-active nitrogen-doped TiO_2 photocatalyst, J. Environ. Sci. 17 (2005) 562–565.

[23] Y.T. Lin, C.H. Weng, H.J. Hsu, Y.H. Lin, C.C. Shiesh, The synergistic effect of nitrogen dopant and calcination temperature on the visible-light-induced photoactivity of N-doped TiO_2, Int. J. Photoenergy. 2013 (2013) 1–13.

[24] Y. Nosaka, M. Matsushita, J. Nishino, A.Y. Nosaka, Nitrogen-doped titanium dioxide photocatalysts for visible response prepared by using organic compounds, Sci. Technol. Adv. Mater. 6 (2005) 143–148.

[25] H.L. Qin, G.B. Gu, S. Liu, Preparation of nitrogen-doped titania using sol-gel technique and its photocatalytic activity, Mater. Chem. Phys. 112 (2008) 346–352.

[26] Y. Wang, C. Feng, M. Zhang, J. Yang, Z. Zhang, Visible light active N-doped TiO_2 prepared from different precursors: Origin of the visible light absorption and photoactivity, Appl. Catal. B Environ. 104 (2011) 268–274.

[27] H. Yu, X. Zheng, Z. Yin, F. Tag, B. Fang, K. Hou, Preparation of nitrogen-doped TiO_2 nanoparticle catalyst and its catalytic activity under visible light, Chinese J. Chem. Eng. 15 (2007) 802–805.

[28] M. Alzamani, A. Shokuhfar, E. Eghdam, S. Mastali, Study Of Annealing Temperature Variation On The Structural Properties Of Dip-Coated TiO_2-SiO_2 Nanostructured Films, Iran. J. Mater. Sci. Eng. 10 (2013) 39–45.

[29] M. Bideau, B. Claudel, C. Dubien, L. Faure, H. Kazouan, On the "immobilization" of titanium dioxide in the photocatalytic oxidation of spent waters, J. Photochem. Photobiol. A Chem. 91 (1995) 137–144.

[30] Z. Zhang, S.M. Meunier, J. Gamage, Z. Duvnjak, Design and characterization of a novel rotating corrugated drum reactor for wastewater treatment, Int. J. Photoenergy. 2010 (2010).

[31] R. van Grieken, J. Marugán, C. Sordo, C. Pablos, Comparison of the photocatalytic disinfection of E. coli suspensions in slurry, wall and fixed-bed reactors, Catal. Today. 144 (2009) 48–54.

[32] R. Portela, S. Suárez, R.F. Tessinari, M.D. Hernández-Alonso, M.C. Canela, B. Sánchez, Solar/lamp-irradiated tubular photoreactor for air treatment with transparent supported photocatalysts, Appl. Catal. B Environ. 105 (2011) 95–102.

[33] M. Adams, N. Skillen, C. McCullagh, P.K.J. Robertson, Development of a doped titania immobilised thin film multi tubular photoreactor, Appl. Catal. B Environ. 130–131 (2013) 99–105.

[34] M.J. Yu, B.W. Kim, Photocatalytic cell disruption of Giardia lamblia in a UV/TiO_2 immobilized optical-fiber reactor, J. Microbiol. Biotechnol. 14 (2004) 1105–1113.

[35] G. Vincent, P.M. Marquaire, O. Zahraa, Abatement of volatile organic

compounds using an annular photocatalytic reactor: Study of gaseous acetone, J. Photochem. Photobiol. A Chem. 197 (2008) 177–189.

[36] Z. Zhang, W. a. Anderson, M. Moo-Young, Radiation modeling of air phase corrugated plate photocatalytic reactor, Dyn. Contin. Discret. Impuls. Syst. Ser. B Appl. Algorithms. 11 (2004) 59–68.

[37] E. Sahle-Demessie, S. Bekele, U.R. Pillai, Residence time distribution of fluids in stirred annular photoreactor, Catal. Today. 88 (2003) 61–72.

[38] O. Richter, H. Hoffmann, B. Kraushaar-Czarnetzki, Effect of the rotor shape on the mixing characteristics of a continuous flow Taylor-vortex reactor, Chem. Eng. Sci. 63 (2008) 3504–3513.

[39] N.F. Gray, Pathogen Control in Drinking Water, Microbiol. Waterborne Dis. Microbiol. Asp. Risks Second Ed. (2013) 537–569.

[40] S. Krauss, C. Griebler, Pathogenic Microorganisms and Viruses in Groundwater, (2011).

[41] Cell wall of Gram-positive bacteria with Gram-negative bacteria, (2015). https://www.boundless.com/biology/textbooks (accessed June 16, 2015).

[42] D.O.F. Philosophy, A TiO_2 Photoelectrocatalytic System For Wastewater Detoxification And Disinfection ,(2009).

[43] E. Tigabu, B. Petros, T. Endeshaw, Prevalence of giardiasis and cryptosporidiosis among children in relation to water sources in selected village of Pawi Special District in Benishangul-Gumuz Region, northwestern Ethiopia, Ethiop. J. Heal. Dev. 24 (2010) 205–213.

[44] M. Demena, A. Workie, Water Borne Disease, (2003).

[45] S. Drinking, W. Act, P. Our, H. From, S. To, Drinking Water Treatment, (2004) 32–34.

[46] M.P. Abdullah, L.F. Yee, S. Ata, A. Abdullah, B. Ishak, K.N.Z. Abidin, The study of interrelationship between raw water quality parameters, chlorine demand and the formation of disinfection by-products, Phys. Chem. Earth. 34 (2009) 806–811.

[47] A. Jessen, A. Randall, D. Reinhart, L. Daly, Effectiveness and kinetics of ferrate as a disinfectant for ballast water., Water Environ. Res. 80 (2008) 561–569.

[48] R. Rahmani, M.R. Samarghandi, M.T. Samadi, F. Nazemi, Photocatalytic Disinfection of Coliform Bacteria Using UV TiO_2, Heal. Sci. 9 (2009) 1–6.

[49] S.D. Richardson, Disinfection by-products: formation and occurrence of drinking water, Encycl. Environ. Heal. Vol. 2. (2011) 110–136.

[50] M. Serrano, I. Montesinos, M.J. Cardador, M. Silva, M. Gallego, Seasonal evaluation of the presence of 46 disinfection by-products throughout a drinking water treatment plant, Sci. Total Environ. 517 (2015) 246–258.

[51] D. Venieri, E. Chatzisymeon, M.S. Gonzalo, D. Mantzavinos, irradiation in water and wastewater : culture techniques never say the whole truth, (2011) 1744–1750.

[52] P. Xu, M.L. Janex, P. Savoye, A. Cockx, V. Lazarova, Wastewater disinfection by ozone: Main parameters for process design, Water Res. 36 (2002) 1043–1055.

[53] D. Bermúdez-Aguirre, G. V. Barbosa-Cánovas, Disinfection of selected vegetables under nonthermal treatments: Chlorine, acid citric, ultraviolet light and ozone, Food Control. 29 (2013) 82–90.

[54] J.G. Den Blanken, Comparative disinfection of treated sewage with chlorine and ozone. Effect of nitrification, Water Res. 19 (1985) 1129–1140.

[55] G. Li, A TiO_2 Photoelectrocatalytic System for Wastewater Detoxification and Disinfection, Griffith University, (2009).

[56] Y. Zhang, Y. Zhuang, J. Geng, H. Ren, Y. Zhang, L. Ding, K. Xu, Science of the

Total Environment Inactivation of antibiotic resistance genes in municipal wastewater effluent by chlorination and sequential UV / chlorination disinfection, 513 (2015) 125–132.

[57] Safe Drinking Water Foundation, Conventional Water Treatment: Coagulation and Filtration, (2000) 1–6.

[58] C. Ray, R. Jain, Disinfection Systems, Low Cost Emergency Water Purification Technologies. Water Purif. Technol. (2014) 55–86.

[59] O.-M. Lee, H.Y. Kim, W. Park, T.-H. Kim, S. Yu, A comparative study of disinfection efficiency and regrowth control of microorganism in secondary wastewater effluent using UV, ozone, and ionizing irradiation process, J. Hazard. Mater. 295 (2015) 201–208.

[60] V. Lazarova, P. Savoye, M.L. Janex, E.R. Blatchley, M. Pommepuy, Advanced wastewater disinfection technologies: State of the art and perspectives, Water Sci. Technol. 40 (1999) 203–213.

[61] D. Wang, J.R. Bolton, S. a. Andrews, R. Hofmann, Formation of disinfection by-products in the ultraviolet/chlorine advanced oxidation process, Sci. Total Environ. 518–519 (2015) 49–57.

[62] C. Tian, R. Liu, H. Liu, J. Qu, Disinfection by-products formation and precursors transformation during chlorination and chloramination of highly-polluted source water: Significance of ammonia, Water Res. 47 (2013) 5901–5910.

[63] B. a. Lyon, A.D. Dotson, K.G. Linden, H.S. Weinberg, The effect of inorganic precursors on disinfection byproduct formation during UV-chlorine/chloramine drinking water treatment, Water Res. 46 (2012) 4653–4664.

[64] W.K. Jo, R.J. Tayade, Facile photocatalytic reactor development using nano-TiO_2 immobilized mosquito net and energy efficient UVLED for industrial dyes

effluent treatment, J. Environ. Chem. Eng. 4 (2016) 319–327.

[65] K.K. Jyoti, a. B. Pandit, Ozone and cavitation for water disinfection, Biochem. Eng. J. 18 (2004) 9–19.

[66] U. Von Gunten, Ozonation of drinking water: Part II. Disinfection and by-product formation in presence of bromide, iodide or chlorine, Water Res. 37 (2003) 1469–1487.

[67] A.R. Ribeiro, O.C. Nunes, M.F.R. Pereira, A.M.T. Silva, An overview on the advanced oxidation processes applied for the treatment of water pollutants defined in the recently launched Directive 2013/39/EU, Environ. Int. 75 (2015) 33–51.

[68] Us Epa, Ozone Chemistry, EPA Guid. Man. (1999) 1–52.

[69] N.F. Gray, Ozone Disinfection, Second Edi, Elsevier, 2013.

[70] M. and Alvarado, Ozone Disinfection for Drinking Water, (2010).

[71] A. Cesaro, D. Mantzavinos, Water And Wastewater Disinfection By Ultrasound Irradiation- A Critical Review, 16 (2014) 561–577.

[72] K.Y.K. Wong, Ultrasound As a role or Synergistic Disinfectiant Drinking Water, (2002) 1–113.

[73] S. Rahim Pouran, A.A. Abdul Raman, W.M.A. Wan Daud, Review on the application of modified iron oxides as heterogeneous catalysts in Fenton reactions, J. Clean. Prod. 64 (2014) 24–35.

[74] A. Selvakumar, M.E. Tuccillo, S. Muthukrishnan, A.B. Ray, Use of Fenton's Reagent as a Disinfectant, Remediat. J. 19 (2009) 135–142.

[75] H. Hassan, B. Hameed, Fenton-like Oxidation of Acid Red 1 Solutions Using Heterogeneous Catalyst Based on Ball Clay, Int. J. Environ. Sci. Dev. 2 (2011) 218–222.

[76] N. De la Cruz, R.F. Dantas, J. Giménez, S. Esplugas, Photolysis and TiO_2 photocatalysis of the pharmaceutical propranolol: Solar and artificial light, Appl. Catal. B Environ. 130–131 (2013) 249–256.

[77] I. García-Fernández, I. Fernández-Calderero, M.I. Polo-López, P. Fernández-Ibáñez, Disinfection of urban effluents using solar TiO_2 photocatalysis: A study of significance of dissolved oxygen, temperature, type of microorganism and water matrix, Catal. Today. (2014).

[78] K.J. Klabunde, M.N. Weerasinghe, Photocatalysts for Elimination of Toxins on Surfaces and in Air Using UV and Visible Light, (2013) 1–17.

[79] M.L. Rodrigues, M. Alvarez, F.L. Fonseca, A. Casadevall, Binding of the wheat germ lectin to Cryptococcus neoformans suggests an association of chitinlike structures with yeast budding and capsular glucuronoxylomannan, Eukaryot. Cell. 7 (2008) 602–609.

[80] J. Mo, Y. Zhang, Q. Xu, J.J. Lamson, R. Zhao, Photocatalytic purification of volatile organic compounds in indoor air: A literature review, Atmos. Environ. 43 (2009) 2229–2246.

[81] Z. Cheng, K. Ting, Y. Tao, A. Goh, X. Yin, Nano-Semiconductors As Photocatalysts, 20 (2010) 281–286.

[82] X. Wei, G. Zhu, J. Fang, J. Chen, Synthesis , Characterization , and Photocatalysis of Well-Dispersible Phase-Pure Anatase TiO 2 Nanoparticles, Int. J. Photoenergy. 2013 (2013).

[83] D.P. Macwan, P.N. Dave, S. Chaturvedi, A review on nano-TiO_2 sol–gel type syntheses and its applications, J. Mater. Sci. 46 (2011) 3669–3686.

[84] P.C. Ricci, C.M. Carbonaro, L. Stagi, M. Salis, A. Casu, S. Enzo, F. Delogu, Anatase-to-rutile phase transition in TiO_2 nanoparticles irradiated by visible light, J. Phys. Chem. C. 117 (2013) 7850–7857.

[85] B. Sun, P.G. Smirniotis, Interaction of anatase and rutile TiO_2 particles in aqueous photooxidation, Catal. Today. 88 (2003) 49–59.

[86] V. Diesen, Heterogeneous TiO 2 Photocatalysis - Fundamental Chemical Aspects and Effects of Solid Phase Alterations, (2013) 962–1123.

[87] D.M. Blake, P.-C. Maness, Z. Huang, E.J. Wolfrum, J. Huang, W. a. Jacoby, Application of the Photocatalytic Chemistry of Titanium Dioxide to Disinfection and the Killing of Cancer Cells, Sep. Purif. Rev. 28 (1999) 1–50.

[88] J. Kumar, A. Bansal, Photocatalysis by Nanoparticles of Titanium Dioxide for Drinking Water Purification: A Conceptual and State-of-Art Review, Mater. Sci. Forum. 764 (2013) 130–150.

[89] A.O. Ibhadon, P. Fitzpatrick, M. Sciences, C. Road, C. Innovation, C.T. Park, Heterogeneous Photocatalysis: Recent Advances and Applications, (2013) 1–29.

[90] A.H. Jawad, M. a. Nawi, Fabrication, optimization and application of an immobilized layer-by-layer TiO_2/Chitosan system for the removal of phenol and its intermediates under 45-W fluorescent lamp, React. Kinet. Mech. Catal. 106 (2012) 49–65.

[91] R.C. Pawar, C.S. Lee, Basics of Photocatalysis, Catal. Sci. Technol. (2015) 1–23.

[92] A. Zaleska, Doped-TiO_2: A Review, Recent Patents Eng. 2 (2008) 157–164.

[93] Y. Wang, C. Feng, M. Zhang, J. Yang, Z. Zhang, Visible light active N-doped TiO_2 prepared from different precursors: Origin of the visible light absorption and photoactivity, Appl. Catal. B Environ. 104 (2011) 268–274.

[94] M. Pelaez, N.T. Nolan, S.C. Pillai, M.K. Seery, P. Falaras, A.G. Kontos, P.S.M. Dunlop, J.W.J. Hamilton, J.A. Byrne, K. O'Shea, M.H. Entezari, D.D. Dionysiou, A review on the visible light active titanium dioxide photocatalysts for environmental applications, Appl. Catal. B Environ. 125 (2012) 331–349.

[95] R.S. Reports, Application of Titanium Dioxide Photocatalysis to Construction

Materials, (2011).

[96] M.J. Wu, T. Bak, P.J.O. Doherty, M.C. Moffitt, J. Nowotny, T.D. Bailey, C. Kersaitis, Photocatalysis of Titanium Dioxide for Water Disinfection : Challenges and Future Perspectives, 2014 (2014).

[97] B. Ohtani, K. Iwai, H. Kominami, T. Matsuura, Y. Kera, S. Nishimoto, Titanium(IV) oxide photocatalyst of ultra-high activity for selective N-cyclization of an amino acid in aqueous suspensions, Chem. Phys. Lett. 242 (1995) 315–319.

[98] G. Yang, Z. Jiang, H. Shi, T. Xiao, Z. Yan, Preparation of highly visible-light active N-doped TiO2 photocatalyst, J. Mater. Chem. 20 (2010) 5301.

[99] M. Baek, J. Hong, J. Yoon, J. Suh, Photocatalytic Degradation of Humic Acid by Fe-TiO 2 Supported on Spherical Activated Carbon with Enhanced Activity, 2013 (2013) 4–9.

[100] M.R. Hoffmann, M.R. Hoffmann, S.T. Martin, S.T. Martin, W. Choi, W. Choi, D.W. Bahnemannt, D.W. Bahnemannt, Environmental Applications of Semiconductor Photocatalysis, Chem. Rev. 95 (1995) 69–96.

[101] Y. Cai, M. Strømme, K. Welch, Disinfection Kinetics and Contribution of Reactive Oxygen Species When Eliminating Bacteria with TiO_2 Induced Photocatalysis, J. Biomater. Nanobiotechnol. 5 (2014) 200–209.

[102] M. Cho, H. Chung, W. Choi, J. Yoon, Linear correlation between inactivation of E. coli and OH radical concentration in TiO_2 photocatalytic disinfection, Water Res. 38 (2004) 1069–1077.

[103] O.K. Dalrymple, Mechanistic Modeling of Photocatalytic Water Disinfection, (2011).

[104] X. Lin, J. Li, S. Ma, G. Liu, K. Yang, M. Tong, D. Lin, Toxicity of TiO_2 nanoparticles to Escherichia coli: effects of particle size, crystal phase and

water chemistry, PLoS One. 9 (2014) e110247.

[105] Z. Zhang, J. Gamage, Applications of photocatalytic disinfection, Int. J. Photoenergy. 2010 (2010).

[106] R. van Grieken, J. Marugán, C. Pablos, L. Furones, A. López, Comparison between the photocatalytic inactivation of Gram-positive E. faecalis and Gram-negative E. coli faecal contamination indicator microorganisms, Appl. Catal. B Environ. 100 (2010) 212–220.

[107] Y. Cai, Titanium Dioxide Photocatalysis in Biomaterials Applications, 2013.

[108] D.M. A. Alrousan, P.S.M. Dunlop, T. a. McMurray, J.A. Byrne, Photocatalytic inactivation of E. coli in surface water using immobilised nanoparticle TiO_2 films, Water Res. 43 (2009) 47–54.

[109] G. Balasubramanian, D.D. Dionysiou, M.T. Suidan, I. Baudin, J.M. Laîné, Evaluating the activities of immobilized TiO2 powder films for the photocatalytic degradation of organic contaminants in water, Appl. Catal. B Environ. 47 (2004) 73–84.

[110] P. Lei, F. Wang, X. Gao, Y. Ding, S. Zhang, J. Zhao, S. Liu, M. Yang, Immobilization of TiO_2 nanoparticles in polymeric substrates by chemical bonding for multi-cycle photodegradation of organic pollutants, J. Hazard. Mater. 227–228 (2012) 185–194.

[111] R.A. Aziz, I. Sopyan, Synthesis of TiO_2-SiO_2 powder and thin film photocatalysts by sol-gel method, Indian J. Chem. - Sect. A Inorganic, Phys. Theor. Anal. Chem. 48 (2009) 951–957.

[112] S. Alijani, M. Vaez, A.Z. Moghaddam, Photocatalytic Degradation of Acid Red 73 Using TiO_2 Nanoparticles Immobilized on Alumina Foam, Int. J. Environ. Sci. Dev.5 (2014) 2–5.

[113] M. a Lazar, S. Varghese, S.S. Nair, Photocatalytic Water Treatment by

Titanium Dioxide: Recent Updates, Catalysts. 2 (2012) 572–601.

[114] A. Hänel, P. Moreń, A. Zaleska, J. Hupka, Photocatalytic Activity of TiO_2 Immobilized on glass Beads, Physicochecal Probl. Miner. Process ,45 (2010) 49–56.

[115] J. Zhu, T. Wang, X. Xu, P. Xiao, J. Li, Pt nanoparticles supported on SBA-15: Synthesis, characterization and applications in heterogeneous catalysis, Appl. Catal. B Environ. 130–131 (2013) 197–217.

[116] S. Sakthivel, M. V Shankar, M. Palanichamy, B. Arabindoo, V. Murugesan, Photocatalytic decomposition of leather dye Comparative study of TiO_2 supported on alumina and glass beads, 148 (2002) 153–159.

[117] A. S. El-Kalliny, S.F. Ahmed, L.C. Rietveld, P.W. Appel, Immobilized photocatalyst structure assuring optimal light distribution in a solar reactor, Drink. Water Eng. Sci. Discuss. 7 (2014) 59–94.

[118] S. Buzby, M.A. Barakat, H. Lin, C. Ni, S.A. Rykov, J.G. Chen, S. Ismat Shah, Visible light photocatalysis with nitrogen-doped titanium dioxide nanoparticles prepared by plasma assisted chemical vapor deposition, J. Vac. Sci. Technol. B Microelectron. Nanom. Struct. 24 (2006) 1210.

[119] K. Natarajan, T.S. Natarajan, H.C. Bajaj, R.J. Tayade, Photocatalytic reactor based on UV-LED/TiO_2 coated quartz tube for degradation of dyes, Chem. Eng. J. 178 (2011) 40–49.

[120] E.F. Duffy, F. Al Touati, S.C. Kehoe, O. A. McLoughlin, L.W. Gill, W. Gernjak, I. Oller, M.I. Maldonado, S. Malato, J. Cassidy, R.H. Reed, K.G. McGuigan, A novel TiO_2-assisted solar photocatalytic batch-process disinfection reactor for the treatment of biological and chemical contaminants in domestic drinking water in developing countries, Sol. Energy. 77 (2004) 649–655.

[121] D. Hao, Z. Yang, C. Jiang, J. Zhang, Photocatalytic activities of TiO_2 coated on

different semiconductive SiC foam supports, J. Mater. Sci. Technol. 29 (2013) 1074–1078.

[122] M. Tasbihi, C.R. Ngah, N. Aziz, A. Mansor, A.Z. Abdullah, L.K. Teong, A.R. Mohamed, Lifetime and regeneration studies of various supported TiO_2 photocatalysts for the degradation of phenol under UV-C light in a batch reactor, Ind. Eng. Chem. Res. 46 (2007) 9006–9014.

[123] S.N. Hosseini, M. Borghei, M. Vossoughi, N. Taghavinia, Photocatalytic degradation of phenol in aqueous phase with TiO_2 immobilized on three different supports with a simple method, (2008) 46–50.

[124] C. Kuo, Y. Yang, Exploring the Photodegradation of Bisphenol A in a Sunlight / Immobilized N-TiO_2 System, 23 (2014) 379–384.

[125] P. Kongsong, L. Sikong, S. Niyomwas, V. Rachpech, Photocatalytic antibacterial performance of glass fibers thin film coated with N-doped SnO_2/TiO_2, Sci. World J. 2014 (2014).

[126] S. Ahmed, M.G. Rasul, W.N. Martens, R. Brown, M. A. Hashib, Heterogeneous photocatalytic degradation of phenols in wastewater: A review on current status and developments, Desalination. 261 (2010) 3–18.

[127] M. Lazar, S. Varghese, S. Nair, Photocatalytic Water Treatment by Titanium Dioxide: Recent Updates, Catalysts. 2 (2012) 572–601.

[128] P. Pongwan, B. Inceesungvorn, K. Wetchakun, S. Phanichphant, N. Wetchakun, Highly efficient visible-light-induced photocatalytic activity of Fe-doped TiO_2 nanoparticles, Eng. J. 16 (2012) 143–151.

[129] V. Caratto, L. Setti, S. Campodonico, M.M. Carnasciali, R. Botter, M. Ferretti, Synthesis and characterization of nitrogen-doped TiO_2 nanoparticles prepared by sol–gel method, J. Sol-Gel Sci. Technol. 63 (2012) 16–22.

[130] H.U. Lee, S.C. Lee, S. Choi, B. Son, S.M. Lee, H.J. Kim, J. Lee, Efficient visible-

light induced photocatalysis on nanoporous nitrogen-doped titanium dioxide catalysts, Chem. Eng. J. 228 (2013) 756–764.

[131] S. Darzi, A. Mahjoub, S. Sarfi, Visible-Light-Active Nitrogen Doped TiO_2 Nanoparticles Prepared by Sol-Gel Acid Catalyzed Reaction, Iran. J. Mater. Sci. 9 (2012) 17–23.

[132] B. Tryba, Increase of the photocatalytic activity of TiO_2 by carbon and iron modifications, Int. J. Photoenergy. 2008 (2008).

[133] D. Wojcieszak, M. Mazur, M. Kurnatowska, D. Kaczmarek, J. Domaradzki, L. Kepinski, K. Chojnacki, Influence of Nd-Doping on Photocatalytic Properties of TiO_2 Nanoparticles and Thin Film Coatings, 2014 (2014).

[134] A.M. Ferrari-Lima, R.G. Marques, M.L. Gimenes, N.R.C. Fernandes-Machado, Synthesis, characterisation and photocatalytic activity of N-doped TiO_2-Nb_2O_5 mixed oxides, Catal. Today. 254 (2014) 119–128.

[135] K. Natarajan, T.S. Natarajan, H.C. Bajaj, R.J. Tayade, Photocatalytic reactor based on UV-LED/TiO_2 coated quartz tube for degradation of dyes, Chem. Eng. J. 178 (2011) 40–49.

[136] a. R. Khataee, M. Zarei, L. Moradkhannejhad, S. Nourie, B. Vahid, Nitrogen Doping of Commercial TiO_2 Nanoparticles for Enhanced Photocatalytic Degradation of Dye Under Visible Light: Central Composite Design Approach, Adv. Chem. Lett. 1 (2013) 24–31.

[137] A. Di Paola, M. Bellardita, L. Palmisano, Brookite, the Least Known TiO_2 Photocatalyst, Catalysts. 3 (2013) 36–73.

[138] S.M. Gupta, M. Tripathi, A review of TiO_2 nanoparticles, Chinese Sci. Bull. 56 (2011) 1639–1657.

[139] N. Luo, Z. Jiang, H. Shi, F. Cao, T. Xiao, P.P. Edwards, Photo-catalytic conversion of oxygenated hydrocarbons to hydrogen over heteroatom-doped

TiO_2 catalysts, Int. J. Hydrogen Energy. 34 (2009) 125–129.

[140] M. Zhu, C. Zhai, L. Qiu, C. Lu, A.S. Paton, Y. Du, M.C. Goh, New Method to Synthesize S-Doped TiO $_2$ with Stable and Highly Efficient Photocatalytic Performance under Indoor Sunlight Irradiation, ACS Sustain. Chem. Eng. 3 (2015) 3123–3129.

[141] R. Asahi, Visible-Light Photocatalysis in Nitrogen-Doped Titanium Oxides, Science (80). 293 (2001) 269–271.

[142] W. Jo, S. Shin, H. Chun, Application of Glass Fiber-Based N-Doped Titania under Visible-Light Exposure for Photocatalytic Degradation of Aromatic Pollutants, Int. J. Photoenergy. 2014 (2014).

[143] P.J. Brown, The Crystal Structure of Solids, Physics Today. 3, 1974.

[144] W. Guo, Y. Shen, G. Boschloo, A. Hagfeldt, T. Ma, Influence of nitrogen dopants on N-doped TiO_2 electrodes and their applications in dye-sensitized solar cells, Electrochim. Acta. 56 (2011) 4611–4617.

[145] J. Wang, Zhiqun, Lin, Low-cost Nanomaterials:Toward Greener and More Efficient Energy Applications, 2014.

[146] Y. Lee, J. Chae, M. Kang, Comparison of the photovoltaic efficiency on DSSC for nanometer sized TiO_2 using a conventional sol-gel and solvothermal methods, J. Ind. Eng. Chem. 16 (2010) 609–614.

[147] T.K. Tseng, Y.S. Lin, Y.J. Chen, H. Chu, A review of photocatalysts prepared by sol-gel method for VOCs removal, Int. J. Mol. Sci. 11 (2010) 2336–2361.

[148] M. Wong, W. Chu, D. Sun, H. Huang, J. Chen, P. Tsai, N. Lin, M. Yu, S. Hsu, S. Wang, H. Chang, A.P.P.L.E.N.M. Icrobiol, Visible-Light-Induced Bactericidal Activity of a Nitrogen-Doped Titanium Photocatalyst against Human Pathogens, Appl. Environ. Microbiol. 72 (2006) 6111–6116.

[149] P. Wu, J.A. ImLay, J. Ku, Biomaterials Mechanism of Escherichia coli

inactivation on palladium-modified nitrogen-doped titanium dioxide, Biomaterials. 31 (2010) 7526–7533.

[150] T.S. Le, Q.B. Ngo, V.D. Nguyen, H.C. Nguyen, T.H. Dao, X.T. Tran, E.N. Kabachkov, I.L. Balikhin, Photocatalytic equipment with nitrogen-doped titanium dioxide for air cleaning and disinfecting, Adv. Nat. Sci. Nanosci. Nanotechnol. 5 (2014) 15017.

[151] J.H. Castillo-Ledezma, A. López-Malo, M. Pelaez, D.D. Dionysiou, E.R. Bandala, Modeling the Enhanced Photocatalytic Solar Disinfection of Escherichia coli Using Nitrogen-Doped TiO 2, J. Surfaces Interfaces Mater. 2 (2014) 334–342.

[152] N.O.R.F. Zainudin, A.Z. Abdullah, A. Rahman, Development of Supported TiO_2 Photocatalyst Based Adsorbent For Photocatalytic Degradation Of Phenol, Int. Conf. Environ. 2008 (2008).

[153] D.P. Subagio, M. Srinivasan, M. Lim, T.T. Lim, Photocatalytic degradation of bisphenol-A by nitrogen-doped TiO_2 hollow sphere in a vis-LED photoreactor, Appl. Catal. B Environ. 95 (2010) 414–422.

[154] A. Acevedo, E. A. Carpio, J. Rodríguez, M. A. Manzano, Disinfection of Natural Water by Solar Photocatalysis Using Immobilized TiO_2 Devices: Efficiency in Eliminating Indicator Bacteria and Operating Life of the System, J. Sol. Energy Eng. 134 (2012) 011008-011011.

[155] A. D. Belapurkar, P. Sherkhane, S.P. Kale, Disinfection of drinking water using photocatalytic technique, Curr. Sci. 91 (2006) 73–76.

[156] J.R. Guimarães, A. S. Barretto, Photocatalytic inactivation of Clostridium perfringens and coliphages in water, Brazilian J. Chem. Eng. 20 (2003) 403–411.

[157] Y.-S. Chai, J.-C. Lee, B.-W. Kim, Photocatalytic disinfection of E. Coli in a

suspended TiO2/UV reactor, Korean J. Chem. Eng. 17 (2000) 633–637.

[158] U.I. Gaya, A.H. Abdullah, Heterogeneous photocatalytic degradation of organic contaminants over titanium dioxide: A review of fundamentals, progress and problems, J. Photochem. Photobiol. C Photochem. Rev. 9 (2008) 1–12.

[159] D. Venieri, E. Chatzisymeon, M.S. Gonzalo, R. Rosal, D. Mantzavinos, Inactivation of Enterococcus faecalis by TiO_2-mediated UV and solar irradiation in water and wastewater: culture techniques never say the whole truth, Photochem. Photobiol. Sci. 10 (2011) 1744.

[160] M.N. Chong, Nano-photocatalytic Mineralization and Disinfection for Water Reclamation : From Catalyst Engineering to Process Optimization and Modelling,PhD Thesis. (2010).

[161] K.W. Kim, S.H. You, S.S. Park, G.H. Kang, W.T. Bae, D.W. Shin, Effect of experimental conditions on photocatalytic efficiency in TiO_2 powder slurry systems, J. Ceram. Process. Res. 9 (2008) 530–537.

[162] D. Mukherjee, Development of a Novel TiO_2-polymeric Photocatalyst for Water Purification both under UV and Solar illuminations, PhD Thesis. (2011).

[163] A.G. Rincón, C. Pulgarin, Comparative evaluation of Fe^{3+} and TiO_2 photoassisted processes in solar photocatalytic disinfection of water, Appl. Catal. B Environ. 63 (2006) 222–231.

[164] C. Kormann, D.W. Bahnemann, M.R. Hoffmann, Photolysis of chloroform and other organic molecules in aqueous TiO_2 suspensions, Environ. Sci. Tech. 25 (1991) 494–500.

[165] J. A. Herrera Melián, J.M. Doña Rodríguez, A. Viera Suárez, E. Tello Rendón, C. Valdés Do Campo, J. Arana, J. Pérez Peña, The photocatalytic disinfection of urban waste waters, Chemosphere. 41 (2000) 323–327.

[166] J.-M. Herrmann, J. Disdier, P. Pichat, Photocatalytic deposition of silver on

powder titania: Consequences for the recovery of silver, J. Catal. 113 (1988) 72–81.

[167] L. Stewart, L.K. Stewart, Tungsten trioxide and titanium dioxide photocatalytic degradations of quinoline, MSc Thesis. (2009).

[168] V. Augugliaro, E. García-López, V. Loddo, S. Malato-Rodríguez, I. Maldonado, G. Marcì, R. Molinari, L. Palmisano, Degradation of lincomycin in aqueous medium: Coupling of solar photocatalysis and membrane separation, Sol. Energy. 79 (2005) 402–408.

[169] A. Fujishima, K. Honda, Electrochemical photolysis of water at a semiconductor electrode., Nature. 238 (1972) 37–38.

[170] M. Rastegar, K.R. Shadbad, A. R. Khataee, R. Pourrajab, Nanoparticles, Environ. Technol. 33 (2012) 995–1003.

[171] T. Zhang, T. Oyama, A. Aoshima, H. Hidaka, J. Zhao, N. Serpone, Photooxidative N-demethylation of methylene blue in aqueous TiO_2 dispersions under UV irradiation, J. Photochem. Photobiol. A Chem. 140 (2001) 163–172.

[172] S.S. Block, V.P. Seng, D.W. Goswami, Chemically Enhanced Sunlight for Killing Bacteria, J. Sol. Energy Eng. 1 (2016)85-89.

[173] V. Cohen-Yaniv, N. Narkis, R. Armon, Photocatalytic inactivation of Flavobacterium and E. coli in water by a continuous stirred tank reactor (CSTR) fed with suspended/immobilised TiO_2 medium, Water Sci. Technol. 58 (2008) 247–252.

[174] W. Jo, R.J. Tayade, New Generation Energy-Efficient Light Source for Photocatalysis: LEDs for Environmental Applications, Ind. Eng. Chem. Res. (2014) 2073−208.

[175] C. Is, Ultraviolet Light Emitting Diodes Ultraviolet Light Emitting Diodes, (2000).

[176] A. C. Chevremont, A. M. Farnet, B. Coulomb, J.L. Boudenne, Effect of coupled UV-A and UV-C LEDs on both microbiological and chemical pollution of urban wastewaters, Sci. Total Environ. 426 (2012) 304–310.

[177] M. Izadifard, G. Achari, C. Langford, Application of Photocatalysts and LED Light Sources in Drinking Water Treatment, Catalysts. 3 (2013) 726–743.

[178] D. Sannino, P. Ciambelli, V. Palma, V. Vaiano, R.S. Mazzei, Improved performances of a fluidized bed photoreactor by a microscale illumination system, Int. J. Photoenergy. 2009 (2009).

[179] C. Fogarty, Photocatalytic Oxidation of Ciprofloxacin Under UV-LED Light: PhD Thesis (2013).

[180] S. Izotov, A. Sitdikov, V. Soldatkin, V. Tuev, A. Olisovets, Study of Phosphors for White LEDs, Procedia Technol. 18 (2014) 14–18.

[181] N. Aslan, Y. Cebeci, Application of Box-Behnken design and response surface methodology for modeling of some Turkish coals, Fuel. 86 (2007) 90–97.

[182] M. Kete, E. Pavlica, F. Fresno, G. Bratina, U.L. Stangar, Highly active photocatalytic coatings prepared by a low-temperature method, Environ. Sci. Pollut. Res. 21 (2014) 11238–11249.

[183] P. Kongsong, L. Sikong, S. Niyomwas, V. Rachpech, Photocatalytic Antibacterial Performance of Glass Fibers Thin Film Coated with N-Doped SnO_2/TiO_2, Sci. World J. 2014 (2014) 1–9.

[184] D.A.H. Hanaor, I. Chironi, I. Karatchevtseva, G. Triani, C.C. Sorrell, Single and mixed phase TiO_2 powders prepared by excess hydrolysis of titanium alkoxide, Adv. Appl. Ceram. 111 (2012) 149–158.

[185] N. Daneshvar, D. Salari, A. Niaei, M.H. Rasoulifard, a R. Khataee, Immobilization of TiO 2 Nanopowder on Glass Beads for the Photocatalytic Decolorization of an Azo Dye C.I. Direct Red 23, J. Environ. Sci. Heal. Part A.

40 (2005) 1605–1617.

[186] M.A. Nawi, S.M. Zain, Enhancing the surface properties of the immobilized Degussa P-25 TiO_2 for the efficient photocatalytic removal of methylene blue from aqueous solution, Appl. Surf. Sci. 258 (2012) 6148–6157.

[187] S. Malato, P. Fernández-Ibáñez, M.I. Maldonado, J. Blanco, W. Gernjak, Decontamination and disinfection of water by solar photocatalysis: Recent overview and trends, Catal. Today. 147 (2009) 1–59.

[188] X. Li, P. Liu, Y. Mao, M. Xing, J. Zhang, Preparation of homogeneous nitrogen-doped mesoporous TiO_2 spheres with enhanced visible-light photocatalysis, Appl. Catal. B Environ. 164 (2015) 352–359.

[189] Y.T. Lin, C.H. Weng, H.J. Hsu, Y.H. Lin, C.C. Shiesh, The synergistic effect of nitrogen dopant and calcination temperature on the visible-light-induced photoactivity of N-doped TiO_2, Int. J. Photoenergy. 2013 (2013).

[190] Y.-H. Lin, C.-H. Weng, A.L. Srivastav, Y.-T. Lin, J.-H. Tzeng, Facile Synthesis and Characterization of N-Doped TiO_2 Photocatalyst and Its Visible-Light Activity for Photo-Oxidation of Ethylene., J. Nanomater. 2015 (2015) 1–10.

[191] Z. Lin, A. Orlov, R.M. Lambert, M.C. Payne, New insights into the origin of visible light photocatalytic activity of nitrogen-doped and oxygen-deficient anatase TiO_2, J. Phys. Chem. B. 109 (2005) 20948–20952.

[192] E.M. Samsudin, S.B. Abd Hamid, J.C. Juan, W.J. Basirun, A.E. Kandjani, S.K. Bhargava, Controlled nitrogen insertion in titanium dioxide for optimal photocatalytic degradation of atrazine, RSC Adv. 5 (2015) 44041–44052.

[193] A. Matthews, The crystallization of anatase and rutile titanium dioxide under hydrothermal conditions, Am. Mineral. 61 (1976) 419–424.

[194] K.M. Reddy, D. Guin, S. V Manorama, Selective synthesis of nanosized TiO_2 by hydrothermal route : Characterization , structure property relation , and

photochemical application, (2004) 2567–2575.

[195] D. Verhov, M. Le, N. Veronovski, Z. Samard, Gel-Sol Synthesis of Rutile Nanoparticles, Acta Chim. Slov. (2014) 468–479.

[196] J. Zhou, B. Song, G. Zhao, G. Han, Effects of acid on the microstructures and properties of three-dimensional TiO_2 hierarchical structures by solvothermal method, Nanoscale Res. Lett. 7 (2012) 1.

[197] S.M. Klein, J.H. Choi, D.J. Pine, F.F. Lange, Synthesis of rutile titania powders: Agglomeration, dissolution, and reprecipitation phenomena, J. Mater. Res.6 (2003) 1457–1464.

[198] J. Zhu, T. Wang, X. Xu, P. Xiao, J. Li, Pt nanoparticles supported on SBA-15: Synthesis, characterization and applications in heterogeneous catalysis, Appl. Catal. B Environ. 130–131 (2013) 197–217.

[199] W. Hui-Lei, L. Xiao-Heng, Synthesis of N-doped Mesoporous Titania with High Visible-light Photocatalytic Activity, J. Inorg. Mater. 29 (2014) 997. doi:10.15541/jim20140125.

[200] T. Horikawa, M. Katoh, T. Tomida, Preparation and characterization of nitrogen-doped mesoporous titania with high specific surface area, Microporous Mesoporous Mater. 110 (2008) 397–404. doi:10.1016/j.micromeso.2007.06.048.

[201] K.-I. Liu, C.-Y. Su, T.-P. Perng, Highly porous N-doped TiO_2 hollow fibers with internal three-dimensional interconnected nanotubes for photocatalytic hydrogen production, RSC Adv. 5 (2015) 88367–88374.

[202] G. Li, L. Chen, M.E. Graham, K.A. Gray, A comparison of mixed phase titania photocatalysts prepared by physical and chemical methods: The importance of the solid-solid interface, J. Mol. Catal. A Chem. 275 (2007) 30–35.

[203] J.A. Rengifo-Herrera, E. Mielczarski, J. Mielczarski, N.C. Castillo, J. Kiwi, C. Pulgarin, Escherichia coli inactivation by N, S co-doped commercial TiO2

powders under UV and visible light, Appl. Catal. B Environ. 84 (2008) 448–456.

[204] S. Sato, R. Nakamura, S. Abe, Visible-light sensitization of TiO_2 photocatalysts by wet-method N doping, Appl. Catal. A Gen. 284 (2005) 131–137.

[205] N.C. Saha, H.G. Tompkins, Titanium nitride oxidation chemistry: An x-ray photoelectron spectroscopy study, J. Appl. Phys. 72 (1992) 3072–3079.

[206] H. Diker, C. Varlikli, K. Mizrak, A. Dana, Characterizations and photocatalytic activity comparisons of N-doped nc-TiO2 depending on synthetic conditions and structural differences of amine sources, Energy. 36 (2011) 1243–1254.

[207] F. Peng, L. Cai, H. Yu, H. Wang, J. Yang, Synthesis and characterization of substitutional and interstitial nitrogen-doped titanium dioxides with visible light photocatalytic activity, J. Solid State Chem. 181 (2008) 130–136.

[208] M. Mollavali, C. Falamaki, S. Rohani, Preparation of multiple-doped TiO_2 nanotube arrays with nitrogen, carbon and nickel with enhanced visible light photoelectrochemical activity via single-step anodization, Int. J. Hydrogen Energy. 40 (2015) 12239–12252.

[209] J. Wang, D.N. Tafen, J.P. Lewis, Z. Hong, A. Manivannan, M. Zhi, M. Li, N. Wu, Origin of photocatalytic activity of Nitrogen-doped TiO_2 nanobelts, J. Am. Chem. Soc. 131 (2009) 12290–12297.

[210] M.H. Chan, F.H. Lu, Preparation of titanium oxynitride thin films by reactive sputtering using air/Ar mixtures, Surf. Coatings Technol. 203 (2008) 614–618.

[211] X. Chen, X. Chen, C. Burda, C. Burda, The Electronic Origin of the Visible-Light Absorption Properties of C-, N- and S-Doped TiO_2 Nanomaterials, J. Am. Chem. Soc. (2008) 5018–5019.

[212] C. Di Valentin, G. Pacchioni, A. Selloni, S. Livraghi, E. Giamello, Characterization of paramagnetic species in N-doped TiO 2 powders by EPR spectroscopy and DFT calculations, J. Phys. Chem. B. 109 (2005) 11414–11419.

[213] H. Irie, Y. Watanabe, K. Hashimoto, Nitrogen-Concentration Dependence on Photocatalytic Activity of $TiO_{2-x}N_x$ Powders, J. Phys. Chem. B. 107 (2003) 5483–5486.

[214] C. Di Valentin, G. Pacchioni, A. Selloni, Origin of the different photoactivity of N-doped anatase and rutile TiO2, Phys. Rev. B. 70 (2004) 85116.

[215] I. Nakamura, N. Negishi, S. Kutsuna, T. Ihara, S. Sugihara, K. Takeuchi, Role of oxygen vacancy in the plasma-treated TiO_2 photocatalyst with visible light activity for NO removal, J. Mol. Catal. A Chem. 161 (2000) 205–212.

[216] F. Dong, W. Zhao, Z. Wu, S. Guo, Band structure and visible light photocatalytic activity of multi-type nitrogen doped TiO_2 nanoparticles prepared by thermal decomposition, J. Hazard. Mater. 162 (2009) 763–770.

[217] A. Selvaraj, R. Parimiladevi, K.B. Rajesh, Synthesis of Nitrogen Doped Titanium Dioxide (TiO_2) and its Photocatalytic Performance for the Degradation of Indigo Carmine Dye, J. Environ. Nanotechnol. 2 (2013) 28–31.

[218] T. Wang, X. Yan, S. Zhao, B. Lin, C. Xue, G. Yang, S. Ding, B. Yang, C. Ma, G. Yang, G. Yang, A facile one-step synthesis of three-dimensionally ordered macroporous N-doped TiO_2 with ethanediamine as the nitrogen source, J. Mater. Chem. A. 2 (2014) 15611.

[219] J. A. Navio, C. Cerrillos, C. Real, Photo-induced Transformation, upon UV Illumination in Air, of Hyponitrite Species $N_2O_2^{2-}$ Preadsorbed onTiO2 Surface, Surf. Interface Anal. 24 (1996) 355–359.

[220] J. A. Navio, C. Cerrillos, C. Real, Photo-induced Transformation, upon UV Illumination in Air, of Hyponitrite Species N2O22- Preadsorbed onTiO2 Surface, Surf. Interface Anal. 24 (1996) 355–359.

[221] J. Saien, Z. Mesgari, Highly efficient visible-light photocatalyst of nitrogen-doped TiO2 nanoparticles sensitized by hematoporphyrin, J. Mol. Catal. A

Chem. 414 (2016) 108–115.

[222] D.-H. Wang, L. Jia, X.-L. Wu, L.-Q. Lu, A.-W. Xu, One-step hydrothermal synthesis of N-doped TiO_2/C nanocomposites with high visible light photocatalytic activity, Nanoscale. 4 (2012) 576–584.

[223] G. Liu, X. Wang, L. Wang, Z. Chen, F. Li, G.Q. (Max) Lu, H.M. Cheng, Drastically enhanced photocatalytic activity in nitrogen doped mesoporous TiO_2 with abundant surface states, J. Colloid Interface Sci. 334 (2009) 171–175.

[224] J. Ananpattarachai, Y. Boonto, P. Kajitvichyanukul, Visible light photocatalytic antibacterial activity of Ni-doped and N-doped TiO_2 on Staphylococcus aureus and Escherichia coli bacteria., Environ. Sci. Pollut. Res. 23 (2015) 4111–4119.

[225] X.D. Wang, K. Zhang, X.L. Guo, G.D. Shenb, J.Y. Xiang, Synthesis and characterization of N-doped TiO_2 Loaded onto activated carbon fiber with enhanced visible-light photocatalytic activity, New J. Chem. 38 (2014) 6139–6146.

[226] Y. Chen, X. Cao, B. Lin, B. Gao, Origin of the visible-light photoactivity of NH_3-treated TiO_2: Effect of nitrogen doping and oxygen vacancies, Appl. Surf. Sci. 264 (2013) 845–852.

[227] D.A. Kumar, J.M. Shyla, F.P. Xavier, Synthesis and characterization of TiO_2/SiO_2 nano composites for solar cell applications, Appl . Nanosci. 2 (2012) 429–436.

[228] Y. Hu, C.X. Shan, J. Wang, J.M. Zhu, C.Q. Gu, W.T. Ni, D. Zhu, A.H. Zhang, Fabrication of functionalized SiO_2/TiO_2 nanocomposites via amidation for the fast and selective enrichment of phosphopeptides, New J. Chem. 39 (2015) 6540–6547.

[229] A. Mahyar, M.A. Behnajady, N. Modirshahla, Characterization and photocatalytic activity of SiO_2-TiO_2 mixed oxide nanoparticles prepared by sol-

gel method, Indian J. Chem. 49 (2010) 1593–1600.

[230] J. Yu, J.C. Yu, The Effect of SiO_2 Addition on the Grain Size and Photocatalytic Activity of TiO_2 Thin Films, J. Sol-Gel Sci. Technol. 24 (2002) 95–103.

[231] Y. huo, Y. jin, J. zhu, H. li, Highly active $TiO_{2-x-y}N_xF_y$ visible photocatalyst prepared under supercritical conditions in NH_4F/EtOH fluid, Appl. Catal. B Environ. 89 (2009) 543–550.

[232] J. A. Navio, C. Cerrillos, C. Real, Photo-induced transformation, upon UV Illumination in air, of hyponitrite species$N_2O_2^{2-}$ preadsorbed on TiO_2 surface, Surf. Interface Anal. 24 (1996) 355–359.

[233] A. Kasgoz, K. Yoshimura, T. Misono, Y. Abe, Preparation and Properties of SiO_2-TiO_2 Thin Films from Silicic Acid and Titanium Tetrachloride, Sol-Gel Sci. Technol. 191 (1994) 185–191.

[234] H.S. Lee, S.M. Koo, J.W. Yoo, TiO_2-SiO_2 nanoparticles for suppressing photocatalytic activities and improving hydrophilicity, J. Ceram. Process. Res. 13 (2012) 300–303.

[235] S. Latthe, S. Liu, C. Terashima, K. Nakata, A. Fujishima, Transparent, Adherent, and Photocatalytic SiO_2-TiO_2 Coatings on Polycarbonate for Self-Cleaning Applications, Coatings. 4 (2014) 497–507.

[236] A.M. El-Toni, S. Yin, T. Sato, Control of silica shell thickness and microporosity of titania-silica core-shell type nanoparticles to depress the photocatalytic activity of titania, J. Colloid Interface Sci. 300 (2006) 123–130.

[237] H.S. Lee, S.M. Koo, J.W. Yoo, TiO_2-SiO_2 nanoparticles for suppressing photocatalytic activities and improving hydrophilicity, J. Ceram. Process. Res. 13 (2012) 300–303.

[238] H.N. Pham, T. McDowell, Photocatalytically-mediated disinfection of water using TiO_2 as a catalyst and spore-forming *Bacillus pumilus* as a model, J.

Environ. Sci. Health (2008) 627–636.

[239] M. Long, J. Wang, H. Zhuang, Y. Zhang, H. Wu, J. Zhang, Performance and mechanism of standard nano-TiO_2 (P-25) in photocatalytic disinfection of foodborne microorganisms - *Salmonella typhimurium* and *listeria monocytogenes*, Food Control. 39 (2014) 68–74.

[240] D.S. Kim, S.-Y. Kwak, Photocatalytic inactivation of *E. coli* with a mesoporous TiO_2 coated film using the film adhesion method., Environ. Sci. Technol. 43 (2009) 148–151.

[241] A. Pal, S.O. Pehkonen, L.E. Yu, M.B. Ray, Photocatalytic inactivation of Gram-positive and Gram-negative bacteria using fluorescent light, J. Photochem. Photobiol. A Chem. 186 (2007) 335–341.

[242] A.G. Rincón, C. Pulgarin, Use of coaxial photocatalytic reactor (CAPHORE) in the TiO_2 photo-assisted treatment of mixed *E. coli* and *Bacillus sp*. and bacterial community present in wastewater, Catal. Today. 101 (2005) 331–344.

[243] K. Shang, S. Ai, Q. Ma, T. Tang, H. Yin, H. Han, Effective photocatalytic disinfection of *E.coli* and *S.aureus* using polythiophene / MnO_2 nanocomposite photocatalyst under solar light irradiation, DES. 278 (2011) 173–178.

[244] R. van Grieken, J. Marugán, C. Pablos, L. Furones, A. López, Comparison between the photocatalytic inactivation of Gram-positive *E. faecalis* and Gram-negative *E. coli* faecal contamination indicator microorganisms, Appl. Catal. B Environ. 100 (2010) 212–220.

[245] M.B. Fisher, D. a. Keane, P. Fernández-Ibáñez, J. Colreavy, S.J. Hinder, K.G. McGuigan, S.C. Pillai, Nitrogen and copper doped solar light active TiO_2 photocatalysts for water decontamination, Appl. Catal. B Environ. 130–131 (2013) 8–13.

[246] V. Arya and Ligy Philip, Visible and solar light photocatalytic disinfection of

bacteria by N-doped TiO_2, Water Sci. Technol. Water Supply. (2014) 924–930.

[247] H. a. Foster, I.B. Ditta, S. Varghese, A. Steele, Photocatalytic disinfection using titanium dioxide: Spectrum and mechanism of antimicrobial activity, Appl. Microbiol. Biotechnol. 90 (2011) 1847–1868.

[248] R. Nakano, M. Hara, H. Ishiguro, Y. Yao, T. Ochiai, K. Nakata, T. Murakami, J. Kajioka, K. Sunada, K. Hashimoto, A. Fujishima, Y. Kubota, Broad Spectrum Microbicidal Activity of Photocatalysis by TiO_2, Catalysts. 3 (2013) 310–323.

[249] Z. Huang, P. Maness, D.M. Blake, E.J. Wolfrum, S.L. Smolinski, W.A. Jacoby, Bactericidal mode of titanium dioxide photocatalysis, Photochem. Photobiol. A Chem. 130 (2000) 163–170.

[250] H.A. Foster, I.B. Ditta, S. Varghese, A. Steele, Photocatalytic disinfection using titanium dioxide: Spectrum and mechanism of antimicrobial activity, Appl. Microbiol. Biotechnol. 90 (2011) 1847–1868.

[251] P. Maness, S. Smolinski, D.M. Blake, Z. Huang, E.J. Wolfrum, W. A. Jacoby, Bactericidal Activity of Photocatalytic TiO_2 Reaction: toward an Understanding of Its Killing Mechanism, Appl. Environ. Microbiol. 65 (1999) 4094–4098.

[252] B. Viswanathan, K.R. Krishanmurthy, Nitrogen incorporation in TiO_2: Does it make a visible light photo-active material, Int. J. Photoenergy. 2012 (2012).